LUND UNIVERSITY

ANNEALED GLASS FAILURE MODELLING

A Weakest-Link Approach with Statistical Analysis

DAVID KINSELLA

Structural Mechanics

Doctoral Thesis

DEPARTMENT OF CONSTRUCTION SCIENCES
DIVISION OF STRUCTURAL MECHANICS

ISRN LUTVDG/TVSM--21/1032--SE (1-156) | ISSN 0281-6679
ISBN 978-91-7895-709-5 (print) | ISBN 978-91-7895-710-1 (pdf)
DOCTORAL THESIS

ANNEALED GLASS FAILURE MODELLING

A Weakest-Link Approach with Statistical Analysis

DAVID KINSELLA

Printed by V-husets tryckeri LTH, Lund, Sweden, January 2021 *(Pl)*.

For information, address:
Division of Structural Mechanics,
Faculty of Engineering LTH, Lund University, Box 118, SE-221 00 Lund, Sweden.
Homepage: www.byggmek.lth.se

Preface

This thesis is submitted in partial fulfilment of the requirements for the degree of Doctor of Philosophy in Structural Mechanics at Lund University. The work presented in this thesis was carried out at the Department of Construction Sciences at the Faculty of Engineering LTH, Lund University. Financial support was provided by the Swedish glass associations, Glasbranschföreningen, Svensk Planglasförening, and Balkongföreningen. The work was supervised by Professor Kent Persson, Professor Erik Serrano, Senior Lecturer Susanne Heyden, Senior Lecturer Johan Lindström, and Senior Lecturer Marcin Kozłowski. The thesis consists of five parts in the form of four journal articles, referred to as Paper A, B, D, and E, and one conference paper, referred to as Paper C. Paper A, B, and D have been published in international peer-reviewed journals, while Paper E is submitted for possible publication in an international peer-reviewed journal. Paper C has been peer-reviewed and published in the proceedings of an international conference. A synopsis binds the five papers together.

Lund, 19th January 2021
David Kinsella

Acknowledgements

It is inevitable for a project of this length that there will be a great many to whom I owe my thanks. First, I thank my supervisors for numerous points of assistance, encouragement, and guidance. I am particularly grateful to Kent Persson and Erik Serrano without whose help and effort this thesis could not have been completed. Their expertise and critical reflections have been pivotal throughout the whole process. I gratefully acknowledge Marcin Kozłowski who contributed with inspiring perspectives, offered practical advice, and provided good company. I am especially grateful to Johan Lindström for immense help on matters of mathematical statistics and for valuable contributions, critical reflections, and inspiring propositions. I thank Susanne Heyden for constructive reading of some of my nearly finished manuscripts, for showing meticulous attention to certain aspects of the text while offering insightful advice. My thanks are also due to Jessica Dahlström for assistance in the laboratory. I would furthermore like to acknowledge the support of Anders Sjöström and Joachim Hein on how to use the facilities at LUNARC, the Center for Scientific and Technical Computing at Lund University. I am grateful to the late Per-Johan Gustafsson for helpful support and sustained encouragement. Thanks to Matti Ristinmaa for doing a sterling work as Head of Department. Thanks also to Marc Vandebroek who provided valuable criticism and a broadened theoretical horizon on Paper A, B, and C. I am indebted to the generosity shown to me by the remarkable group of PhD Candidates within the divisions of Structural Mechanics, Geotechnical Engineering, Engineering Acoustics, and Solid Mechanics: Hanna, Karin, Linus, Jens, Jan, Nikolas, Gustaf, Vedad, Wael, Anders, Juan, Johan, and others. I thank the rest of the staff at the Department of Construction Sciences who have contributed to a pleasant workplace environment. The excellent service provided by the librarians at Lund University was essential to the retrieval and management of scientific information within the specific research area, thanks to Tora Kristiansen and Andreas Karman, among others. My sincere gratitude is expressed to Gustaf Larsson, Wael Mohamed, and Liene Sable for the wonderful company they afforded me while sharing the office room. Finally, my gratitude goes to my beloved Sofie, for her continued support and deep understanding and sensitivity.

Abstract

Novel and increased use of glass in building construction has been made possible, as a result of methods of mass production introduced during the 20th century and advanced computational structural analyses. With modern use of glass structures, a range of demands emerge which need to be addressed in the strength design process. The aim of the thesis work has been to develop experimentally verified prediction models that can be used as design tools for advanced glass structures. The first part of the thesis consists of an introduction and overview with a background and motivation for the work carried out, the aim and objectives, along with a summary of the appended papers, and a conclusion and outlook with suggestions for further work. The second part of the thesis consists of five appended publications, Paper A to E. Paper A presents results from a wide-ranging survey of laboratory tests which was conducted pertaining to the strength of new annealed soda-lime float glass tested in an ambient environment. With a basis in the survey, four standard statistical distributions were compared with respect to their performance as strength models, namely the normal, lognormal, Weibull, and Gumbel. It was concluded that the extreme value distributions provide basic models for edge failures but perform poorly for surface fracture origins. In Paper B, C, and E, various numerical implementations of finite-size and flaw-size based weakest-link systems were developed and applied to model the failure stress and fracture origins on the surface of plates subject to lateral loading, in addition to a consideration of strength-scaling size effects. Applications were made to a range of different load cases including small plates subject to ring-on-ring and ball-on-ring loading, large linearly supported plates subject to uniform pressure, and large panels with complex geometry subject to impact loading. In Paper E, results were presented from laboratory tests which were carried out on two series of annealed glass plates subject to ring-on-ring and ball-on-ring loading in an investigation of the distribution of failure stress and fracture origin, and their dependence on the surface area exposed to greatest tension. The Weibull effective areas were expressed in closed-form and employed to calculate a strength-scaling size effect. According to the observed surface strength data, the weakest-link premise of the ordinary Weibull model is rendered intractable and more sophisticated approaches are warranted. Finally, it was concluded that there is a need for additional research on the surface condition of glass that can lead to more reliable information about the suitable choice of model parameters. In Paper D it was considered that the Weibull distribution parameters that are fitted to laboratory measurements of as-cut, arrised, ground, and polished edge strength exhibit considerable variability. Estimates for the characteristic 5%-fractile edge strength were obtained in a hierarchical modelling approach by considering the Weibull parameters as nested random variables. It was shown that glass supplier random effects are important to consider in addition to effects on the observed strength due to environmentally assisted crack growth, applied stress rate, and edge length exposed to maximum stress.

Populärvetenskaplig sammanfattning

Glas är ett genomsiktligt material som används i byggnader för att utforma miljöer som är ljusa och upplevs som öppna. Modernt byggnadsglas används i konstruktioner som utsätts för betydande laster jämfört med ett traditionellt fönsterglas. Som exempel kan nämnas trappsteg, balustrader, golv, tak och väggpaneler där glasets geometriska utformning kan vara mer eller mindre komplex. Det finns ett behov av att utveckla metoder som kan användas för att dimensionera moderna glaskonstruktioner. En följd av bristen på metoder är att stora säkerhetsfaktorer måste tillgripas. Det medför att materialåtgången blir onödigt stor vilket leder till tunga konstruktioner med extra produktionskostnader och större energiåtgång under transporten från glasverket till byggarbetsplatsen. Avhandlingsarbetet syftar till att utveckla modeller för hållfastheten och metoder som kan användas för att göra förutsägelser om styrkan i avancerade glaskonstruktioner. I förlängningen kan modellerna tillämpas i beräkningshjälpmedel som används av konstruktören.

En genomgång av forskningslitteraturen resulterade i en bred sammanställning av hållfasthetsmätningar. Dessa har använts för att pröva en rad hypoteser om glasets hållfasthet och för att anpassa en nydanande modell för kanthållfastheten. Bland annat undersöktes hur de vanligast förekommande bearbetningarna av glaskanten påverkar den uppmätta hållfastheten. I teorin är glas ett mycket starkt material. I praktiken är emellertid hållfasthetsvärdet begränsat och förknippat med en betydande statistisk spridning. Experiment visar även att brottets läge sällan sker just där den största påkänningen finns. Spridningen i uppmätt hållfasthet kan förklaras genom att anta att glasytan är bemängd med en mångfald mikroskopiska defekter som har vissa slumpmässiga egenskaper. Defekterna uppstår på grund av olika betingelser redan under framställningen, hanteringen, transporten och senare medan glaset brukas och underhålls. I närheten av defekterna koncentreras spänningarna och når kritiska nivåer som leder till brott. Därför är glas ett sprött material som tenderar att gå till brott till synes utan förvarning. I avhandlingsarbetet har hållfasthetsmodeller utvecklats som bygger på att defekterna representeras av plana sprickor med en förenklad geometrisk konfiguration. Beräkningsmodellerna tillämpades på fallstudier inbegripet en avancerad glaskonstruktion i en lokal i en offentlig byggnad. Konstruktionsdelen utsätts för en mjuk stötlast som i princip motsvarar utfallet av att en människa av en olyckshändelse faller in mot glaset. Tillämpningar gjordes även i ett studium av glasplattor som böjs till brott under kontrollerade former i experiment. En möjlighet är att använda modellerna som beräkningshjälpmedel i certifieringsprocesser av glaskonstruktionsdelar för att minska behovet av dyra och tidskrävande experiment. En annan möjlighet är att införliva vissa av metoderna i befintliga beräkningshjälpmedel som redan används av glasbranschen i Sverige för att utföra effektivare dimensionering av konstruktioner.

Contents

Part I

Introduction and overview

1 Introduction

1.1 BACKGROUND

Glass has been used in buildings since the time of ancient Rome. The functional role of traditional window glass is to shut out the cold and weather while allowing for transmission of daylight. Roman baths, for instance, depended on their heating among other things on large glazed windows to retain the hot air in the rooms and achieve some solar gain, as well as to provide natural light (Addis 2007). In addition, significant architectural use is evident in e.g. medieval cathedrals where stained glass windows, which were made possible through skilful addition of metallic salts during manufacture, satisfied trends for style and design (Addis 2007, Macfarlane & Martin 2002). Until only recently, glass in building construction was limited to such functional and architectural use. Methods of mass production introduced in the 20th century together with new techniques for post-processing the manufactured glass, and advanced computational structural analyses have created opportunity for novel and increased use of glass in construction (Fröling 2013, Haldimann et al. 2008). Exposure to natural light is important for human well-being, however, the reality is that we spend up to 80%-90% of our time indoors (Christoffersen 2011, Marqueze et al. 2015). The benefit of glass in buildings on human health and well-being can be profound. With modern use of glass in building construction, the structural role of the glass unit is significant due to its exposure to considerable loading as it is utilized as beam, pillar, plate, or panel element. The strength design must take into account various static load cases due to e.g. snow load or secondary structural members, and dynamic load cases due to e.g. accidental impacting from

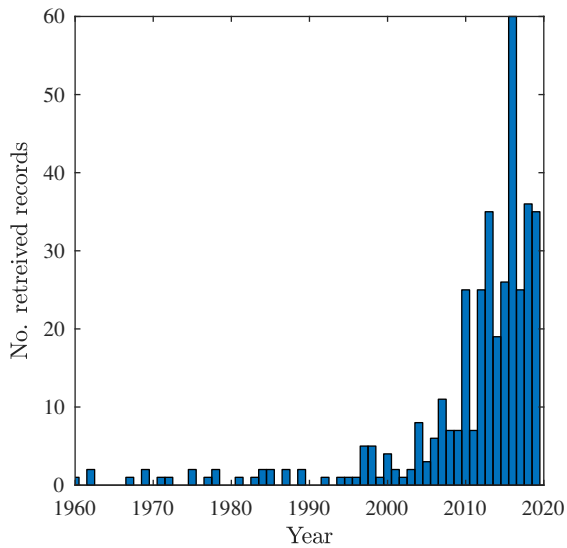

Figure 1.1: Number of retrieved records per year in Scopus (www.scopus.com) from search phrase (1.1). The data includes the year 2019.

a soft body. Hence, with modern use of glass in structures there emerges new opportunities as well as demands on the design process which may involve a whole range of different design alternatives to be evaluated. There is a need for improved methods to be developed which can be applied in a safe strength design of advanced glass structures. When methods are lacking, an overly conservative strength design is adopted which leads to considerably more material than necessary being used in structures. This leads to additional production costs and also requires more energy to be spent in transporting the manufactured units from the production site to the construction site. Optimally designed glass structures are a matter of safety, cost efficiency, as well as sustainability.

Research into structural use of glass in building is an emerging field. This is reflected in the increased number of dedicated scientific journals and conferences as well as in the overall number of peer-reviewed publications that deal with the topic. As an indication of the increase in research activity, consider the statistics generated by the following search string in the Scopus database (www.scopus.com) which is an abstract and citation database for scientific journals, books, and conference proceedings.

$$\{\text{structural glass}\} \tag{1.1}$$

The search is limited to the title, abstract, and keywords fields, in addition to the subject area “engineering”. The number of retrieved records per year is illustrated in the bar graph in Fig. 1.1. Evidently, engineering structural glass is being researched at an increased rate.

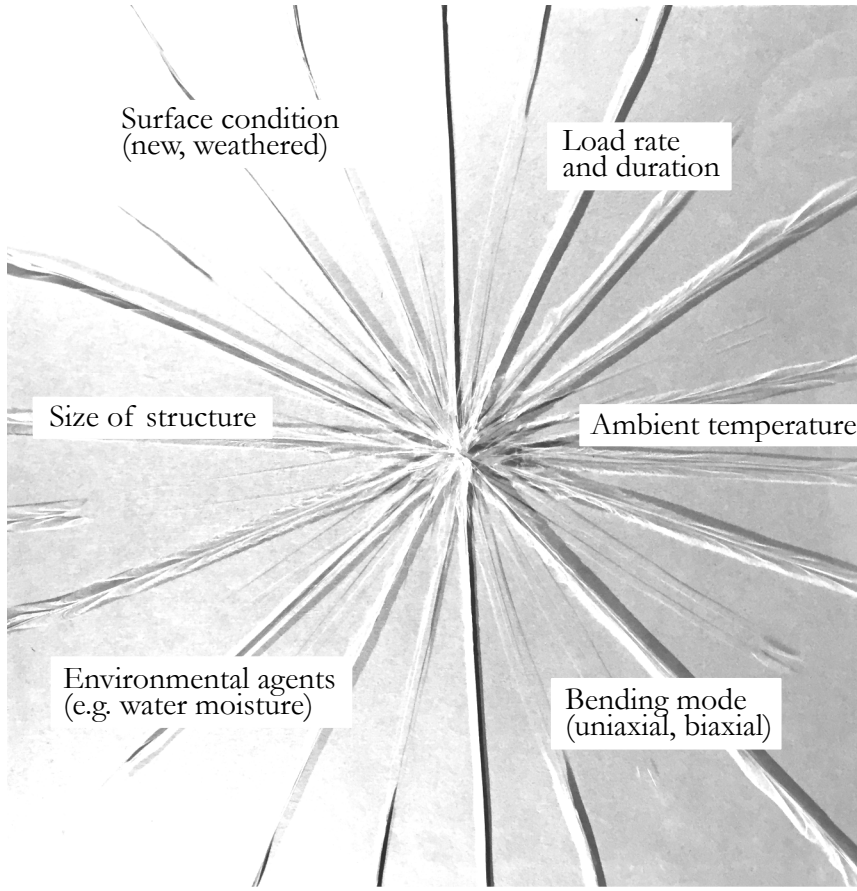

Figure 1.2: The strength of glass depends on a range of factors.

The strength of glass depends on a range of factors, see Fig. 1.2. To begin with, it can only be revealed by destroying the glass. As a matter of fact, the strength depends on the load history, environment, and temperature, as well as the overall size of structure exposed to tension, and the state of surface, the condition of which might be new as-received or aged and weathered. The simultaneous action of stress and environmental conditions promote a fatigue phenomenon in glass. The combined effect of load-history and climate on strength can be accounted for by implementing the stress corrosion rate theory or some empirical formula.

A substantial number of experiments on annealed glass have been conducted over the past decades. Those tests provide statistics about the strength and the location of fracture origins. The results demonstrate that the strength exhibits a large variation ranging over one order of magnitude. Also, the fracture origin often does not coincide with the location of maximum tensile stress. There is an element of randomness to the phenomenon of glass fracture that clearly warrants a stochastic

approach to modelling and a statistical treatment of empirical data, more so perhaps than for any other conventional building material in present use. In spite of efforts to devise probabilistic strength models for glass, it remains a great challenge to model and predict the strength value for some structural unit in general.

On a macroscopic scale and to the naked eye, the glass surface appears smooth almost without defect. With glass manufactured using the float process production method, the surface seems also to be perfectly flat. Theoretically, such material could be extremely strong. And yet, on a microscopic scale, it is assumed that the surface contains numerous and minute flaws that limit the practical strength to such magnitudes that are commonly observed in experiments. Present techniques for modelling and predicting the strength are based either on a fracture mechanical method that takes as starting point the microscopic scale of events, or on some phenomenological approach that starts out from a macroscopic scale. As an example of the latter we may take the adoption of a standard statistical distribution such as the normal distribution to model fracture stress. Current failure prediction models, however, are limited in scope. At best, they are suited to particular test arrangements and environmental conditions. In fact, the failure prediction remains a formidable challenge in the general case of a structural unit with boundary conditions that can vary from very rigid to fairly flexible with continuous support or point fixings, where the load is either distributed or concentrated, and with the geometrical properties of glass depending on e.g. aspect ratio and the existence of boreholes. Additionally, although failure prediction generally pertains to the strength value, it can also be useful to make predictions about the failure origin. There is need for further development of a failure prediction model that can be conducive to the improvement of design methodology, structural standards and building codes.

The failure prediction and strength design of a glass structure is dependent on a range of theories and methods at the material as well as the structural level as illustrated in Fig. 1.3. Fracture mechanical theories consider the microscopic behaviour of solids and form a basis of failure prediction models for use with brittle materials. At the structural level, mechanical models allow for the determination of the stresses and strains in plates and beams due to bending under various forms of loading and support conditions. In combination, fracture mechanical and structural mechanical models provide a powerful tool for the analysis of brittle specimens subjected to bending loads. However, the phenomenon of static fatigue complicates prediction-making. Experimental test results can be used to validate the models at the structural level, to make investigations into the surface condition at the material level e.g. through the estimation of a surface flaw size density function, and to quantify the rate of subcritical crack growth. Ultimately, it is necessary to employ probability theory and methods of statistical inference at both the material and the structural level to account for the various aspects of glass failure, e.g., to represent surface microcrack concepts, and to draw inference about model para-

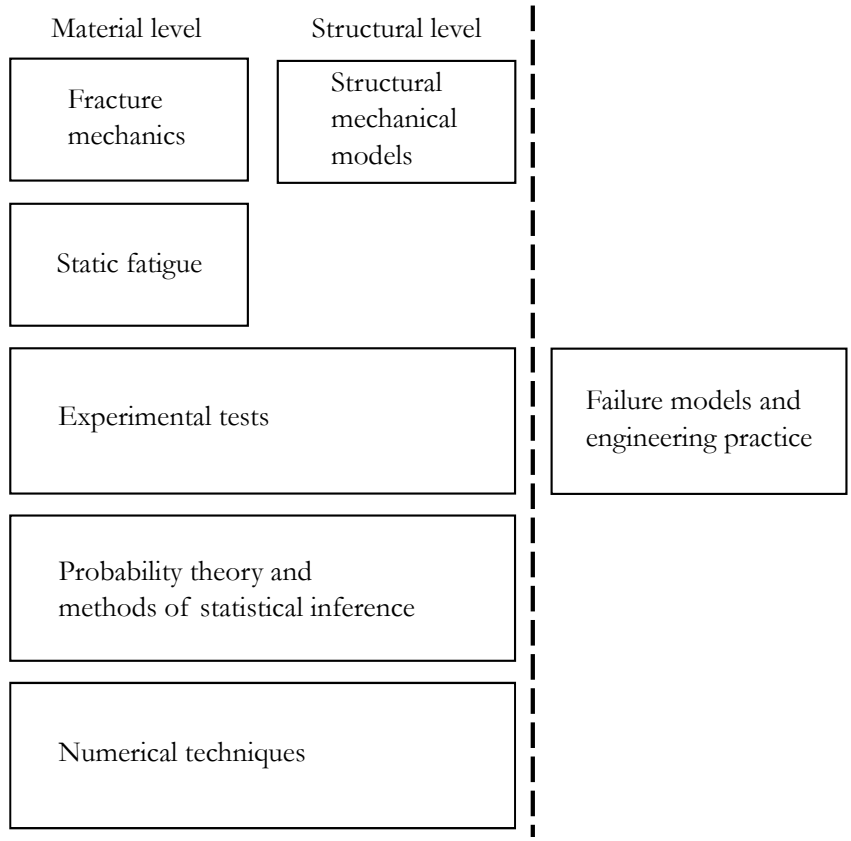

Figure 1.3: Engineering practice dependencies.

meters and performance. Some of the methods thus employed are made feasible by use of numerical techniques such as the finite element method (FEM) which is key to computing the stresses and strains in solids subjected to arbitrary boundary conditions. Finally, the failure prediction model has to be put to practical use by carefully considering the requirements and directives of modern building codes and structural standards.

Monolithic panes of annealed float glass are an important object for modelling because according to the structural standards, e.g. EN 16612:2019, the strength of a glass pane is based on the so-called characteristic value for the bending strength of annealed glass. In practice, a glass pane may be tempered to increase the breaking stress, and a laminated structure may be formed by bonding together multiple plies of glass, see further Sec. 2.1.1. In either case, knowledge of the strength of a monolithic pane of annealed glass is key to making strength-predictions.

1.2 AIM AND OBJECTIVES

The main aim of the research is to develop experimentally verified models that can be used as design tools for failure prediction of advanced glass structures subjected to various loads and boundary conditions. To reach the aim, the following objectives are considered which are dependent on a range of theories and methods as presented in Fig. 1.3.

a) Create an overview of glass failure modelling approaches according to basic features and underlying assumptions. What are some of the utilities and drawbacks in general when it comes to various modelling approaches?

b) Collect and organize empirical data on the strength of new monolithic annealed float glass that is tested in ambient conditions. Survey the laboratory tests reported in scientific journals, conference proceedings, and academic dissertations.

c) Appraise the performance of the most pertinent standard statistical distributions when those are applied to model the strength observed in laboratory tests. Does the edge strength data exhibit significantly different features compared to the surface strength tests?

d) Develop a surface strength model assuming random sampling of Griffith flaws in Monte Carlo simulations of glass specimens extracted from virtual jumbo panes. How should the surface condition be represented, e.g., what would the stochastic properties of the Griffith flaws be?

e) Apply the surface strength model to simulate the fracture origin and strength of plates subject to various forms of loading. Illustrate how the method can be used as a practical tool, e.g., in tests where the survival probability for some structural component is assessed.

f) Investigate the surface strength-scaling size effect. For example, calculate and compare the Weibull effective areas for nominally equal specimens subject to diverse bending setups that expose dissimilar surface areas to maximum tension.

g) Conduct laboratory tests to study the distribution of strength, fracture origin, and strength-scaling size effects, and to verify the Weibull effective area solutions and the numerical surface strength model.

h) Perform an in-depth analysis of the edge strength based on surveyed data measurements. How do common edge treatments differ from one another if at all? Can the empirical data be used to assess the possible influence that the supplier or manufacturer has on the random variability in the observed test results?

1.3 LIMITATIONS

Certain limitations are necessary for the work carried out in the thesis. The main focus is on monolithic panes of float glass that are new, in the as-received condition. It is generally assumed that the glass is stressed in an ambient environment meaning that the temperature and relative humidity correspond to indoor conditions. Flaws in the bulk are disregarded and it is assumed that failure is governed by surface flaws. It is assumed that the shape of flaws can be represented by planar cracks. Mode III crack displacement is not considered in a fracture criterion. Crack healing effects are not taken into account in the strength modelling. The analysis and discussion of structural standards is limited mainly to previous drafts for a European standard for strength of glass in building, prEN 16612:2013, prEN 16612:2017, and the subsequent EN 16612:2019.

2
Glass material

The background information and facts in Sec. 2.1 are based on Le Bourhis (2008) where no reference is cited explicitly.

2.1 MANUFACTURE

Soda-lime silicate glass is an amorphous and inorganic ceramic material. The manufacture involves a long process line, see Fig. 2.1. Glass for use in structures is composed of the following raw materials which are selected in the batching operation, viz. sand, sodium carbonate, calcium carbonate, and various metal oxides. The composition of raw material is indicated in Tab. 2.1. The material composition is further standardized in EN 572-1. The role of sodium in the batch is to soften the glass network and reduce the melting temperature to a practical regime while the addition of calcium stabilizes the network (McLellan & Shand 1984). Various metal oxides are added, among other reasons, to facilitate in the fining operation.

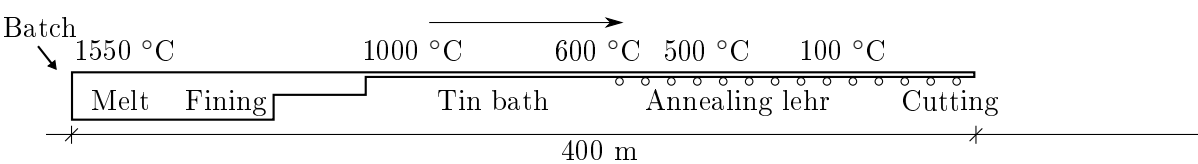

Figure 2.1: Flat glass production line with the float process. Adapted from Haldimann (2006) and Le Bourhis (2008).

Table 2.1: Raw material composition in a batch of soda-lime silicate float glass (Le Bourhis 2008).

Raw material	Sand	Sodium carbonate	Calcium carbonate	Metal oxides
Concentration (%)	54	24	16	2

Table 2.2: Typical values for a range of material properties (Le Bourhis 2008)

Density (kg m^{-3})	2500
Thermal conductivity (W $(mK)^{-1}$)	1.00
Thermal expansion coeff. (10^{-6} K^{-1})	8.5
Surface energy (J m^{-2})	0.6

The melting is done in a furnace which is usually combustion heated.

The glass material is formed by a network of Si – O which have covalent bonds and that is modified by Na^+ and $Ca_2{}^+$ ions through ionic bonds. The glass network is characterized by a short-range order; after about five interatomic distances, order almost vanishes. In three dimensions, the Si and O atoms arrange to form tetrahedral elements with a Si atom at the centre. The elemental tetrahedrons are connected by the sharing of corners. The addition of Na^+ causes rupture of O – O bonds, however, the pair of tetrahedra still interact electrostatically. The modification of the network induces a decrease in viscosity. This is of great practical importance because it lowers the melting temperature of glass significantly. In pure silica the melting temperature is about 1700 °C while in soda glass it is only about 790 °C after addition of 25% soda to silica. Values for a range of material properties are given in Tab. 2.2. At room temperature, the viscosity is so high that no flow can be observed.

In the fining operation, the glass composition and temperature is made uniform through convection, and bubbles are eliminated. In the float process, the glass melt is floated on a bed of molten tin at a temperature of about 1100 °C under a nitrogen atmosphere. As the glass exits the float, it has a temperature of about 600 °C. Then, it enters the annealing lehr where it is cooled down to room temperature. The thermal history is carefully controlled to design the residual stresses. The glass is usually cut into standard size panes with the dimensions 6×3.21 m^2 (EN 572-1). The standard thicknesses are given in EN 572-1. Some experiments (Krohn et al. 2002, Tummula & Foster 1975) indicate that the tin side of the float glass contains more severe flaws than the air side. However, to the extent that there may be a marginal difference in strength between the tin and air sides of glass, this should not necessarily be attributed to the diffusion of tin atoms, but to the contact of the tin side with the rollers as the glass exits the float (Haldimann 2006).

There are many production parameters with importance for the mechanical properties of the glass end-product and some of the most important ones with respect to the edge strength are explained in Kinsella & Lindström (2020), which can also be found in Paper D. In addition to the edge treatments considered in Paper D, the strength of the water-cut edge profile was investigated by, among others, Veer & Rodichev (2012).

The flat glass that exits the annealing lehr in the float glass production line can be further processed in several ways to produce various products with added value. Here follows a description of the operations that are most pertinent to glass products for structural use. The processing can be done on the manufacturing site or off-site, e.g. with a supplier. The basic, un-processed product is in this context understood to be the monolithic pane of annealed float glass with an as-cut edge.

2.1.1 Tempering

Tempering produces a glass sheet with all surfaces subjected to compressive stresses which are counter-balanced by tensile stresses in the interior. The compressive surface stresses have to first be overcome before the tempered glass can be broken, unless the fracture is initiated from the interior (Tooley 1984). Thermal tempering is performed by heating up the glass article close to the transition temperature at about 650 °C and rapidly quenching it by chilling the surface with blasts of air (McLellan & Shand 1984). The rapidly cooled glass material is subjected to a thermal gradient while it passes through the viscous-elastic domain which results in the build-up of compressive residual stresses at the surface. The thermal and structural histories during tempering are complex and include unknown thermal transfer coefficients. However, a simple model for the through-the-thickness stress distribution can be achieved by assuming a constant rate of cooling and supposing that no structural relaxation takes place.

A fully tempered glass pane usually has a breaking stress that is increased by a factor of 2.5 to 3.5 compared to annealed glass (McLellan & Shand 1984). According to EN 16612:2019, the strength of toughened safety glass is about 2.5 times as great as that of ordinary annealed glass while the strength of heat strengthened glass is about 1.5 times as great. Upon failure, a fully tempered pane shatters into small cubes and this is referred to as dicing. The dice are unlikely to cause serious injury. Thermally toughened glass is standardized in EN 12150-1. Heat-strengthened glass is produced similarly to fully tempered glass but with a lower rate of quenching which produces smaller compressive surface stresses. On failure, heat-strengthened glass does not dice into small fragments like fully tempered glass. Instead, it retains a large fracture pattern similar to annealed glass. Heat-strengthened glass is standardized in EN 1863-1.

After thermal toughening has been performed, any occurring nickel sulphide (NiS) inclusions undergo a slow transformation at room temperature to a lower density phase that can prompt spontaneous failure of the glass article. The phase-transformation can be accelerated in a heat-soak treatment that prevents transformation from taking place during service. A heat-soak test is standardized in EN 14179-1 that greatly reduces the risk of breakage due to NiS-inclusions during use of thermally toughened components.

Chemical tempering is performed by immersing the glass in a molten salt bath. The outer surface of the glass is strengthened through an ion exchange process. It is possible to achieve much higher surface compression with chemical tempering than with thermal tempering. However, the ion exchange depth is limited which results in a much smaller compression depth compared to thermally tempered articles. Moreover, the ion diffusion rates are very slow for ordinary soda-lime-silica glass which is widely used in building applications (Tooley 1984).

2.1.2 Laminated glass

Laminated glass is formed by bonding together two panes by a tough polymer in an autoclave. Polyvinyl butyral (PVB) is the most common choice of interlayer material and normally two foils are used, each foil having a thickness of 0.38 mm. However, there exist a whole range of alternative interlayer materials that offer higher stiffness, greater temperature resistance, etc. Laminated glass units achieve a greatly improved post-fracture behaviour compared to monolithic units due to the way in which the polymer interlayer absorbs energy from impacting objects, retains the fractured pieces of glass providing structural redundancy, and limits the risk of flying shards (McLellan & Shand 1984). The product standard for laminated glass and laminated safety glass can be found in EN 14449. For the standard that governs the determination of interlayer viscoelastic properties, see EN 16613.

2.1.3 Insulating glass units

An insulating glass unit is composed of two or more glass panes with closed cavities which reduce heat transfer due to radiation, conduction, and convection. A low-conductivity gas fill is normally used between the panes. Radiative heat transfer can be further limited by tinted or coated glazing. The product standard for insulating glass units can be found in EN 1279-5.

2.2 CONSTITUTIVE MODELLING

To model a glass material specimen under general loading, a continuum body in Euclidian space is considered. Suppose a motion that generates a spatial displacement field $\boldsymbol{u}$ (for the equations of motion, see further Sec. 3.3.1). The strain tensor $\boldsymbol{\epsilon}$ describes the deformation completely (Saabye Ottosen & Ristinmaa 2005). For small displacement gradients and with the displacements resolved into components parallel to the coordinate axes x, y, and z, it is given by

$$\boldsymbol{\epsilon} = \begin{bmatrix} \epsilon_{xx} & \epsilon_{xy} & \epsilon_{xz} \\ \epsilon_{yx} & \epsilon_{yy} & \epsilon_{xz} \\ \epsilon_{zx} & \epsilon_{zy} & \epsilon_{zz} \end{bmatrix} \tag{2.1}$$

where the elongation strains are

$$\epsilon_{xx} = \frac{\partial u_1}{\partial x}, \qquad \epsilon_{yy} = \frac{\partial u_2}{\partial y}, \qquad \epsilon_{zz} = \frac{\partial u_3}{\partial z} \tag{2.2}$$

and the shearing strains are (Timoshenko & Woinowsky-Krieger 1959)

$$\epsilon_{xy} = \frac{1}{2}\left(\frac{\partial u_1}{\partial y} + \frac{\partial u_2}{\partial x}\right), \quad \epsilon_{xz} = \frac{1}{2}\left(\frac{\partial u_1}{\partial z} + \frac{\partial u_3}{\partial x}\right), \quad \epsilon_{yz} = \frac{1}{2}\left(\frac{\partial u_2}{\partial z} + \frac{\partial u_3}{\partial y}\right). \tag{2.3}$$

The Cauchy stress tensor contains all the information necessary to determine the traction vector $\boldsymbol{t}$ for arbitrary sections through a given point, and it is given by (Saabye Ottosen & Ristinmaa 2005)

$$\boldsymbol{\sigma} = \begin{bmatrix} \sigma_{xx} & \tau_{xy} & \tau_{xz} \\ \tau_{yx} & \sigma_{yy} & \tau_{yz} \\ \tau_{zx} & \tau_{zy} & \sigma_{zz} \end{bmatrix} \tag{2.4}$$

Both the strain and stress matrices in (2.1) and (2.4) are symmetric and for sake of notational simplicity a vector representation is used (see further Sec. 3.3.2) in the form of Eq. (2.5) and (2.6), viz.

$$\boldsymbol{\epsilon} = \begin{bmatrix} \epsilon_{xx} & \epsilon_{yy} & \epsilon_{zz} & \epsilon_{xy} & \epsilon_{xz} & \epsilon_{yz} \end{bmatrix}^T, \tag{2.5}$$

and,

$$\boldsymbol{\sigma} = \begin{bmatrix} \sigma_{xx} & \sigma_{yy} & \sigma_{zz} & \tau_{xy} & \tau_{xz} & \tau_{yz} \end{bmatrix}^T. \tag{2.6}$$

The isotropic linear elastic response is expressed using Hooke's generalized law in

$$\boldsymbol{\sigma} = \boldsymbol{D}\boldsymbol{\epsilon} \tag{2.7}$$

with (2.5) and (2.6), and with

$$\boldsymbol{D} = \frac{E}{(1+\nu)(1-2\nu)} \begin{bmatrix} 1-\nu & \nu & \nu & 0 & 0 & 0 \\ \nu & 1-\nu & \nu & 0 & 0 & 0 \\ \nu & \nu & 1-\nu & 0 & 0 & 0 \\ 0 & 0 & 0 & \frac{1}{2}(1-2\nu) & 0 & 0 \\ 0 & 0 & 0 & 0 & \frac{1}{2}(1-2\nu) & 0 \\ 0 & 0 & 0 & 0 & 0 & \frac{1}{2}(1-2\nu) \end{bmatrix} \tag{2.8}$$

where E is Young's modulus and ν is Poisson's ratio (Saabye Ottosen & Ristinmaa 2005). See Paper E for a table containing representative values of the elastic properties in glass. A state of plane strain exists when the only non-zero strains are ϵ_{xx}, ϵ_{yy}, and ϵ_{xy}. In plane stress, the only non-zero stresses are σ_{xx}, σ_{yy}, and τ_{xy}.

The assumption of material linear elasticity is insufficient for modelling of nonlinearly elastic and viscoelastic materials such as are present in e.g. the interlayers in laminated glass and in certain types of gasket in laterally supported plates. For a further treatment of hyperelastic material modelling the reader is referred to Holzapfel (2000).

2.3 STATIC FATIGUE AND FRACTURE

Material fatigue means that the strength deteriorates over time. The earliest record of fatigue in glass is found in Grenet (1899) who subjected rectangular plates and small rods of glass to three-point bending at various rates of loading. He observed a decrease in strength as the load-duration was increased. Subsequently, many experiments have manifested environmentally assisted fatigue in glass, see e.g. Baker & Preston (1946*a*,*b*), Culf (1957), Mould & Southwick (1959). The environment comprises agents such as water, usually in the form of humidity. Static fatigue is not observed at temperatures below -196 °C (Le Bourhis 2008). It has been demonstrated that static fatigue is not aggrevated by cyclic loading, see e.g. Lü (1997). Fatigue in glass is conventionally termed static fatigue, perhaps to distinguish it from cyclic fatigue which is common in the steel engineering literature (Haldimann 2006). Present theories that explain static fatigue are based on the assumption of pre-existing surface flaws, see Sec. 2.3.2.

The phenomenon of fracture is the loss of contact between parts of a material. Glass is brittle because it does not yield under strain. Breakage may be sudden and catastrophic as in a laboratory strength test or a dropped glass, or it may be slowly progressing in stages such as a crack growing in an automobile windshield (Quinn 2016). Fracture is usually prompted by the extension of one or multiple cracks with possible branching of the cracks. The fracture pattern can provide a wealth of information about, e.g., whether failure was thermally or mechanically driven, whether the stress was large or small, and whether the stresses were uniaxial or multiaxial (Quinn 2016). As an example of the use of fractography in practice, consider that thermally toughened glass according to EN 12150-1:2015 should break in a prescribed manner that can be verified in a fragmentation test. The test involves to perform a particle count after fracture within a predefined surface area, and to measure the diameter of the longest particle. The basis for this is the fact that the amount of crack branching is dependent on the magnitude of residual compressive stresses that are present. For a further treatment of visual examination of fracture

patterns (fractography), see e.g. Mencik (1992) and Quinn (2016).

The fracture origin can mean a point where the fracture has started (Mencik 1992). The notion of fracture origin adopted in the appended papers A to E corresponds with Quinn (2016) who uses a broader definition that takes into account not just a location but also an object, and hence it refers to the location of a flaw or defect. In this context, a flaw does not imply something defective and should not be confused with such.

Suppose that the strength is determined by the work necessary to separate the atoms in a given plane which slices the material in two. From a purely theoretical point of view then, the inert strength can be estimated at (Le Bourhis 2008, Orowan 1949, Polanyi 1921)

$$\sigma_f = \sqrt{\frac{E\gamma}{\rho_0}} \tag{2.9}$$

where γ is the surface energy of the cleavage surface, and ρ_0 is the Si−O distance. Taking $E = 70$ GPa, $\rho_0 = 0.15$ nm, and the value of γ from Tab. 2.2, the strength is found to be about 16 GPa (Le Bourhis 2008). However, experiments on annealed float glass demonstrate that this value is incorrect by more than two orders of magnitude, see further Paper A and E. It is well-known that a scratch can reduce the strength of a glass sheet. In fact, glass is cut into the desired dimensions by flexuring a pane that has been scored on the surface with the use of a cutting wheel (Le Bourhis 2008).

In the appended papers, fracture mechanics models are used to explain how some material flaw might prompt the onset of fracture in a solid. The basis is a representation of the flaw as a crack, and assuming that cracks propagate in response to stresses and strains. A crack is a flat separation bounded within the material by a leading edge which is approximated by a simple curve (Mencik 1992). A flaw can refer to many sorts of defects depending on the scale of things (submicroscopic, microscopic, macroscopic), for a broader discussion see Mencik (1992). In the following, a crack refers to an idealization. It is a concept that represents the type of flaw that is thought to prompt failure in glass. This is sometimes referred to as Griffith flaws.

Here follows a brief overview of the background to fracture mechanics. For a more in-depth treatment of this topic, see e.g. Hellan (1984). Based on linear elasticity theory, Inglis (1913) presented a logical explanation for the weakening effect of a material flaw. He considered the elastic stresses near the edge of an elliptical through-the-thickness hole in an infinite plate of isotropic material subjected to uniform uniaxial tension. It was found that the crack warps the stress field. The maximum stress at the tip of the elliptical hole with radius of curvature ρ due to

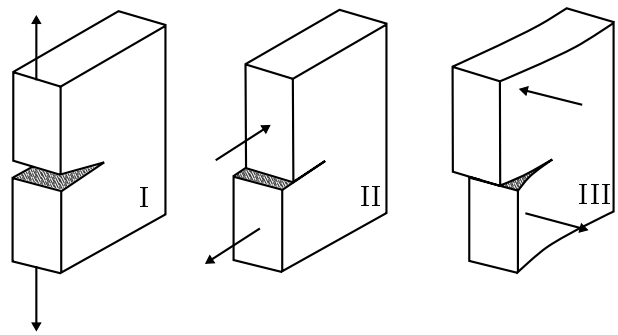

Figure 2.2: Crack displacement modes: mode I opening, mode II sliding, and mode III tearing. Adapted from Broek (1983).

farfield stress σ was calculated to be

$$\hat{\sigma} = \sigma\left(1 + 2\sqrt{\frac{a}{\rho}}\right) \approx 2\sigma\sqrt{\frac{a}{\rho}}, \text{if } \rho \ll a \tag{2.10}$$

where $\hat{\sigma}$ denotes the crack tip stress and a is the half major axis. Supposing that an elliptical crack represents a real material flaw, Inglis' (1913) model explains how a flaw is capable of prompting failure for farfield stresses well below the theoretical bond strength. Taking the radius of curvature to correspond to the intermolecular dimensions of the material and the maximum stress to correspond to the material strength, Inglis' theory of strength shows that the following quantity is a constant, viz.

$$\text{constant} = \frac{1}{2}\hat{\sigma}\sqrt{\rho} \approx \sigma\sqrt{a} \tag{2.11}$$

Griffith (1920) adopted Inglis' (1913) stress solution and developed a fracture condition based on a consideration of the elastic energy released upon crack growth. A closed and reversible thermodynamic system is studied that consists of a solid material and an external load applied quasi-statically. The first and seconds laws of thermodynamics combined then produce the following equation

$$\dot{U}_{\text{internal}} = \frac{\delta W}{dt} \tag{2.12}$$

where U denotes the internal energy and $\delta W/dt$ is the rate of mechanical work input (Saabye Ottosen & Ristinmaa 2005). Specifically, Griffith considered a plate (the same as was studied by Inglis) of infinite extension with a traction-free central elliptical cavity of length $2a$. The plate is subjected to a remote uniaxial stress σ. Griffith supposed that the internal energy is composed of elastic strain energy, U, and potential surface energy. He introduced as a state variable, a, the surface area per unit thickness of the plate. In this case the rate of external work performed equals to zero, and the system equation becomes

$$4a\gamma - \dot{U} = 0 \tag{2.13}$$

where γ is the surface tension. The system tends towards a state of minimum potential energy. The condition that the crack extends is

$$\frac{d}{da}\left(4a\gamma - \dot{U}\right) = 0 \tag{2.14}$$

Griffith recognizes the fact that the linear elastic solution to the strain near the tip of the cavity is no longer valid. However, he argues that if the traction-free crack is sufficiently large, the error in strain energy calculated according to linear elasticity theory is negligible. Griffith adopts an atomistic view on surface energy as the energy required to overcome surface traction and increase the surface of a body. When a body is split in two the work necessary to overcome the molecular attractions corresponds directly to the surface energy.

The condition for crack growth in Eq. (2.14) means that the rate of elastic energy release, typically denoted by G in most literature, is balanced by the energy consumed during crack propagation. The critical energy release rate which can be determined experimentally, is a measure of material toughness. The fracture criterion is expressed in

$$G \geq G_{\mathrm{Ic}} \tag{2.15}$$

where G_{Ic} denotes the mode I critical energy release rate. The three modes of cracking denoted by mode I, II, and III, respectively, are illustrated in Fig. 2.2 (Irwin 1958). Mode I refers to crack opening due to displacements normal to the crack plane surfaces. Mode II and III describe in-plane and out-of-plane shearing displacement cracking (Broek 1983). With the elliptical crack used in Inglis' solution, which pertains to pure mode I crack opening, the breaking stress under plane stress conditions is

$$\text{constant} = \sqrt{\frac{2E\gamma}{\pi}} = \sigma\sqrt{a} \tag{2.16}$$

where γ is the surface energy. In fact, both theories in (2.11) and (2.16) predict the invariance of the quantity $\sigma\sqrt{a}$, see also Suo (2016) for a discussion of this.

Another way of representing the fracture condition is provided by a characterization of the elastic stress field near the crack tip (Broek 1983). A solution in rectangular coordinates was found by Westergaard (1939) for a sharp through-the-thickness crack in an infinite plate subjected to uniform biaxial tension. The basic equation for in-plane loaded elastic plates is written by means of Airy's stress function, χ, as follows,

$$\nabla^2(\nabla^2\chi) = 0 \tag{2.17}$$

where ∇ is a linear operator; for a derivation see Hellan (1984). The stress function is a scalar valued function that specifies the three stress components acting in a given point. The boundary conditions for a wedge-like crack, as illustrated in Fig. 2.3, are in polar coordinates

$$\sigma_\theta = \tau_{r\theta} = 0 \qquad \text{for } \theta = \pm\alpha \tag{2.18}$$

The sharp crack representation is obtained by letting $\alpha \to \pi$. By use of the Euler identity, Irwin (1957) showed that the following expressions for the stress field near the crack tip approximate those of Westergaard (1939). Expressed in polar coordinates, the stresses near the crack tip were calculated to be

$$\sigma_x = \sigma\sqrt{\frac{a}{2r}}\cos\frac{\theta}{2}\left(1-\sin\frac{\theta}{2}\right)\sin\frac{3\theta}{2} \tag{2.19}$$

$$\sigma_y = \sigma\sqrt{\frac{a}{2r}}\cos\frac{\theta}{2}\left(1+\sin\frac{\theta}{2}\right)\sin\frac{3\theta}{2} \tag{2.20}$$

$$\tau = \sigma\sqrt{\frac{a}{2r}}\sin\frac{\theta}{2}\cos\frac{\theta}{2}\cos\frac{3\theta}{2} \tag{2.21}$$

where a is the semi-crack length. The formulation of a fracture criterion in the appended papers is directly based on Irwin (1957) who introduced the stress intensity factor (SIF) which is denoted by K_I in the case of mode I opening displacements. Considering Eq. (2.19), (2.20), and (2.21), it follows that

$$\sigma_{ij} = \frac{K_\mathrm{I}}{\sqrt{2\pi r}} f_{ij}(\theta) \tag{2.22}$$

where $K_\mathrm{I} = \sigma\sqrt{\pi a}$, and the SIF completely determines and characterizes the stress field at the crack tip (Broek 1983). Irwin demonstrates how, under the assumption of linear elasticity, the work done to close the crack corresponds exactly to the crack driving force, G, when the stresses near the crack tip are approximated by those obtained with the Westergaard solution, so that

$$G_\mathrm{I} = \frac{\beta K_\mathrm{I}^2}{E} \qquad \beta = \begin{cases} 1 & \text{for plane stress} \\ 1-\nu^2 & \text{for plane strain} \end{cases} \tag{2.23}$$

provided the crack moves in the plane of the existing crack. Eq. (2.23) is derived from the expressions for stress and displacement in the vicinity of the crack tip by considering the relation between crack driving force and separation work that applies in a purely elastic body. For a more in-depth treatment of this including the general situation with anti-symmetrical displacement modes, see Hellan (1984). The fundamental difference between Irwin (1957) and Griffith (1920) is that while Irwin's analysis is predicated on a crack tip singularity, i.e. a mathematically sharp crack, Griffith's approach is general and does not really depend on such a representation of the flaw. Consequently, the equations given by Irwin (1957) that express the crack driving force in terms of the stress-intensity factor are restricted to those cases where the crack tip is conceived as a singularity. It is not evident that this model was constructed by starting from the real world and stripping out complicating factors; the stipulation of a crack tip singularity does not present a key feature of the real world. "Although the model world is simpler than the real world, the one is not a simplification of the other." (Knuuttila 2009, Sugden 2002). What

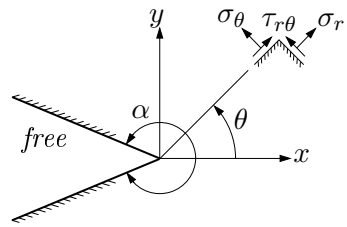

Figure 2.3: Polar stresses at a wedge-like notch. Adapted from Hellan (1984).

kind of realism is viable for glass fracture theory? Irwin's model offers explanatory power and is practically useful. As applied science aims at knowledge, simplicity and manageability is a concern and simplifying assumptions may be introduced even at the expense of truthlikeness (Niiniluoto 1993). With an instrumentalist approach, the unrealism of an assumption may not matter since the goal of science is to develop hypotheses that give valid and meaningful predictions about the phenomenon; unrealistic assumptions need not mean adopting a non-realist attitude towards the theory (Knuuttila 2009). For a further discussion of the viability of the sharp crack tip model from different perspectives, see e.g. Lawn et al. (1985) versus Han & Tomozawa (1989) and Tomozawa (1996). It lies beyond the scope of the present work to operate outside the sharp crack-tip singularity paradigm. However, just to see how the SIF would be altered if the crack tip geometry is not a singularity, consider the Creager (1966) solution which presents the elastic stress field equations for blunt cracks in a form equivalent to the usual sharp crack tip stress fields. Creager & Paris (1967) note that the tips of blunt cracks are imbedded within the usual crack tip stress field and that these usual field equations are disturbed only for mode I and mode II stress states and only in the immediate vicinity of the crack tip.

2.3.1 Surface flaws

As a representation of surface flaws in glass, Papers A through E consider mainly two types of part-through flat edge cracks, viz. the long straight-fronted plane edge crack and the semi-circular edge crack. The semi-circular edge crack is also known as the half-penny crack. It is assumed that the crack is contained in a semi-infinite specimen. For other crack shapes, however, it is possible to define a geometry factor Y associated with the crack shape such that

$$K_{\mathrm{I}} = Y\sigma\sqrt{\pi a} \tag{2.24}$$

Flaw location distribution is generally assumed to be uniform over the surface, see e.g. Wachtman et al. (2009) and Haldimann (2006). In Wereszczak et al. (2014), an empirical flaw location distribution was obtained in laboratory measurements

using optical scanning techniques. Wereszczak et al. (2014) has already been cited frequently in recent attempts to model glass strength using a flaw-size approach in Monte Carlo simulations, see also Paper B and E. However, due to the low resolution of the diagram in the journal article print (Wereszczak et al. 2014), it is hard to reproduce the observed spatial distribution. In addition, the measurements were limited to an examination of two glass panes comprising four surface sides. The conclusions drawn from this study are interesting but require further experimentation to be corroborated.

Regarding the representation of the surface condition in glass, the following should be noted. A single population concept was used by a number of researchers. Freudenthal (1968) assumed a Cauchy distributed flaw size distribution. Poloniecki & Wilshaw (1971) and Poloniecki (1974) proposed a flaw size density function in the form of an inverse gamma distribution which was based on empirical results and which was subsequently adopted in the strength model by De Jayatilaka & Trustrum (1977). The Pareto distribution for flaw size is a logical basis for deriving the Weibull distribution, see Wachtman et al. (2009). Yankelevsky (2014) assumed a flaw size distribution function that can be interpreted as a truncated exponential distribution. A number of researchers implement into their strength models a right-truncated flaw size distribution assuming arguments such as the following: Due to optical and aesthetic performance requirements on commercial glass, strict production controls "usually assure that glass with large defects are discarded and not placed on the market." (Pisano & Royer-Carfagni 2017) And, a "consequence of the factory production control is that it eliminates those elements that present cracks whose size is above a certain limit. From a statistical point of view, this is equivalent to a lower truncation in the population of glass strength." (Bonati et al. 2018)

Several authors have considered dual flaw populations concepts. In fact, the empirical data suggests that flaw size in glass is bimodal. Consider e.g. Krohn et al. (2002) who performed fractographic analyses of broken glass plates which had been subjected to double ring bending tests. It was concluded that "there is some evidence for a second flaw population to be contributing to the low strength of the float glass specimens." A statistical model for characterizing glass strength when two flaw populations are superimposed due to abrasive phenomena was proposed by Pisano & Royer-Carfagni (2017) and Bonati et al. (2018). Pathirana et al. (2017) implemented a dual population of lognormally distributed flaw sizes in Monte Carlo simulations of Griffith flaws. Kinsella & Persson (2018*b*), see Paper B, implemented a dual flaws population concept consisting of a Pareto flaw size distribution corresponding to large, "rogue" flaws of which there were assumed to be only a small number on a given plate, and a Fréchet flaw size distribution corresponding to numerous small flaws according to an argument based on extreme value theory.

It is interesting to note the reasoning in Mencik (1992) who distinguishes between

four surface flaw populations according to their supposed origin. Accordingly, there are large cracks caused by contact damage which limit the strength to 20-60 MPa. Then, there are microscopic and submicroscopic cracks smaller than 100 microns in size whose origin lie in the glass formation process as well as in contact damage. These small flaws of the second category are numerous; on a given square centimetre there may be hundreds or even tens of thousands. Then, there are flaws that arise due to foreign microscopic particles that adhere firmly to the surface at higher temperatures during manufacturing in the glassworks. Such flaws act as fracture initiators for failure at several hundred or thousands of MPa of tensile stress. Their effect is generally overlapped by flaws of the first two categories of origin. Finally, there are flaws occurring during manufacture and subsequent heat-treatment due to changes in the surface resulting from reactions with the environment, e.g. in the form of volatilization. Again, their effect is generally overlapped by the more severe flaws in the first two categories of origin. Hence, according to Mencik (1992), there can be a very large number of potentially fracture-inducing flaws even in a single square centimetre, many of which would be pertinent to the technical strength in the range of about 20 MPa to over 200 MPa.

At present, when some glass plate is tested in bending and its strength recorded in a typical experiment such as presented in Paper E, it cannot be known exactly what shape of flaw that prompted the observed fracture, nor can it be found out in reality which orientation the hypothetical crack plane had with respect to the stress field. A thorough investigation of each fracture site using a confocal microscope may provide some insight into the fracture process but such detailed investigation is rare when the main purpose is to measure the strength distribution. And, in reality, the flaw may have a complex shape and it may not be evident how a size and orientation should be assigned. Lindqvist (2013) attempted to measure the critical flaw size by performing fractographical studies of the failure origin before and after destructive testing and was unable to establish a clear relationship between the observed strength and the measured flaw depth. The laboratory investigation conducted by Haldimann (2006) also bears testimony to the tremendous challenge involved in attempts to probe the actual sizes of flaws that caused failure in glass specimens broken in bending. It is usually possible to identify a smooth mirror-like zone around the flaw that prompted failure using an optical microscope (Quinn 2016). There exist empirical relations between the critical stress and the mirror zone radius, although such formulae do not always produce reliable results when comparisons are made with the calculated fracture stress (Johar 1981). As a matter of fact there is a need for greater insight into the surface condition in glass. At present, however, there is a lack of methods and technology available by which to probe the surface flaws. Indeed, there are published papers on the strength of glass that appear to sidestep the usual paradigm of Griffith flaws, instead looking to other explanations for failure, see Zubkov & Kondratieva (2014) for an example. It lies beyond the scope of the present work to operate outside the established paradigm of Griffith flaws in glass.

When it comes to the representation of flaws in glass, it can be said in general that it is assumed that the effect of bulk flaws, if they are present at all, is overlapped by the effect of surface flaws. Glass is mostly stressed in bending which results in the surface stresses being larger than the stresses in the bulk.

The production method which includes scribing, cutting and grinding operations alters the condition of the edge in glass. Hence, the edge condition is not necessarily comparable to the surface. For a longer discussion of the edge versus surface condition, see Kinsella et al. (2018) which can also be found in Paper A.

2.3.2 Subcritical crack growth

Present theories that explain static fatigue are based on the concept of preexisting cracks that grow subcritically, i.e. at a rate much smaller than at catastrophic failure. Subcritical crack growth can be characterized by velocities of the order μm s^{-1} to mm s^{-1} while crack velocity at rupture is of the order km s^{-1} (Lawn 1993).

Stress corrosion

Subcritical crack growth due to stress corrosion provides an explanation for static fatigue (Charles 1958*a*). There has been much debate over the chemical reaction that supposedly takes place at the crack tip, see e.g. Lawn et al. (1985), Han & Tomozawa (1989), and Tomozawa (1996). Charles (1958*b*) supposed that the corrosion rate conforms to an arbitrary power function of the crack tip stress, i.e.

$$v \propto \hat{\sigma}^n \tag{2.25}$$

where v denotes the corrosion rate, $\hat{\sigma}$ denotes the crack tip stress, and n is the stress corrosion parameter. The crack tip stress $\hat{\sigma}$ was estimated by Charles (1958*b*) through adoption of the Inglis (1913) solution of the stress at the tip of an elliptical flaw, Eq. (2.10). Charles (1958*b*) obtained the value $n = 16$ through analysis of experimental data results from four-point bending tests carried out on 3000 glass rods, 100 mm long and 2.5 mm in diameter, while using a dead-weight loading system. The tests were performed at various temperatures between -170 °C and 242 °C in an atmosphere at 100% relative humidity. Moreover, Charles (1958*b*) assumed the temperature dependence to be a simple Arrhenius one, i.e.

$$v \propto e^{\left(-\frac{1}{T}\right)} \tag{2.26}$$

where T denotes the absolute temperature.

Wiederhorn (1967) observed that the corrosion rate in soda-lime-silicate glass is approximately proportional to the relative humidity, i.e.

$$v \propto \mathrm{RH} \tag{2.27}$$

Eq. (2.27) was verified using the double-cantilever cleavage arrangement in tests on microscope slide specimens into which cracks with a predetermined length were introduced (Wiederhorn 1967).

Brown (1972) developed an equation which states that the cumulative effect of an arbitrary stress history on a given crack is constant. This equation was integrated into a theory sometimes referred to as Brown's Load Duration Theory. The work done by Charles (1958*a*,*b*) and Wiederhorn (1967) form a basis for this theory, where it is assumed that

$$v \propto \mathrm{RH}\, e^{\left(-\frac{\hat{\sigma}}{T}\right)} \tag{2.28}$$

The dependence on stress in Eq. (2.28) was approximated by a power term. After carrying out an integration and substituting the crack tip stress for the farfield stress, Brown (1972) obtained the following formula which is given below in original notation

$$\int_0^{t_f} \mathrm{RH} \cdot \exp\left(-\frac{\gamma_0}{RT}\right) \left(\frac{\sigma}{T}\right)^n dt = \text{constant} \tag{2.29}$$

where γ_0 and R are constants, t_f is the time until failure, and n is the stress corrosion parameter. The right-hand side of Eq. (2.29) contains various constants including the distance traversed by the subcritically propagated crack. However, when the stress intensity is below a certain threshold limit, stress corrosion is no longer observed in experiments (Wiederhorn & Tornsend 1970). With the use of Eq. (2.29), the threshold limit value of stress corrosion is neglected. In Paper E it is shown how the threshold limit can be accounted for in numerical implementations of finite-size weakest-link systems. In a design situation, however, it is conservative to neglect the threshold limit.

Consider now a given crack which has been subjected to a certain amount of stress corrosion, the corrosion being measured in terms of the distance traversed by the growing crack. If the environmental conditions are assumed to be held constant, Eq. (2.29) provides for an equivalence class of stress histories. Specifically, it is derived from Eq. (2.29) that

$$\int_0^{t_{1,f}} \sigma_1^n(\tau)\, d\tau = \int_0^{t_{2,f}} \sigma_2^n(\tau)\, d\tau \tag{2.30}$$

where $(\sigma_1,t_{1,f})$ and $(\sigma_2,t_{2,f})$ correspond to a pair of stress histories and load-durations until fracture.

Eq. (2.30) has been employed by various researchers to calculate 3 s and 60 s constant stress-equivalent strength values, see e.g. Beason (1980), Mencik (1992)

and Calderone (1999). It is the constant stress which when applied during 3 s or 60 s, respectively, would produce the same amount of stress corrosion assuming the environmental conditions are identical. This transformation enables the comparison of test results carried out at different load-rates and with different load-durations. More specifically, the t-sec constant stress-equivalent strength is

$$\sigma_{t,\text{const}} = \left(\frac{\int_0^{t_f} \sigma^n(\tau) d\tau}{t} \right)^{\frac{1}{n}} \tag{2.31}$$

For a linear stress rate $\dot{\sigma}$ at the crack tip, the stress history is given by

$$\sigma(t) = \dot{\sigma} t \tag{2.32}$$

from which it follows that the fracture stress at time t_f is

$$\sigma_f = \dot{\sigma} t_f \tag{2.33}$$

Hence,

$$\int_0^{t_f} \sigma^n(\tau)\, d\tau = \int_0^{t_f} (\dot{\sigma}\tau)^n \; d\tau = \frac{\dot{\sigma}^n t_f^{n+1}}{n+1} = \frac{\sigma_f^{n+1}}{\dot{\sigma}(n+1)} \tag{2.34}$$

where Eq. (2.33) was used in the last step. For two constant-rate stress histories, $\sigma_1(t)$ and $\sigma_2(t)$, Eq. (2.34) can be rewritten

$$\frac{\sigma_{1,f}^{n+1}}{\dot{\sigma}_1} = \frac{\sigma_{2,f}^{n+1}}{\dot{\sigma}_2} \tag{2.35}$$

Extensive use of Eq. (2.35) was made to normalize fracture stress values in a wide-ranging survey of laboratory strength tests which can be found in a report by this author, see Kinsella (2018) and Sec. 3.4. However, the practical utility of normalizing stresses according to Eq. (2.31) and (2.35) depends on the fact that the environmental conditions are actually similar. For a longer discussion of the applicability of equations such as (2.31) from a practical perspective, see e.g. Mencik (1992) and Haldimann (2006).

Stress corrosion can be divided into four regions according to the rate of crack propagation (Wiederhorn 1967). Consider the logarithm of crack growth velocity as function of mode I SIF, see Paper E for an illustration of this in the form of a graph. In region I, the crack growth velocity is generally modelled with Eq. (2.25) as a basis. Region 0 denotes the domain in which no stress corrosion is observable. The threshold limit value for detectable stress corrosion is about 0.25 MPa $\text{m}^{-\frac{1}{2}}$, however, the estimates for this parameter value vary somewhat, see further e.g. Wiederhorn & Tornsend (1970), Freiman et al. (1985), and Gehrke et al. (1991). Regions II and III are generally not relevent for the strength design of glass structures because once the mode I SIF enters these regions, the time scale is very short and catastrophic failure is imminent (Fischer-Cripps & Collins 1995).

Evans (1974) proposed the following expression for the crack growth velocity.

$$v = AK_{\mathrm{I}}^{n} \tag{2.36}$$

Eq. (2.36) represents an empirically based approximation of the crack growth velocity which is valid for region I. In Eq. (2.36), A and n are crack growth velocity parameters and n is moreover identical to the stress corrosion parameter in Charles (1958*b*) stress corrosion theory. Eq. (2.36) can be reformulated as

$$v = v_0 \left(\frac{K_{\mathrm{I}}}{K_{\mathrm{I}c}} \right)^{n} \tag{2.37}$$

The benefit of Eq. (2.37) is that the crack growth velocity parameter v_0 has the same unit as the velocity v. This is also the formulation used in the appended papers A to E.

A classical explanation for the chemical reaction that takes place during stress corrosion is given by Charles & Hillig (1962). It is supposed that stress enhanced hydrolysis happens at the crack tip according to the following formula

$$\mathrm{Si{-}O{-}Si} + \mathrm{H_2O} \longrightarrow \mathrm{Si{-}OH} + \mathrm{HO{-}Si}$$

and this represents stress corrosion in region I. In region II, it is believed that the rate of stress corrosion depends strongly on the environment since it is limited by the transport of reactants to the crack tip (Le Bourhis 2008). However, no general consensus exists so far about the exact reaction that happens during stress corrosion, see e.g. Haldimann (2006) and Ciccotti (2009) for a longer discussion of this.

3

Strength calculation and measurements

3.1 INTRODUCTION

The strength of glass is a property that can only be revealed by destroying the sample specimen. Glass is much stronger in compression than in tension so that in practice, only the tensile strength is considered. One way to evaluate the strength would be to grip the specimen at two ends and pull it thus subjecting the surface to uniform stress. However, for practical reasons, this arrangement is usually avoided because of the risk that the specimen would either slip or else fail at the grips. In practice, glass plates are usually put to the test in a bending device that subjects part of the specimen to significant tensile stress. The bending stresses in a beam subject to four-point bending are calculated according to Bernoulli-Euler theory and closed-form expressions are given in Paper D. Closed-form expressions are also given in Paper E for the in-plane stresses due to ring-on-ring and ball-on-ring bending. In the case of laterally supported plates subjected to uniform pressure, the stress distribution is non-linear and highly dependent on the boundary conditions, see e.g. Kinsella & Persson (2018*a*) which can also be found in Paper C. Closed-form solutions for the stress are not always available and numerical computation is used instead. A background for numerical computation using finite elements is given in Sec. 3.3. Strength measurements and statistics are commented on in Sec. 3.4 with a brief background to probability theory and methods of statistical inference.

The strength is generally defined as the major (in-plane) principal tensile stress component at the fracture location, and this is what the strength refers to in the appended papers A to E. However, the strength determined from a bending test is sometimes defined as the maximum tensile stress that is reached within some predefined area of the specimen, e.g. within the load span in the case of four-point bending, irrespective of whether the fracture site was contained in the same area or not. For convenience, it is referred to as the apparent strength.

For instance, in a three-point bending setup, the apparent strength is determined by the stress at the midpoint where the load is introduced. Hence, the strength (at the failure origin) is generally smaller than the recorded apparent strength because it is not unusual for the fracture origin to be located some distance away from the midpoint. Furthermore, there are reports in the literature of a substantial proportion of fractures occurring from outside the loading ring area in some double ring bending tests (Reid 2007). Likewise, with a four-point bending arrangement it is not unusual for fracture to occur outside the load span. In fact, not every experimenter records the fracture location. Others simply discard the data point when the fracture origin was located outside the predefined loading area. However, discarding observations for such reason is not necessarily sound practice. Speaking of the double ring bending device, Reid (2007) notes that "failure outside the loading ring is a real physical phenomenon that cannot be eliminated by any experimental technique, because it is an inescapable consequence of the spatial variability of glass strength." According to a recent review of the test results from hundreds of large laterally supported panes subjected to uniform pressure, it was found that none failed at the location of maximum principal tensile stress (Natividad et al. 2016).

3.2 TIME-VARIANT STRENGTH

In an ordinary environment with a normal atmosphere, the strength cannot be revealed without intervening with the glass so as to alter the inert strength significantly. Hence, what might have been the strength at the onset of testing, the so-called inert strength, is reduced while putting the specimen to the test. Ultimately, delayed fracture might happen, e.g. when the specimen breaks under a static load that was sustained to begin with. Measurements of the strength carried out at different load rates and in different environments produce results that can differ substantially even when the test setup, specimen dimensions, and fracture location are otherwise the same. See further Sec. 2.3.2 for a description of stress corrosion.

In order for the strength to be well defined in the time domain, there exist alternative routes. One way is to employ a purely empirical model for the effect of static fatigue to enable a comparison of strength measurements made at different

load-histories. As an example, consider the universal static fatigue curve of Mould & Southwick (1959) who carried out experiments on glass rods subjected to static loads, see also Varshneya (1994),

$$\frac{\sigma}{\sigma_N} = -A \log\left(\frac{t}{t_{0.5}}\right) + B \tag{3.1}$$

In Eq. (3.1) which is valid in the linear portion in the plot of the time to fracture, σ_N is the strength of pristine glass rods immersed in liquid nitrogen, B is a term dependent on the manner of abrasion of the rod while using different grits, $\log t_{0.5}$ is the time corresponding to $\sigma/\sigma_N = 0.5$ and A is the slope in the plots, the slopes of which were found to be approximately the same according to laboratory tests (Mould & Southwick 1959).

Another way to account for static fatigue is to adopt the theory of stress corrosion and employ the logical model that follows, i.e. a subcritical crack growth velocity described by an Arrhenius process that is stress-dependent and temperature-activated. This modelling technique was used in the appended papers and a background was given in Sec. 2.3.2. In the following section, however, it is explained how to calculate the fracture stress without consideration of static fatigue.

3.3 NUMERICAL COMPUTATION

The stresses in, e.g., laterally supported plates subjected to double ring bending or uniform pressure, can be accurately calculated with the finite element (FE) method. The general problem of determining the stresses at an arbitrary location on the surface of a laterally supported plate which is subjected to uniform loading does not have a tractable solution when using analytical formulae except for some elementary cases with special boundary conditions. With the FE method, approximate solutions are obtained to partial differential equations that arise in the modelling of structures. However, the solutions are highly dependent on the boundary conditions.

In practice a combination of analytical calculation and FE-analysis is sometimes employed in strength analysis. As an example of this consider Vandebroek et al. (2014) who calculate the stress due to four-point bending based on Bernoulli-Euler beam theory. The beam is subdivided into 10 equal bins along the longitudinal axis. The stress values in the bins closest to the load introduction points are corrected based on calculations with the FEM. This is done in order to obtain a more accurate measure of the stress concentration that occurs due to non-linearities at the load introduction points. In a similar vein, Blank et al. (1994) recommend in some cases to use a weighted mean value from FE-analyses to take into account the variations in stress in the transversal direction due to double curvature of a bent beam that is loaded out-of-plane in four-point bending.

3.3.1 Equations of motion

Here follows an outline of the differential equations of motion with respect to the current or spatial configuration. The presentation follows the format found in Holzapfel (2000). A continuum body is considered as already introduced in Chap. 2; the body contains a set of particles that occupy an arbitrary region Ω with boundary surface $\partial\Omega$ at time t. The spatial mass density is ρ. The balance of linear momentum is adopted according to the generalized form of Newton's principles of motion, i.e.

$$\frac{D}{Dt}\int_{\Omega}\rho\dot{\mathbf{u}}\,dv = \mathbf{F}(t) \tag{3.2}$$

where it is assumed that the structure of forces, $\mathbf{F}(t)$, acting on the body are such that they can be separated into traction and body forces, respectively, i.e.

$$\mathbf{F}(t) = \int_{\partial\Omega}\mathbf{t}\,ds + \int_{\Omega}\mathbf{b}\,dv \tag{3.3}$$

where $\mathbf{t}$ is the Cauchy traction vector (see Eq. (2.6)) and $\mathbf{b} = \rho\mathbf{g}$ with $\mathbf{g}$ the constant gravitational acceleration. It is supposed that there exists a spatial tensor field $\boldsymbol{\sigma}$ with the property that $\mathbf{t} = \boldsymbol{\sigma}\mathbf{n}$ where $\mathbf{n}$ is an outward normal vector of unit length to the surface. It can be shown that $\boldsymbol{\sigma}$ is symmetric. Cauchy's first equation of motion is derived from the system-governing equilibrium Eq. (3.2) and (3.3) while applying Cauchy's stress theorem and Gauss' divergence theorem, i.e.

$$\int_{\Omega}(\mathrm{div}\boldsymbol{\sigma} + \mathbf{b} - \rho\ddot{\mathbf{u}})\,dv = \mathbf{0} \tag{3.4}$$

Since Eq. (3.4) holds for any volume v, it is deduced that

$$\mathrm{div}\boldsymbol{\sigma} + \mathbf{b} = \rho\ddot{\mathbf{u}} \tag{3.5}$$

which is the strong form of the equation of motion. Providing that the problem is static, the boundary conditions are

$$\begin{cases}\mathbf{u} = \bar{\mathbf{u}} & \text{on} \quad \partial\Omega_u \\ \mathbf{t} = \bar{\mathbf{t}} & \text{on} \quad \partial\Omega_\sigma\end{cases} \tag{3.6}$$

where displacement $\bar{\mathbf{u}}$ and load $\bar{\mathbf{t}}$ are prescribed functions on the boundary.

The strong form, Eq. (3.5), contains functions whose derivates might not be defined. The weak form is developed while noting that functions have well-defined integrals even when the derivative is undefined thus allowing for access to the underlying solution. An arbitrary test function $\mathbf{v}$ is introduced with the property that $\mathbf{v} = \mathbf{0}$ on the boundary surface $\partial\Omega$. The test function represents a virtual displacement field on the current configuration. After multiplication by $\mathbf{v}$, integration over Ω, and application of Gauss' divergence theorem, it can be shown that (Holzapfel 2000)

$$\int_{\Omega}(\boldsymbol{\sigma} : \mathrm{grad}\mathbf{v} + \rho\ddot{\mathbf{u}}\cdot\mathbf{v})\,dv = \int_{\Omega}\mathbf{b}\cdot\mathbf{v}\,dv + \int_{\partial\Omega}\mathbf{t}\cdot\mathbf{v}\,ds \tag{3.7}$$

Eq. (3.7) is the weak form with the natural and essential boundary conditions, respectively, which for the case of a static problem are the same as in Eq. (3.6). Henceforth, a quasi-static condition is assumed which implies that the second term on the left-hand side of Eq. (3.7) vanishes.

3.3.2 Finite Element Method

The finite element formulation is based on the weak form of the equation of motion, Eq. (3.7), and Galerkin's method (Bathe 2006, Saabye Ottosen & Petersson 1992). In the following, the matrix notation from Chap. 2 is used for the stress tensor. In addition, the vector differential operator is

$$\boldsymbol{\nabla} = \begin{bmatrix} \frac{\partial}{\partial x} & 0 & 0 \\ 0 & \frac{\partial}{\partial y} & 0 \\ 0 & 0 & \frac{\partial}{\partial z} \\ \frac{\partial}{\partial y} & \frac{\partial}{\partial x} & 0 \\ \frac{\partial}{\partial z} & 0 & \frac{\partial}{\partial x} \\ 0 & \frac{\partial}{\partial z} & \frac{\partial}{\partial y} \end{bmatrix} \tag{3.8}$$

The independent displacement vector field $\mathbf{u}$ is discretized at the nodes in a finite element mesh and a shape function is associated with each unique node. The displacement field is approximated throughout the body by

$$\mathbf{u} = \mathbf{N}\mathbf{a} \tag{3.9}$$

where $\mathbf{N}$ is a matrix that represents a global shape function. The vector $\mathbf{a}$ represents the nodal displacements and is a vector of size equal to the total number of degrees of freedom. Following Galerkin's method, test functions are selected according to

$$\mathbf{v} = \mathbf{N}\mathbf{c} \tag{3.10}$$

where $\mathbf{c}$ is an arbitrary constant vector. Combining Eq. (3.9) and (3.10) with Eq. (3.7) yields

$$\int_\Omega \mathbf{c}'(\nabla\mathbf{N})'\sigma \, dv = \int_{\partial\Omega} \mathbf{c}'\mathbf{N}'\mathbf{t} \, ds + \int_\Omega \mathbf{c}'\mathbf{N}'\mathbf{b} \, dv \tag{3.11}$$

which can be simplified to

$$\int_\Omega (\nabla\mathbf{N})'\sigma \, dv = \int_{\partial\Omega} \mathbf{N}'\mathbf{t} \, ds + \int_\Omega \mathbf{N}'\mathbf{b} \, dv \tag{3.12}$$

since $\mathbf{c}$ is arbitrary and constant (the prime symbol denotes the transpose of a matrix). In the special case of a linear elastic material it follows from Eq. (3.9) while assuming $\boldsymbol{\sigma} = \mathbf{D}\nabla\mathbf{u}$ that

$$\int_\Omega (\nabla\mathbf{N})'\mathbf{D}(\nabla\mathbf{N})\mathbf{a} \, dv = \int_{\partial\Omega} \mathbf{N}'\mathbf{t} \, ds + \int_\Omega \mathbf{N}'\mathbf{b} \, dv \tag{3.13}$$

Eq. (3.13) can be rewritten in a compact form as

$$\mathbf{Ka} = \mathbf{f}_l + \mathbf{f}_b \tag{3.14}$$

with

$$\mathbf{K} = \int_\Omega (\nabla \mathbf{N})' \mathbf{D} (\nabla \mathbf{N})\, dv \tag{3.15}$$

$$\mathbf{f}_l = \int_\Omega \mathbf{N}' \mathbf{b}\, dv \tag{3.16}$$

$$\mathbf{f}_b = \int_{\partial\Omega} \mathbf{N}' \mathbf{t}\, ds \tag{3.17}$$

where $\mathbf{K}$ represents the stiffness matrix, $\mathbf{f}_l$ is the body force vector, and $\mathbf{f}_b$ is the boundary force vector. Also, the essential boundary conditions must be specified in the nodes.

3.4 MEASUREMENTS AND STATISTICS

Thirty years ago Dalgliesh & Taylor (1990) commented about experimental measurements of glass strength: "Test results available from around the world refer to about 5000 panes broken in total." Those tests were not exclusively performed on the float type of glass, however. And, some experiments involved glass panes which were submerged in water while testing. About 500 of the tests mentioned by Dalgliesh & Taylor (1990) were performed on weathered glass, i.e. glass exposed to service conditions in buildings. Additionally, all test results were not such that a value for the fracture stress could be given because frequently, a failure load or pressure was reported from laboratory testing but not the associated fracture origin; in the case of linearly supported plates subjected to lateral loading, then a fracture stress value is not readily determined. For all these reasons, the majority of tests referred to by Dalgliesh & Taylor (1990) are not directly useful for an estimation of the fracture stress of new annealed float glass tested in ambient conditions.

A survey (Kinsella 2018) was recently carried out of experimental data on the strength of annealed float glass panes in the as-recieved condition which were tested in an ambient environment. Many of the tests were conducted using a loading device that generated a constant stress rate at the fracture location. The survey was a basis for Paper A and D.

In addition, laboratory tests were carried out on nominally identical glass plates subject to ring-on-ring and ball-on-ring bending. The test device was designed to expose a dissimilar portion of the surface area to considerable tension in an investigation of strength-scaling relating to size effect. The experimental results and further details including a schematic of the device, can be found in Paper E.

The strength of monolithic panes of annealed float glass which are tested in ambient conditions scatters considerably. The overall strength ranges from about 20 MPa to well over 200 MPa and coefficients of variation as high as 25% are common with annealed glass strength data (Beason et al. 1998). An investigation was performed to determine the performance of standard statistical distributions when modelling glass strength, see Paper A. A basic question addressed in this study was: is a Weibull distribution better or worse than a normal or lognormal distribution for modelling the strength with, generally speaking? In addition, another type of extreme value distribution was considered, namely the Gumbel distribution, which can also be derived from failure based mechanics using a weakest-link system. Another question addressed was whether there exists a basic difference in performance for the statistical models between edge and surface strength data. Also, the impact of sample size on data analysis was considered. A more in-depth treatment of edge strength was performed in Paper D with a Weibull statistical framework in a hierarchical model where the Weibull scale and shape parameters were treated as nested random variables. Glass supplier effect on strength was considered as a mixed-effect in a linear statistical model. Such a consideration, e.g., would hardly have been feasible without an empirical basis in wide-ranging measurements.

3.4.1 Probability theory

This section provides some of the background to probability theory and is based on the textbook presentation by Gut (1995). In probability theory, one assumes a sample space, Ω, which contains the set of elementary events ω. For any collection of such events, A, its probability is defined, $P(A)$, so that it satisfies the three Kolmogorov axioms. A random variable X is a function from the probability space to the real numbers

$$X : \Omega \to \mathbb{R} \tag{3.18}$$

The cumulative distribution function (CDF), F_X, provides a complete description of a random variable and is defined by

$$F_X(x) = P(X \leq x) \quad \text{for} \quad x \in \mathbb{R} \tag{3.19}$$

For a discrete distribution the probability function, p_X, is defined by

$$p_X(x) = P(X = x) \quad \text{for} \quad x \in \mathbb{Z} \tag{3.20}$$

For a continuous distribution the density function, f_X, has the property that

$$F_X(x) = \int_{-\infty}^{x} f_X(y)dy \quad \text{for} \quad x \in \mathbb{R} \tag{3.21}$$

A random variable can be characterized by its moments. The kth moment, m_k, is defined by

$$m_k = \begin{cases} \sum_i x_i^k p_X(x_i) & \text{if } X \text{ is discrete} \\ \int_{\mathbb{R}} x^k f_X(x) dx & \text{if } X \text{ is continuous} \end{cases} \tag{3.22}$$

provided that the sum or integral is absolutely convergent. The first moment is the mean denoted by $E(X)$, i.e. the expected value. The variance, $Var(X)$, is a measure of dispersion

$$Var(X) = \begin{cases} \sum_k (x_k - E(X))^2 p_X(x_k) & \text{if } X \text{ is discrete} \\ \int_{\mathbb{R}} (x - E(X))^2 f_X(x) dx & \text{if } X \text{ is continuous} \end{cases} \tag{3.23}$$

3.4.2 Methods of statistical inference

This section provides some of the background to statistical inference theory and is based on the textbook presentation by Young & Smith (2005). Statistical inference is an important tool used to draw conclusions of the underlying distribution of a random variable X on the basis of its observed value x. Typically, there are a number of n observations so that the data has the form $\mathbf{x} = (x_1, \ldots, x_n) \in \mathbb{R}^n$. In a parametric model, the distribution of X is of known analytical form, but involves a finite number, d, of real unknown parameters $\boldsymbol{\theta} = (\theta_1, \theta_2, \ldots, \theta_d)$. The parameter space is defined by the region $\boldsymbol{\Theta} \subseteq \mathbb{R}^d$ of possible values of $\boldsymbol{\theta}$.

In a hypothesis test, the following is considered.

$$H_0 : \boldsymbol{\theta} \in \boldsymbol{\Theta_0} \quad \text{versus} \quad H_1 : \boldsymbol{\theta} \in \boldsymbol{\Theta_1} \tag{3.24}$$

where $\boldsymbol{\Theta_0}$ and $\boldsymbol{\Theta_1}$ are two disjoint subsets of $\boldsymbol{\Theta}$ that possibly, but not necessarily, satisfy the condition that $\boldsymbol{\Theta_0} \cup \boldsymbol{\Theta_1} = \boldsymbol{\Theta}$. The unknown parameter value $\boldsymbol{\theta}$ is the quantity to make inference about. According to the likelihood principle, the general problem of inference for $\boldsymbol{\theta}$ is solved by examining the likelihood function, $L(\boldsymbol{\theta})$. In the case when $\mathbf{X} = (X_1, X_2, \ldots, X_n)$ is an independent identically distributed sample, and after observing $\mathbf{x}$, the likelihood function is defined by

$$L(\boldsymbol{\theta}) = \prod_i f(x_i, \boldsymbol{\theta}) \tag{3.25}$$

In Eq. (3.25), $L(\boldsymbol{\theta})$ is viewed as a function of $\boldsymbol{\theta}$ for the fixed value $\mathbf{x}$. The maximum likelihood estimate, $\hat{\boldsymbol{\theta}}(\mathbf{x})$, is defined to be the value of $\boldsymbol{\theta}$ that maximizes the likelihood function.

When parametric models are applied to find solutions to real-world problems, the question arises if this distribution adequately fits the sampled data. A goodness-of-fit test is one way of measuring the potential of a statistical model. The general test of fit is a test of the null-hypothesis

$$H_0 : \text{A random sample of } n \text{ observations of } X \text{ comes from } F_0(x, \boldsymbol{\theta}) \tag{3.26}$$

where $F_0(x, \boldsymbol{\theta})$ is the hypothetical distribution under consideration.

Next, consider tests based on the empirical distribution function (EDF) which is a step function that estimates the CDF that generated the observed data points. Suppose a random sample $X_1, \ldots, X_n$ drawn from a distribution with CDF F_X. The Kaplan-Meier EDF is defined by (Forbes et al. 2011, Wasserman 2006)

$$\hat{F}_n(x) = \begin{cases} 0 & \text{for } x < X_{(1)} \\ \frac{i}{n} & \text{for } X_{(i)} \leq x < X_{(i+1)},\ i = 1, \ldots, n-1 \\ 1 & \text{for } x \geq X_{(n)} \end{cases} \tag{3.27}$$

where $X_{(i)}$ denotes the ith order statistic. An EDF statistic measures the discrepancy between the EDF and a hypothetical distribution. A classic EDF statistic is the Kolmogorov-Smirnov statistic defined by

$$D = \sup_x \left\{ |\hat{F}_n(x) - F_0(x, \boldsymbol{\theta})| \right\} \tag{3.28}$$

and it measures the largest vertical difference between $\hat{F}_n(x)$ and $F_0(x, \boldsymbol{\theta})$. A generally superior set of EDF statistics are based on the class of quadratic statistics of the form (D'Agostino & Stephens 1986)

$$Q = n \int_{\mathbb{R}} \left(\hat{F}_n(x) - F_0(x, \boldsymbol{\theta}) \right)^2 \omega(x)\, dF_0(x, \boldsymbol{\theta}) \tag{3.29}$$

where $\omega(x)$ is a weight function. The Anderson-Darling (Anderson & Darling 1952) statistic is obtained by choosing

$$\omega(x) = (F_0(x, \boldsymbol{\theta})(1 - F_0(x, \boldsymbol{\theta})))^{-1} \tag{3.30}$$

This statistic was employed in Paper A, B, and E.

4

Failure modelling approaches

A background to glass failure prediction models can be found, e.g., in Haldimann (2006) and Haldimann et al. (2008) who provide, among other things, a thorough comparison of the North American ASTM E-1300 with various European counterparts including the prEN 13474. Lamon (2016) examines strength models for application on brittle materials in general and considers statistical-probabilistic theories based on flaw size density as well as flaw strength density. Rinne (2009) provides an in-depth treatment of the Weibull distribution.

4.1 OVERVIEW

The strength (and sometimes fracture origin) prediction of a glass structure is a challenging task which is based on a range of theories and techniques depending on the modelling approach. Fig. 4.1 presents an overview of failure modelling approaches with a list of references which have already been cited in the appended papers. The overview in the figure is not intended to be an exhaustive account of all models suggested in literature, but rather to highlight how a selected set of approaches can be categorized with respect to key features. The shaded gray box in Fig. 4.1 corresponds to models that implement stress corrosion theory in one form or another. Many of the modelling approaches involve a weakest-link based system (Peirce 1926, Weibull 1939*b*), the premise of which is further explained in Paper E. The categorization in the figure is influenced by Lamon (2016), who makes a distinction between models that take a macroscopic or phenomenological approach to

fracture on the one hand, and on the other hand those in which failure is derived from pre-existing flaws on the microscopic level, i.e. where flaws are understood to be real physical entities that are operated on by stresses. In the latter case the models can be separated into those with a flaw size approach and those with an elemental strength approach. The flaw size approach depends on a more or less rigorous representation of the surface flaws in terms of a flaw size distribution, a flaw shape, and an orientation of the flaw in the plane. Hence, those models are fundamentally rooted on notions of the physical processes that take place in a brittle material. The elemental strength approach does not depend on a direct representation of the flaw geometry. Instead, it is based on the isotropic material resistance to uniaxial tension leading to a critical stress magnitude for the characterization of flaw severity. The main issue with the elemental strength approach is how to properly deal with failure when it is supposed that the elemental strength is dependent on a multiaxial state of stress. The advantage compared to the flaw size approach is that it more readily conforms to the kind of information that is acquired from laboratory tests on glass; usually the fracture load and origin are measured from which the fracture stress is subsequently calculated. Hypothetical cracks with a size and crack plane orientation are not directly measured with common test setups, although these entities may be inferred from the fracture stress data based on fracture mechanics concepts. In addition, the edge strength model developed in Kinsella & Lindström (2020), which can also be found in Paper D, draws on both a flaw-size based and a macroscopic/phenomenological approach and thus does not fit smoothly into the categorization in the figure.

4.1.1 Flaw-size based approaches

The approaches in Pathirana et al. (2017), De Jayatilaka & Trustrum (1977), Kinsella & Persson (2018*b*), and Yankelevsky (2014) have already been mentioned in Sec. 2.3.1. The common feature is the flaw-size based approach as described by Lamon (2016). The models developed in Haldimann (2006), Yankelevsky et al. (2017), and Osnes et al. (2018) are similarly based on this premise; the latter two present an adoption of the modelling approach already described in Yankelevsky (2014). In addition, in Kinsella et al. (2018) which can also be found in Paper A, the Gumbel distribution is applied as a strength model based on assumptions that infer its position among the flaw-size approaches. The Gumbel distribution is an interesting object to study because it is the extreme value distribution associated with a whole range of standard-type distributions which lie in its domain of attraction, including the exponential, normal, and lognormal distributions. It is apparently rarely applied to model glass strength, in contrast with the Weibull distribution which appears frequently in the literature. Both the Weibull and Gumbel models share key features. They can be derived in a flaw-size based approach using an infinite size weakest-link system and assuming a single population of flaws with a

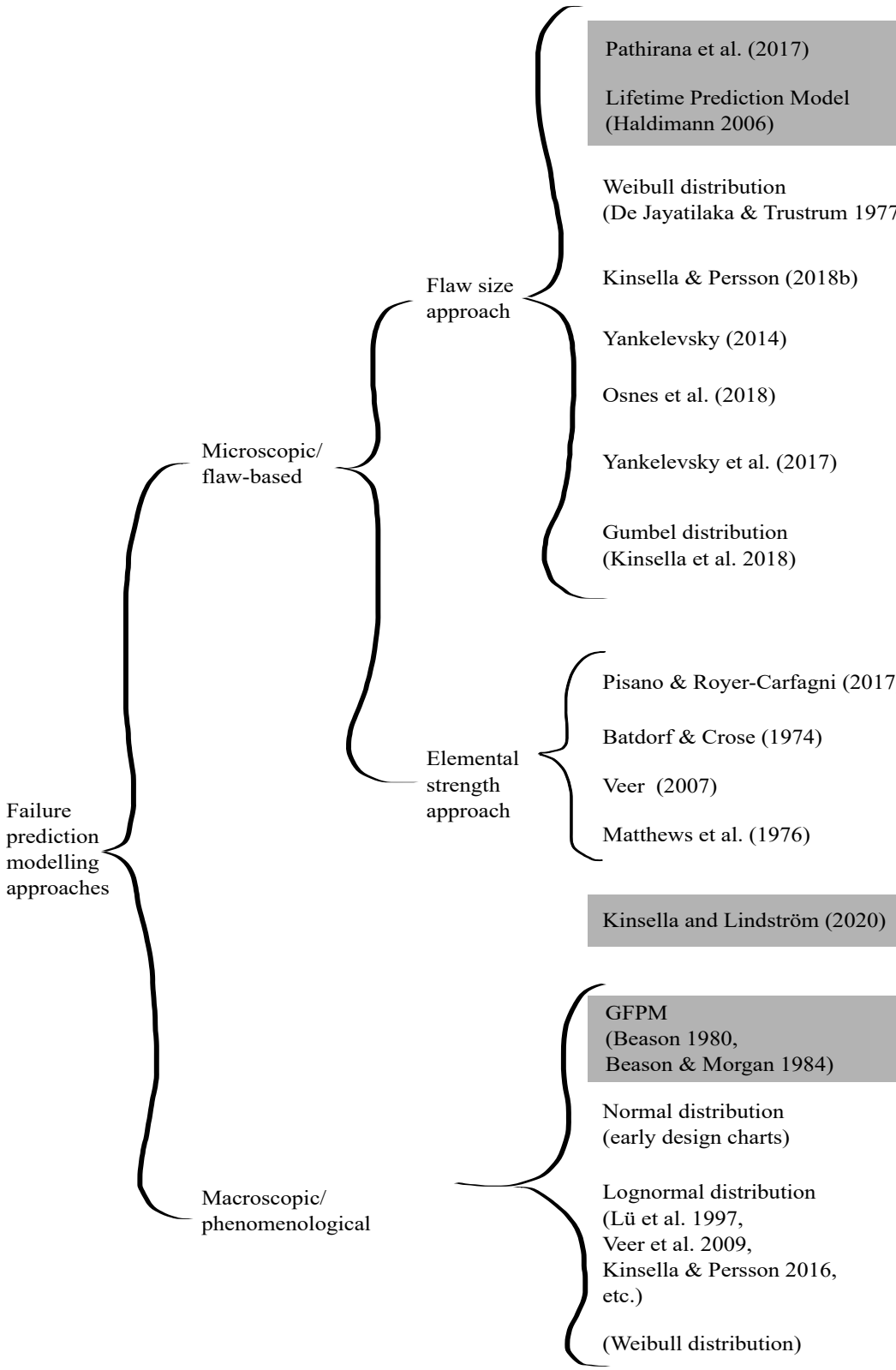

Figure 4.1: Failure modelling approaches.

flaw size distribution that decays either exponentially (to generate the Gumbel type distribution), or as a power-law (to generate the Weibull type distribution). The Gumbel and Weibull distributions represent two of the three types of extreme value distributions, the Fréchet distribution being the third (see Paper B for an account of the latter distribution). In the case of the Weibull distribution, let

$$M_n = \min_{1 \leq i \leq n} \{X_i\} \tag{4.1}$$

denote the minimum value of a sample $\{X_i; 1 \leq i \leq n\}$ of independent and identically distributed random variables. Then, for certain conditions on the sampled variable and provided that M_n is non-degenerate as $n \to \infty$, it holds that the limiting distribution is of the Weibull type. The specific condition for this to happen is that the sampled distribution is bounded from below for some x_u, i.e., $x \in [x_u, \infty)$, and the sampled distribution has a finite number of moments only (the moment is defined in Eq. (3.22)). The uniform distribution over some interval $[A, B]$ as well as the Weibull distribution itself are two prototypes of distributions which lie in the domain of attraction of the type of limiting extreme value distribution that is the Weibull distribution (Rinne 2009).

The Weibull distribution certainly has descriptive virtue (Weibull 1951), and according to a recent survey (Rinne 2009) there are a great number of papers and monographs that demonstrate its successful application in some 180 distinct topics that encompass nearly all scientific disciplines. However, the descriptive virtue can become a liability when the sample sizes are small because the Weibull model maintains its flexibility all the same; in such case, the better fitting means nothing (Danzer et al. 2001). According to Danzer (1994), the size difference between the smallest and largest critical defect is expected to be small for a data set of limited size, e.g. 30 specimens. The flaw-size density function can always be approximated by a power law over a small interval, and "this would explain the good description of small sets of data by the Weibull distribution." (Danzer 1994)

Finally, the failure model in Paper E that emerges from the modified flaw-size concept presented therein is considered as follows and further compared to an ordinary Weibull model. As evidenced in the paper, this model has explanatory power because it is able to model the outcome from both the ring-on-ring and the ball-on-ring tests. To further investigate its potential for prediction-making, consider Fig. 4.2 which shows a series of normalized histograms representing the outcome when the numerical method from Paper E is applied to model the results from various double ring bending tests recorded in literature. In addition, a pair of Weibull distributions are also plotted in each of the diagrams. These are explained in the following. Beginning with the last diagram, i.e., subplot f, the semitransparent bars in blue colour represent the numerical simulation results and the white bars with black edge colour represent the experimental observations from the double ring bending tests recorded in Paper E. The modified flaw-size concept from Paper E is used which means that: 1) a decent fit is simultaneously obtained

with the ball-on-ring test data (not shown in figure) using this method, and; 2) the flaw-size distribution is truncated at a flaw size of about 200 microns. The solid line represents a two-parameter Weibull model fitted to the ring-on-ring experimental data. The dashed line represents the model obtained when a Weibull distribution originally fitted to the ball-on-ring data from Paper E (not shown in figure) is used to predict the outcome of the ring-on-ring tests, based on the effective area strength-scaling. Considering next the first diagram, i.e., subplot a, the white bars represent the experimental results from ring-on-ring bending tests conducted by Simiu et al. (1984). The semitransparent bars represent the outcome when using the same numerical method and flaw-size concept from Paper E as already mentioned. The solid line represents the model obtained when a Weibull distribution originally fitted to the ring-on-ring data from Paper E is scaled using the calculated effective areas to fit the geometrical setup of the test conducted by Simiu et al. (1984). The dashed line represents the model obtained when a Weibull distribution originally fitted to the ball-on-ring data from Paper E is scaled to fit the setup of the test recorded in Simiu et al. (1984). With the diagrams in subplot b to e, the semitransparent bars, and solid and dashed lines, are analogous to the diagram in subplot a, and the white bars now correspond to experimental data from ring-on-ring tests conducted by, in order from b to e, Fink (2000) data set 1, Fink (2000) data set 2, Schula (2015), and Muniz-Calvente et al. (2016). For a list of summary statistics including the load ring radii from these experiments, see also Tab. 3 in Paper B. In order to generate the numerical results illustrated in semitransparent bars, a simplification was made to the numerical modelling tool in Paper E. The in-plane stresses were calculated using the closed-form solutions instead of being obtained in a FE-analysis. In the ring-on-ring setups considered in Fig. 4.2, the geometrical properties of the glass specimens and bending apparatus are quite similar and the fracture loads are generally not exceedingly large. Therefore, the errors obtained due to the simplification are assumed to be negligible within this context; the purpose of the figure is to provide a basic impression that permits a comparative analysis, and not to estimate precisely, e.g., a low-strength quantile. In addition, the applied stress rate was generally around 2 MPa s^{-1} during laboratory testing in a controlled environment in the experiments, thus suggesting that the presence of stress corrosion effects can be assumed to be relatively even among the tests; an exception being the first data set in subplot a where testing was done at around 1 MPa s^{-1}. The following conclusions should be drawn from the results presented in the figure.

The numerical modelling results tend to produce strength predictions (in subplot a, d, and e) that overestimate the strength in the left-hand tail. However, the degree to which it overestimates appears to vary considerably. In at least one case (subplot b) the predicted strength distribution has too little spread. In another case, (in subplot c), a reasonable prediction may be obtained somewhat conservatively, with the exception of a conspicuously strong specimen in the empirical data set at about 200 MPa. When strength prediction is based on a Weibull model originally fitted to the

ring-on-ring tests reported in Paper E (solid line) and scaled according to a Weibull weakest-link system (see further how this is done in Paper E), the results in subplots a through e are very similar to what is obtained with the numerical procedure (shown in semi-transparent bars). As a matter of fact, the overall geometrical dimensions of the specimens and bending setup are similar throughout the considered tests. The strength prediction from a Weibull model originally fitted to ball-on-ring tests (dashed line) and scaled according to a Weibull weakest-link system produces overly conservative results in some cases (notably in subplot f) compared to a model originally fitted to ring-on-ring tests (solid line), but produces a better fit with empirical data in other cases. What appears to be an overly conservative strength model from one experimental campaign may turn out to offer a viable strength prediction in another campaign, when operating within a Weibull weakest-link system. The following should be noted in summary. A Weibull weakest-link scaling system is able to produce reasonable predictions of size effect for relatively small changes in effective area only. Apparently, the surface condition properties exhibit substantial variability from one experimental campaign to another. It may be possible to fit a logical failure model that has explanatory power in one experimental campaign, and also find that the same model performs rather well in another campaign, but in general it is evident that random variability occurs between experimental campaigns to such an extent that the original (well-performing) model can be rendered ineffective. It is not evident how such random variability should be estimated from the outcome of one campaign only. This should probably be further investigated in wide-ranging experiments involving multiple laboratories and glass suppliers.

4.1.2 Elemental-strength based approaches

Batdorf & Crose (1974) and Matthews et al. (1976) present models that are representative of the elemental strength approach to failure modelling. A recent development of the Batdorf model with application to glass can be found in Pisano & Royer-Carfagni (2017) where also a left-truncated strength distribution is developed. In addition, consider the basic model proposed in Veer (2007) for the edge strength of glass using two superposed flaw strength distributions with normally distributed elemental strengths. The concept is based on test results from plates which were machine cut and ground, and subjected to in-plane four-point bending tests. A subset of the data sample is selected by Veer and associated with one type of defect denoted Q and which is supposed to occur once in every two meters of edge length with a mean failure stress of 30 MPa and a coefficient of variation of 7%. The other type of defect denoted N, is deemed to have a frequency of once in every millimetre with a mean failure stress of 60 MPa and a coefficient of variation of 12%.

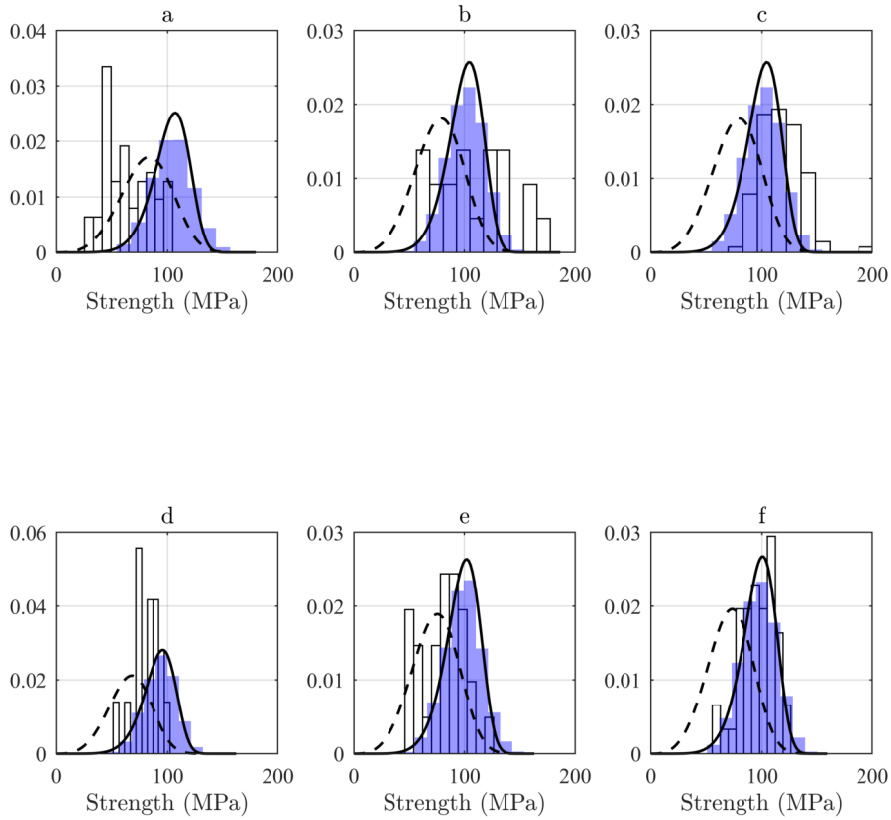

Figure 4.2: Application of numerical method from Paper E on ring-on-ring loading cases. Histograms (white bars) represent test data obtained from: (*a*) Simiu et al. (1984), (*b*) and (*c*) Fink (2000), (*d*) Schula (2015), (*e*) Muniz-Calvente et al. (2016), and (*f*) Paper E.

4.1.3 Macroscopic approaches

According to Weibull (1939*a*), the development of the equation for the Weibull distribution (see e.g. Eq. (1) in Paper A) depends on two basic premises. The first involves a logical deduction of the governing equation in an infinite-sized weakest-link scaling system based on a limiting operation on a finite-sized system. Basically, if the finite-sized system is composed of individual elements (links) with failure probabilities equal to S_0, then the system survival function is

$$1 - S = \prod_{i=1}^{n} (1 - S_0) \tag{4.2}$$

Now, S_0 tends to zero as n tends to infinity while the volume element V vanishes. In the limit, the following approximation holds

$$S_0 \approx f(x) \cdot dV \tag{4.3}$$

where $f(x)$ is a finite non-decreasing function of stress. Taking the logarithm of Eq. (4.2) and approximating $\log(1 - S_0)$ by $-S_0$ for a vanishingly small quantity S_0 while observing Eq. (4.3), Weibull derives

$$\log(1 - S) = -\int f(x)\, dV \tag{4.4}$$

In the case of a uniformly distributed stress in a uniaxial state of loading, this becomes

$$S(x) = 1 - e^{-V \cdot f(x)} \tag{4.5}$$

As a matter of fact, there is a complete analogy so far with a development based on a homogeneous spatial Poisson process with random sized events, see further Mesarovic et al. (1992).

The second premise in Weibull (1939*b*) pertains to the choice of function $f(x)$, the socalled "risk function". Here, Weibull claims that his particular choice represents "the most simple function satisfying the condition" (Weibull 1951) and that "experience has shown that [this] expression ... in many cases gives an excellent reproduction of the observations" (Weibull 1949), that "it appears that good agreement with measuring results may frequently be obtained" (Weibull 1939*b*), etc. When the functional form of the socalled "risk function" is based on such heuristical argument, the Weibull distribution should be categorized among macroscopic/phenomenological failure modelling approaches (Gumbel 1954).

The normal distribution was employed early in, e.g., Pilkington glass design charts assuming a coefficient of variation of 0.20 (Calderone 1999). The normal distribution was employed in fracture statistics by, e.g., Peirce (1926), and more recently considered in Lu et al. (2002) although it seems generally to be neglected in fracture statistics. The use of a normal distribution as a standard model for data is generally due to the Central Limit Theorem (Beirlant et al. 2004) which states that averages of many samples will tend to follow a normal distribution. In spite of the convenience of the normal (and lognormal) distributions, it might be said that they focus on the symptoms instead of the causes of fracture (Lamon 2016); in fact, the physical processes underlying fracture including the presence of microcracks with stochastic properties which prompt failure (Griffith 1920), become masked and concealed when applying a standard statistical distribution such as the normal distribution.

Finally, the Glass Failure Prediction Model (Beason & Morgan 1984) should be located among the macroscopic/phenomenological models. With the GFPM, fracture in glass is assumed to be dependent on the existence of surface microcracks and, it

is further supposed that a biaxial stress correction factor can be applied to account for random crack plane orientations. Specifically, an equivalent stress is calculated "which acts normal to the axis of a flaw" (Beason 1980). While the adoption of the fundamental Eq. (4.5) is stringent, the particular selection and further treatment of the socalled risk function is essentially heuristical. The GFPM does not directly deploy a flaw size density function nor an elemental strength distribution. It relies on a sophisticated procedure for the estimation of the socalled surface flaw parameters which unfortunately cannot be measured directly at present. The way in which the surface flaw parameters represent the actual surface flaws is not evident (Reid 1991). The unit of the surface flaw parameter which is denoted by k depends on the value for m and hence varies from one model fit to another. For instance, with the Dallas glass plates that were extracted from the Johnson Chevrolet Building and subsequently analyzed by Beason (1980), the value of k including its unit was estimated at $3.01 \cdot 10^{-15}$ mm^{10} N^{-6} (Beason & Morgan 1984). For further discussion of this model, see e.g. Haldimann (2006) and Reid (1991).

4.1.4 Miscellaneous approaches

The strength model proposed in Kinsella & Lindström (2020), which can also be found in Paper D, draws on elements from both a flaw size approach and a macroscopic approach towards failure. The linear statistical model is based on an approach with Weibull distributed errors which are explicitly connected to flaw characteristics such as shape and scale parameters in a flaw size Pareto density function. At the same time, the adopted hierarchical approach and the subsequent statistical modelling adds another layer on top of the basic Weibull model which ultimately generates a strength model that has key features in common with a macroscopic/phenomenological treatment of failure, such as when a normal distribution is applied to model data, in the sense that, e.g., size-effects are no longer necessarily understood or obtained directly from a weakest-link system (although such a system is part of the original makeup).

5
Summary of publications

Paper A, B, and D have been published in international peer-reviewed journals, and Paper E has been submitted for possible publication in an international peer-reviewed journal. In addition, Paper C has been peer-reviewed and published in the proceedings of an international conference. The five publications are summarized in the following. In the given descriptions of the contributions by this author, use is made of the Contributor Roles Taxonomy (CRediT), see further, e.g., Brand et al. (2015).

5.1 APPENDED PAPERS

5.1.1 Paper A

Kinsella, D., Lindström, J., Persson, K. (2018): *Performance of Standard Statistical Distributions for Modeling Glass Fracture.* International Journal of Structural Glass and Advanced Materials Research 2, (178.190).

Summary

A comparison is made between four standard statistical distributions, namely the normal, lognormal, Gumbel, and Weibull with respect to the performance in modelling the strength results from a wide-ranging survey of laboratory data on new

annealed float glass when it is tested in an ambient environment. The Weibull distribution outperforms the normal and lognormal distributions and is at least as well-performing as the Gumbel distribution when the fracture data is selected to comprise edge only failure origins. In the case of surface only failure origins, it is indicated that the extreme value distributions perform worse than the normal and lognormal distributions. However, the surface strength is complicated to model and none of the standard distributions which were examined are truly capable of producing a compatible model. The sample size also has a profound impact on the performance of the surface strength models in particular.

Contributions by David Kinsella

David Kinsella was the main author. He contributed to the conceptualization of ideas, development of methodology, creation of models, implementation of computer code and supporting algorithms, and conclusions drawn. He conducted the investigation process and performed the data collection and curation including management activities to annotate and maintain research data. He planned the research activities, prepared the initial manuscript for the published work and participated in reviewing and editing.

5.1.2 Paper B

Kinsella, D., Persson, K. (2018): *A Numerical Method for Analysis of Fracture Statistics of Glass and Simulations of a Double Ring Bending Test.* Glass Structures & Engineering 3(2), 139–152.

Summary

The fracture stress and failure locations in small glass plates subjected to double ring bending are computed with a numerical method that considers the stochastic properties of surface microcracks in a fracture mechanics approach to brittle failure based on a weakest-link system. The results are compared with laboratory data from a double ring bending test recorded in literature. The numerical method is dependent on a representation of the surface flaws condition in glass and two types of flaw-size distributions are fitted according to a single and a dual population concept which are motivated by empirical results and extreme value theory. The effect of using different fracture criteria is investigated, however, the incorporation of mode II shearing displacement into the fracture criterion has only a minor impact on the simulated strength distribution when the glass is subjected to double ring bending.

Contributions by David Kinsella

David Kinsella was the main author. He contributed to the conceptualization of ideas, development of methodology, conclusions drawn, and applied the numerical models, performed the statistical analysis and finite-element computations, and implemented the computer code and supporting algorithms. He planned the research activities, prepared the initial draft for the published work, and participated in reviewing and editing.

5.1.3 Paper C

Kinsella, D., Persson, K. (2018): *An Analysis of Glass Fracture Statistics.* In: Challenging Glass Conference 6: Conference on Architectural and Structural Applications of Glass, Delft, The Netherlands.

Summary

A numerical method is applied to model the failure stress and fracture origin in linearly supported glass panes subjected to various forms of lateral loading including a uniform pressure and an impact from a soft body. The stresses are computed in a finite-element analysis and the strength and failure origins are revealed using a numerical procedure based on a stochastic approach to brittle fracture assuming a weakest-link system and Pareto distributed flaw sizes. Two types of gasket support materials are considered, namely neoprene and nylon, and the softer gasket material produces a greater number of fractures nearer the corners in plates exposed to uniform lateral pressure. A comparison is made with the recorded fracture origins from a number of laboratory tests which are reported in the literature. In addition, failure modelling is performed for a tall vertical panel of laminated glass with a complex geometry that is subjected to dynamic impact loading.

Contributions by David Kinsella

David Kinsella was the main author. He contributed to the conceptualization of ideas, development of methodology, conclusions drawn, planning of research activities, finite-element modelling, and applied the numerical methods, performed the statistical analysis, developed software, and implemented the computer code and supporting algorithms. He prepared the initial draft for the published work and participated in reviewing and editing.

5.1.4 Paper D

Kinsella, D., Lindström, J. (2020): *Using a Hierarchical Weibull Model to Predict Failure Strength of Different Glass Edge Profiles*. International Journal of Structural Glass and Advanced Materials Research 4, (130.148).

Summary

Laboratory measurements of edge strength from four-point bending tests are surveyed from literature and analyzed in a Weibull statistical framework. The estimated Weibull parameters exhibit considerable scatter and a hierarchical modelling approach is adopted in which the Weibull parameters are treated as nested random variables. Estimates are obtained for the characteristic 5%-fractile strength of four common edge profiles as function of load rate and load span while accounting for statistical effects due to glass supplier. A mixture distribution is computed by averaging over the effect of different suppliers to produce a model that represents the strength when no prior knowledge exists for the glass supplier, as would be useful in a practical design situation. In addition, it is suggested that the Weibull shape parameter is scale-dependent for the raw-cut edge profile.

Contributions by David Kinsella

David Kinsella was the main author. He contributed to the conceptualization of ideas, planning of research activities, conclusions drawn, and implementation of computer code. He was a supporting contributor to the development of methodology, creation of models, and application of statistical techniques to analyze the data. He performed the data collection and curation including management activities to annotate and maintain the research data. He prepared the initial draft for the published work and participated in reviewing and editing.

5.1.5 Paper E

Kinsella, D., Serrano, E. (2021): *Failure Modelling of Glass Plates in Biaxial Loading: Using Flaw-Size Based Weakest-Link Systems*. Submitted for possible journal publication.

Summary

Laboratory tests are conducted with a ball-on-ring and ring-on-ring bending setup and the results are modelled using flaw-size based weakest-link systems. With ana-

lytical calculation and numerical computation of the stress field, the effective area and strength-scaling size effect are expressed in closed-form assuming a Weibull system. Using a computationally intensive numerical method, the fracture stress and origins are simulated in virtual glass specimens that contain randomly distributed surface cracks depending on different flaw population concepts. Comparisons of modelled and predicted strength and fracture origin distribution are performed and it is suggested that surface size-effects in glass cannot be represented only by a Weibull strength-scaling because the shape of the observed distributions in experiments differ thus rendering intractable the weakest-link scaling premise of the ordinary Weibull model. The numerical implementations of finite-size weakest-link systems using an exponentially decaying flaw-size distribution produce better predictions for the strength-scaling compared to a Weibull distribution. Low-strength quantiles for the glass in ball-on-ring and ring-on-ring bending are estimated based on results from a large number of virtual tests. However, the simulated ball-on-ring fracture origins exhibit greater spread in the radial direction from the centre point than observed in laboratory tests.

Contributions by David Kinsella

David Kinsella was the main author. He contributed to the conceptualization of ideas, development of methodology, creation of models, conclusions drawn, design of experiments, performing statistical analysis, developing software, and planning of research activities. He applied the analytical and numerical models and performed the finite-element computations. He contributed to the preparation of experiments, the verification of test results, and was a supporting contributor in carrying out the experiments. He prepared the initial draft for the submitted manuscript.

5.2 OTHER CONTRIBUTIONS

The following contributions are related to, but not included in, the thesis.

Kinsella, D., Persson, K. (2016): *On the Applicability of the Weibull Distribution to Model Annealed Glass Strength and Future Research Needs.* In: Challenging Glass Conference 5: Conference on Architectural and Structural Applications of Glass, Ghent, Belgium.

Karlsson, S., Kozlowski, M., Kinsella, D., Haller, K., Andersson, S., Hellman, F., Persson, K. (2018): *Kvalitetshöjning av planglas. Icke-förstörande provning av glasets hållfasthet.* Report no. 2018-001, Smart Housing Småland.

Kozlowski, M., Kinsella, D., Persson, K., Kubica, J., Hulimka, J. (2018): *Structural Analysis of Slender Glass Panel Subjected to Static and Impact Loading*. In: Challenging Glass Conference 6: Conference on Architectural and Structural Applications of Glass, Delft, The Netherlands.

Kinsella, D. (2018): *Survey of Experimental Data on the Strength of Annealed Float Glass Panes in the As-received Condition Tested in an Ambient Atmosphere*. Report TVSM-7166, Division of Structural Mechanics, Lund University.

Kinsella, D. (2018): *Modelling of Annealed Glass Fracture*. Report TVSM-3079, Division of Structural Mechanics, Lund University.

Sable, L., Kinsella, D., Kozlowski, M. (2019): *Influence of EVA, PVB and Ionoplast Interlayers on the Structural Behaviour and Fracture Pattern of Laminated Glass*. International Journal of Structural Glass and Advanced Materials Research 3(1), 62–78.

6
Conclusions and outlook

With respect to objective a), see further the objectives on p. 8 in Sec. 1.2, it is concluded that glass failure modelling approaches can generally be divided into; 1) models with a phenomenological approach towards failure where failure is considered at the macroscopic level and no particular representation of the surface condition is assumed, and; 2) models which consider fracture at the microscopic level by supposing pre-existing material flaws from which failure is derived. Flaws in glass can be represented more or less rigorously with stochastic cracks of a certain shape, size and orientation, or flaws can be represented by an elemental strength distribution. The main issue with the latter approach is how to properly deal with failure when it is supposed that the elemental strength is dependent on a multiaxial state of stress. A problem facing the flaw-size density-based approach is the difficulty to detect flaws due to practical limitations, as well as to distinguish between the potentially fracture-inducing flaws; additionally, flaws may have a complex shape.

With respect to objective b), a survey was performed of laboratory strength measurements on glass tested in an ambient environment and which were conducted within the last 40 years. The experiments which comprise some 3100 tests of individual specimens in nearly 200 samples, record the fracture stress of new and monolithic annealed float glass panes. Four different testing devices were employed in the experiments, namely the three-point and four-point bending devices, the double ring bending device, and the setup that allows for linearly supported plates to be subjected to uniform lateral pressure.

With the results from Paper A (objective c), it is concluded that the Weibull distribution provides a basic model for the surveyed edge strength data, that it outper-

forms a normal or lognormal distribution and is at least as well-performing as an extreme value Gumbel distribution. When the edge strength is considered, there is a tendency towards a unimodal flaw-size distribution that governs failure. In the case of surface strength tests, the extreme value distributions generally make a poor fit with data samples and multiple flaw populations that co-exist on the pristine surface are likely what causes the comparatively better performance of the normal and lognormal distributions. Ultimately, the standard statistical distributions, at least those considered, are insufficient for the modelling of surface strength, and more sophisticated approaches are warranted. From a practical perspective, both the edge and surface condition are important to account for in a strength design situation. Laboratory tests on hundreds of linearly supported plates subject to uniform lateral pressure demonstrate that on average about one in every third fracture occurred along an edge. In the case of linearly supported plates, numerical investigations performed in Paper C show how profound an effect the boundary conditions have on the resulting stress distribution which can attain equally large magnitudes on the "tension" side as the "compression" side of glass, in addition to exposing the edges to potentially critical magnitudes of stress concentration.

With respect to objective d), the models developed in Paper B, C, and E demonstrate how the strength and fracture origin can be simulated in numerical implementations of finite-size weakest-link (FSWL) systems assuming random sampling of Griffith flaws which are distributed over the surface area. The method has great potential for use in connection with failure modelling and prediction-making of glass structures. It is to begin with capable of approximating an ordinary Weibull weakest-link system as a special case. Yet provision is made for greater flexibility as it readily allows for custom surface flaw representations and a range of fracture criteria to be applied. However, the method is dependent on a rigorous representation of the surface condition which is challenging to acquire insight into due to the current lack of techniques by which to probe it. The use of a mixed mode fracture criterion has only a limited impact on the simulated strength distribution compared to a pure mode I criterion, at least in those cases studied which include ring-on-ring bending and linearly supported plates subject to uniform lateral pressure. When the FSWL systems are fitted to laboratory strength data (Paper E), in some cases the predicted fracture origins have significantly larger spread than observed in experiments. More work is required to further investigate simultaneous prediction-making of strength and fracture origins which are intrinsically interconnected in weakest-link systems. More research is needed to better understand which surface condition parameter values to use in numerical implementations of FSWL systems, e.g., pertaining to the flaw density value, or the choice of flaw-size density function. The application of multiple co-existing flaw populations are tractable with this method and more work is required to address the full potential and to deal with ensuing complexities. The results from Paper A pertaining to the observed surface strength characteristics (see objective c) provide justification for an investigation of multiple flaw populations as was pursued in Paper B and E. In addition,

there is random variability in the surface condition properties of glass that occurs between experimental campaigns that should be further addressed in wide-ranging experiments involving multiple laboratories and glass suppliers. It is also important in future work to address the stress corrosion parameters and how in particular the crack growth velocity parameter in Eq. (2.37) should be estimated for use in modelling of the surface condition in a range of environments including the ambient conditions of an indoor laboratory. For example, it would be tractable to treat this parameter as a random variable within the framework of the numerical method.

With respect to objective e), Paper C and E illustrate the application of the surface strength model to a range of different load cases including small plates subject to ring-on-ring and ball-on-ring loading, large linearly supported plates subject to uniform pressure, and large panels with complex geometry subject to impact loading. The analysis of a tall panel and soft impactor as was carried out in Paper C suggests a promising application of the numerical method for implementation of FSWL systems. In the study, an impact load with a fixed weight and fall height was applied on a panel with a complex geometry in a repeated series of virtual tests and the strength and fracture origin were recorded only if the structure was deemed to have failed. This procedure is similar to a certification test and it is anticipated that this can lead to a practicable simulation tool with potential to reduce significantly the need for time-consuming and costly laboratory tests. In addition, possible areas of application would be wide-ranging including, e.g., product certification of photovoltaic solar panels subject to certain predefined loads. It would therefore be of interest to continue the research on FSWL systems and to further calibrate the model parameters in experimental tests.

With respect to objective f), it is shown in Paper E how the theoretical strength-scaling in glass plates subject to ring-on-ring and ball-on-ring bending can be determined on the basis of a Weibull weakest-link system using the calculated effective areas which are expressed in closed-form. However, the results from laboratory tests (objective g) show that usage of the Weibull effective area is error-prone and thus the weakest-link premise of the ordinary Weibull model is rendered intractable from a practical point of view; it leads to non-conservative strength predictions on smaller effective areas, and to too low strength predictions than are viable for glass design on larger areas. To further address surface strength-scaling size effects, the study performed in Paper E could be expanded on by considering larger specimens extracted from a single jumbo pane and subjected to ring-on-ring and ball-on-ring bending using multiple loading ring dimensions in order to probe a greater range of the underlying flaw-size distribution. At the same time, careful attention should be paid to the observed fracture origins to promote a better understanding for their modelling.

With Paper D, an in-depth analysis of the edge strength is performed based on surveyed data measurements (objective h). Different edge treatments are associated

with different strength distribution characteristics, e.g., the polished edge is associated with the largest coefficient of variation on average and the arrised with the smallest whereas as-cut and ground edges lie in-between. The results from Paper A pertaining to the observed edge strength characteristics (see objective c) provide justification for an analysis in a Weibull statistical framework. However, the recorded data shows that the estimated Weibull parameters scatter considerably from one data sample to another even in cases where tests are done on specimens with equal dimensions that are obtained from the same supplier and are subjected to a uniform load rate in an indoor climate. A tractable way of dealing with this variability is to adopt a hierarchical modelling approach in which the Weibull parameters are treated as nested random variables. The as-cut edge may be associated with a scale-dependent shape parameter with an inverse proportionality. Supplier effects on edge strength are significant and important to consider alongside other effects due to, e.g., applied stress rate and length of edge exposed to maximum stress. A 45 MPa characteristic strength value can be conservatively used with arrised, ground, and polished edges if related to a reference length of 100 mm at an applied stress rate of 2 MPa s^{-1}. Static fatigue is best accounted for with a value of stress corrosion parameter equal to about 16.

In summary, the results from Paper A provide justification for key assumptions made in Paper B, D, and E, namely, the consideration of multiple flaw populations in surface fracture modelling, and the analysis of edge strength data within a Weibull statistical framework. In addition, Paper C and E present various applications of the surface strength model including linearly supported plates subject to uniform lateral pressure, a laminated glass panel located in a public hall which is subject to dynamic impact loading, and laboratory results from ring-on-ring and ball-on-ring bending tests with a consideration of surface size effects.

Another important area for future research pertains to the joint modelling of surface and edge fracture. In a numerical implementation of a FSWL system, the unit cells corresponding to the edge perimeter can be sampled from one type of flaw population while the unit cells corresponding to the surface from another. The work carried out and presented in Paper D and E, respectively, could be combined to promote such a model. In Paper D a mixture distribution for the edge strength is computed (see Fig. 8 in the paper) which represents the strength at a 2 MPa s^{-1} stress rate for various load spans and edge types. It also represents the strength when no prior knowledge is had about the particular supplier from which the glass was obtained, thus corresponding to a realistic design situation. The computed mixture distribution could be adapted and used as an elemental strength distribution for application in a FSWL context. When it comes to the surface condition, more research is recommended to produce a reliable representation including further work on multiple flaw population concepts. This should include wide-ranging laboratory testing with glass sampled from numerous suppliers and tested at multiple laboratories. As a starting point, however, the modified flaw-size concept that

was applied in Paper E could be used. Supposing such joint modelling of surface and edge fractures in a FSWL system, the tall panel and soft impactor case from Paper C could be revisited in a future investigation using an elemental strength approach for the edge subregions and a flaw-size approach for the surface subregions. This would present a significantly improved analysis of the structure because the complex geometry in this case results in a substantial portion of the edge and surface to be simultaneously exposed to considerable tension. However, a question to be further addressed is the possible difference in edge strength characteristics when a glass specimen is subjected to an out-of-plane bending load compared to the more commonly adopted configuration of in-plane loading (as in laboratory tests using a four-point bending fixture).

A promising opportunity is to integrate some of the methods covered in the thesis into the ClearSight glass design program which is used by industry in Sweden. ClearSight is a finite element-based design tool that was developed at the Division of Structural Mechanics at Lund University in collaboration with the Swedish glass associations. The program consists of a user interface, a simulation module, a result viewer, and a report window, see further Fröling (2013) for a description of some of the features. ClearSight can be used to determine the strength due to various load cases and boundary conditions with a large number of capabilities including bolt or clamp fixed laminated glass units subjected to, e.g., a uniformly distributed load or a uniform line load along one edge. A special reduced integration scheme is utilized so that only one element layer per material layer in the thickness direction is required which makes for very time-efficient computations in particular for laminated glass units which consist of several material layers. When ClearSight is used as a tool in the design process to evaluate different design alternatives, at present it does so by comparing the computed maximum principal tensile stress with the allowable stress which can be inferred from the standards. The methods presented in this thesis can be applied in a tool like ClearSight to facilitate a strength-design process that accounts for glass material characteristics and is consistent with present knowledge of advanced glass structures in building construction.

References

Addis, B. (2007), *Building: 3000 years of design engineering and construction*, Phaidon Press Limited.

Anderson, T. W. & Darling, D. A. (1952), 'Asymptotic theory of certain "goodness of fit" criteria based on stochastic processes', *Ann. Math. Statist.* (2), 193–212.

Baker, T. C. & Preston, F. W. (1946*a*), 'The effect of water on the strength of glass', *J Appl Phys* **17**, 179–188.

Baker, T. C. & Preston, F. W. (1946*b*), 'Fatigue of glass under static loads', *J Appl Phys* **17**, 170–178.

Batdorf, S. B. & Crose, J. G. (1974), 'A statistical theory for the fracture of brittle structures subjected to nonuniform polyaxial stresses', *J Appl Mech* **41**(2), 459–464.

Bathe, K.-J. (2006), *Finite Element Procedures*, Klaus-Jürgen Bathe.

Beason, W. L. (1980), A Failure Prediction Model for Window Glass, PhD thesis, Texas Tech University, Institute for Disaster Research. NTIS Accession no. PB81-148421.

Beason, W. L., Kohutek, T. L. & Bracci, J. M. (1998), 'Basis for ASTM E 1300 annealed glass thickness selection charts', *J Struct Eng* **124**, 215–221.

Beason, W. L. & Morgan, J. R. (1984), 'Glass failure prediction model', *J Struct Eng* **110**, 197–212.

Beirlant, J., Goegebeur, Y., Teugels, J., Segers, J., De Waal, D. & Ferro, C. (2004), *Statistics of Extremes – Theory and Applications*, John Wiley & Sons.

Blank, K., Duerkop, D., Durchholz, M., Grueters, H., Helmich, G. & Senger, W. (1994), 'Strength tests of flat glass by means of four-point bending', *Glastechnische Berichte* **67**, 9–15.

Bonati, A., Occhiuzzi, A., Pisano, G. & Royer-Carfagni, G. (2018), 'A micro-mechanically motivated model for the strength of heat-treated glass', *Glass Struct Eng* **3**, 153–166.

Brand, A., Allen, L., Altman, M., Hlava, M. & Scott, J. (2015), 'Beyond authorship: attribution, contribution, collaboration, and credit', *Learned Publishing* **28**, 151–155.

Broek, D. (1983), *Elementary Engineering Fracture Mechanics*, 3 edn, Martinus Nijhoff Publishers, The Hague.

Brown, W. G. (1972), A load duration theory for glass design, Technical Report NRCC 12354, National Research Council of Canada.

Calderone, I. J. (1999), The equivalent wind loading for window glass design, PhD thesis, Monash University.

Charles, R. J. (1958*a*), 'Static Fatigue of Glass I', *J Appl Phys* **29**, 1549–1553.

Charles, R. J. (1958*b*), 'Static Fatigue of Glass II', *J. Appl. Phys.* **29**, 1554–1560.

Charles, R. J. & Hillig, W. B. (1962), The kinetics of glass failure by stress corrosion, *in* 'Symposium on Mechanical Strength of Glass and Ways of Improving it', pp. 511–527.

Christoffersen, J. (2011), The importance of light to health and well-being, *in* '4th VELUX Daylight Symposium "Daylight in a Human Perspective"', Lausanne, Switzerland.

Ciccotti, M. (2009), 'Stress-corrosion mechanisms in silicate glasses', *J. Phys. D: Appl. Phys.* **42**(21), 214006.

Creager, M. (1966), The elastic stress field near the tip of a blunt crack, PhD thesis, Lehigh University. Theses and Dissertations 3440.

Creager, M. & Paris, P. C. (1967), 'Elastic field equations for blunt cracks with reference to stress corrosion cracking', *Int J Fract Mech* **3**(4), 247–252.

Culf, C. J. (1957), 'Fracture of glass under various liquids and gases', *J. Soc. Glass Tech.* **41**, 157.

D'Agostino, R. B. & Stephens, M. A., eds (1986), *Goodness-of-fit Techniques*, Marcel Dekker, New York, USA.

Dalgliesh, W. A. & Taylor, D. A. (1990), 'The strength and testing of window glass', *Can J Civ Eng* **17**, 752–762.

Danzer, R. (1994), 'Ceramics: Mechanical performance and lifetime prediction', *The Encyclopedia of Advanced Materials* **1**, 385–398.

Danzer, R., Lube, T. & Supancic, P. (2001), 'Monte Carlo simulations of strength distributions of brittle materials – Type of distribution, specimen and sample size', *Z. Metallkd.* **92**, 773–783.

De Jayatilaka, A. & Trustrum, K. (1977), 'Statistical approach to brittle fracture', *J Mater Sci* **12**, 1426–1430.

EN 12150-1 (2015), 'Glass in building – Thermally toughened soda lime silicate safety glass. Part 1: Definition and description.', CEN.

EN 1279-5 (2018), 'Glass in building – Insulating glass units – Part 5: Product standard', CEN.

EN 14179-1 (2016), 'Glass in building – Heat soaked thermally thoughened soda lime silicate safety glass – Part 1: Definition and description', CEN.

EN 14449 (2005), 'Glass in building – Laminated glass and laminated safety glass – Evaluation of conformity/Product standard', CEN.

EN 16612 (2019), 'Glass in building – Determination of the lateral load resistance of glass panes by calculation', CEN.

EN 16613 (2019), 'Glass in building – Laminated glass and laminated safety glass – Determination of interlayer viscoelastic properties', CEN.

EN 1863-1 (2011), 'Glass in building – Heat strengthened soda lime silicate glass – Part 1: Definition and description.', CEN.

EN 572-1 (2012), 'Glass in building – Basic soda lime silicate glass products – Part 1: Definitions and general physical and mechanical properties', CEN.

Evans, A. G. (1974), 'Slow crack growth in brittle materials under dynamic loading conditions', *Int J Fracture* **10**, 251–259.

Fink, A. (2000), Ein Beitrag zum Einsatz von Floatglas als dauerhaft tragender Konstruktionswerkstoff im Bauwesen, PhD thesis, TU-Darmstadt.

Fischer-Cripps, A. C. & Collins, R. E. (1995), 'Architectural glazings: Design standards and failure models', *Building and Environment* **30**, 29–40.

Forbes, C., Evans, M., Hastings, N. & Peacock, B. (2011), *Statistical distributions*, 4 edn, John Wiley and Sons.

Freiman, S. W., White, G. S. & Fuller, E. R. (1985), 'Environmentally enhanced crack growth in soda-lime glass', *J Am Ceram Soc* **68**(3), 108–112.

Freudenthal, A. M. (1968), Statistical approach to brittle fracture, *in* H. Liebowitz, ed., 'Fracture', Vol. 2, Academic Press, New York.

Fröling, M. (2013), Strength Design Methods for Glass Structures, PhD thesis, Lund University. Report TVSM-1025.

Gehrke, E., Ullner, C. & Hähnert, M. (1991), 'Fatigue limit and crack arrest in alkali-containing silicate glasses', *J. Mater. Sc.* **26**, 5445–5455.

Grenet, L. (1899), 'Mechanical strength of glass', *Bull. Soc. Enc. Industr. Nat. Paris* **4**, 838–48.

Griffith, A. A. (1920), 'The phenomena of rupture and flow in solids', *Phil. Trans. R. Soc.* **A221**, 163.

Gumbel, E. J. (1954), *Statistical theory of extreme values and some practical applications: A series of lectures*, Applied mathematics series, U.S. Govt. Print. Office.

Gut, A. (1995), *An intermediate course in probability*, Springer.

Haldimann, M. (2006), Fracture strength of structural glass elements – Analytical and numerical modelling, testing and design, PhD thesis, Ecole Polytechnique Fédérale de Lausanne EPFL.

Haldimann, M., Luible, A. & Overend, M. (2008), *Structural use of glass*, International Association for Bridge and Structural Engineering.

Han, W.-T. & Tomozawa, M. (1989), 'Mechanism of mechanical strength increase of soda-lime glass by aging', *J. Am. Ceram. Soc.* **72**(10), 1837–43.

Hellan, K. (1984), *Introduction to Fracture Mechanics*, McGraw-Hill.

Holzapfel, G. (2000), *Nonlinear solid mechanics*, Wiley.

Inglis, C. E. (1913), 'Stresses in a plate due to the presence of cracks and sharp corners', *Trans. Inst. Naval. Archit.* **55**, 219.

Irwin, G. R. (1957), 'Analysis of stresses and strains near the end of a crack traversing a plate', *J. Appl. Mech.* **24**, 361.

Irwin, G. R. (1958), Fracture, *in* 'Handbuch der Physik', Vol. 6, Springer, p. 551.

Johar, S. (1981), Dynamic fatigue of flat glass – Phase II, Technical report, Ontario Research Foundation, Department of Metals, Glass and Ceramics.

Kinsella, D. (2018), Survey of experimental data on the strength of annealed float glass panes in the as-received condition tested in an ambient atmosphere, Report TVSM-7166, Division of Structural Mechanics, Lund University.

Kinsella, D. & Lindström, J. (2020), 'Using a Hierarchical Weibull Model to Predict Failure Strength of Different Glass Edge Profiles', *Int J Struct Glass Adv Mater Res* **4**, 130.148.

Kinsella, D., Lindström, J. & Persson, K. (2018), 'Performance of standard statistical distributions for modeling glass fracture', *Int J Struct Glass Adv Mater Res* **2**(178.190).

Kinsella, D. & Persson, K. (2018*a*), An analysis of glass fracture statistics, *in* 'Challenging Glass 6 – Conference on Architectural and Structural Applications of Glass', Delft, The Netherlands.

Kinsella, D. T. & Persson, K. (2016), On the applicability of the Weibull distribution to model annealed glass strength and future research needs, *in* 'Challenging Glass Conference 5', Ghent, Belgium.

Kinsella, D. T. & Persson, K. (2018*b*), 'A numerical method for analysis of fracture statistics of glass and simulations of a double ring bending test', *Glass Struct & Eng* **3**(2), 139–152.

Knuuttila, T. (2009), 'Isolating representations versus credible constructions? Economic modelling in theory and practice', *Erkenntnis* **70**(1), 59–80.

Krohn, M. H., Hellmann, J. R., Shelleman, D. L. & Pantano, C. D. (2002), 'Biaxial flexure strength and dynamic fatigue of soda-lime-silica float glass', *J. Am. Ceram. Soc.* **85**(7), 1777–1782.

Lamon, J. (2016), *Brittle Fracture and Damage for Brittle Materials and Composites*, Elsevier.

Lawn, B. (1993), *Fracture of Brittle Solids*, Cambridge Solid State Science Series, 2 edn, Cambridge University Press, Cambridge, UK.

Lawn, B., Jakus, K. & Gonzalez, A. (1985), 'Sharp vs blunt crack hypothesis in the strength of glass: A critical study using indentation flaws', *J. Am. Ceram. Soc.* **68**(1), 25–34.

Le Bourhis, E. (2008), *Glass*, Wiley-VCH, Weinheim.

Lindqvist, M. (2013), Structural Glass Strength Prediction Based on Edge Flaw Characterization, PhD thesis, Ecole Polytechnique Fédérale de Lausanne EPFL.

Lü, B.-T. (1997), 'Fatigue strength prediction of soda-lime glass', *Theor Appl Fract Mec* **27**, 107–114.

Lu, C., Danzer, R. & Fischer, F. D. (2002), 'Fracture statistics of brittle materials: Weibull or normal distribution', *Phys. Rev. E* **65**, 67102.

Macfarlane, A. & Martin, G. (2002), *Glass. A World History.*, The University of Chicago Press.

Marqueze, E. C., Vasconcelos, S., Garefelt, J., Skene, D. J., Moreno, C. R. & Lowden, A. (2015), 'Natural light exposure, sleep and depression among day workers and shiftworkers at Arctic and Equatorial latitudes', *PLOS ONE* **10**, 1–14.

Matthews, J. R., McClintock, F. A. & Shack, W. J. (1976), 'Statistical determination of surface flaw density in brittle materials', *J. Am. Ceram. Soc.* **59**, 304–308.

McLellan, G. W. & Shand, E. B. (1984), *Glass engineering handbook*, McGraw-Hill.

Mencik, J. (1992), *Strength and Fracture of Glass and Ceramics*, Vol. 12 of *Glass Science and Technology*, Elsevier.

Mesarovic, S., Gasparini, D., Muju, S. & McNelis, M. (1992), 'Probability of crack growth in Poisson field of penny cracks', *J Eng Mech* **118**(5), 961–978.

Mould, R. E. & Southwick, R. D. (1959), 'Strength and static fatigue of abraded glass under controlled ambient conditions: II, Effect of various abrasions and the universal fatigue curve', *J Am Ceram Soc* **42**(12), 582–592.

Muniz-Calvente, M., Ramos, A., Pelayo, F., Lamela, M. J. & Fernandez-Canteli, A. (2016), 'Statistical joint evaluation of fracture results from distinct experimental programs: An application to annealed glass', *Theor Appl Fract Mec* **85**(Part A), 149–157.

Natividad, K., Morse, S. M. & Norville, H. S. (2016), 'Fracture origins and maximum principal stresses in rectangular glass lites', *J Archit Eng* **22**(2), –1—-1.

Niiniluoto, I. (1993), 'The aim and structure of applied research', *Erkenntnis* **38**, 1–21.

Orowan, E. (1949), 'Fracture and strength of solids', *Rep Prog Phys* **12**(1), 185.

Osnes, K., Börvik, T. & Hopperstad, O. S. (2018), 'Testing and modelling of annealed float glass under quasi-static and dynamic loading', *Eng Fract Mech* .

Pathirana, M., Lam, N., Perera, S., Zhang, L., Ruan, D. & Gad, E. (2017), 'Risks of failure of annealed glass panels subject to point contact actions', *Int J Solids Struct* **129**, 177–194.

Peirce, F. T. (1926), '32–X.–Tensile tests for cotton yarns v.–"The weakest link" theorems on the strength of long and of composite specimens', *J. Textile Inst. Trans.* **17**, 355.

Pisano, G. & Royer-Carfagni, G. (2017), 'A micromechanical derivation of the macroscopic strength statistics for pristine or corroded/abraded float glass', *J. Eur. Ceram. Soc.* **37**, 4197–4206.

Polanyi, M. (1921), 'On the nature of the tearing process', *Z. Physik.* (7), 323–7.

Poloniecki, J. D. (1974), Statistical investigation of surface flaws, PhD thesis, The University of Sussex.

Poloniecki, J. D. & Wilshaw, T. R. (1971), 'Determination of surface crack size densities in glass', *Nature Physical Science* **229**, 226–227.

prEN 16612 (2013), 'Glass in building – Determination of the load resistance of glass panes by calculation and testing', CEN.

prEN 16612 (2017), 'Glass in building – Determination of the lateral load resistance of glass panes by calculation', CEN.

Quinn, G. D. (2016), Fractography of ceramics and glasses, Technical report, National Institute of Standards and Technology, Gaithersburg, MD, USA.

Reid, S. G. (1991), Flaws in the Failure Prediction Model of Glass Strength, *in* 'Sixth International Conference on Applications of Statistics and Probability in Civil Engineering', pp. 111–117.

Reid, S. G. (2007), 'Effects of spatial variability of glass strength in ring-on-ring tests', *Civ Eng Environ Syst* **24**, 139–148.

Rinne, H. (2009), *The Weibull Distribution – A Handbook*, Taylor & Francis Group.

Saabye Ottosen, N. & Petersson, H. (1992), *Introduction to the finite element method*, Prentice Hall.

Saabye Ottosen, N. & Ristinmaa, M. (2005), *The mechanics of constitutive modeling*, Elsevier.

Schula, S. (2015), *Charakterisierung der Kratzanfälligkeit von Gläsern im Bauwesen*, Springer.

Simiu, E., Reed, D. A., Yancey, C. W. C., Martin, J. W., Hendrickson, E. M., Gonzalez, A. C., Koike, M., Lechner, J. A. & Batts, M. E. (1984), Ring-on-ring tests and load capacity of cladding glass, NBS Building Series 162, U.S. Department of Commerce – National Bureau of Standards.

Sugden, R. (2002), Credible worlds: The status of the theoretical models in economics., *in* U. Mäki, ed., 'Fact and fiction in economics: Models, realism, and social construction.', Cambridge University Press, Cambridge, pp. 107–136.

Suo, Z. (2016), 'The Griffith paper', `imechanica.org/node/7470`. Accessed: 2020-10-26.

Timoshenko, S. & Woinowsky-Krieger, S. (1959), *Theory of Plates and Shells*, 2 edn, McGraw-Hill book company.

Tomozawa, M. (1996), 'Fracture of glasses', *Ann. Rev. Mater. Sci.* **26**, 43–74.

Tooley, F. V. (1984), *The handbook of glass manufacture*, 3 edn, Books for the glass industry division Ashlee Publishing.

Tummula, R. R. & Foster, B. J. (1975), 'Strength and dynamic fatigue of float glass surfaces', *J. Am. Ceram. Soc.* **58**(3–4), 156–157.

Vandebroek, M., Louter, C., Caspeele, R., Ensslen, F. & Belis, J. (2014), 'Size effect model for the edge strength of glass with cut and ground edge finishing', *Eng Struct* **79**, 96 – 105.

Varshneya, A. (1994), *Fundamentals of Inorganic Glasses*, Academic Press.

Veer, F. A. (2007), 'The strength of glass, a nontransparent value', *HERON* **52**, 87–104.

Veer, F. A., Louter, C. & Bos, F. P. (2009), 'The strength of annealed, heat-strengthened and fully tempered float glass', *Fatigue Fract Eng M* **32**, 18–25.

Veer, F. A. & Rodichev, Y. M. (2012), The strength of water jet cut glass, *in* 'Glass Performance Days 2011', pp. 434–438.

Wachtman, J. B., Cannon, W. R. & Matthewson, M. J. (2009), *Mechanical properties of ceramics*, Wiley, Hoboken, N. J.

Wasserman, L. (2006), *All of nonparametric statistics*, Springer.

Weibull, W. (1939*a*), 'The phenomenon of rupture in solids', *Ingenjörsvetenskapsakademiens handlingar* **153**.

Weibull, W. (1939*b*), 'A statistical theory of the strength of materials', *Ingenjörsvetenskapsakademiens handlingar* **151**.

Weibull, W. (1949), 'A statistical representation of fatigue failures in solids', *Kungl. tekniska högskolans handlingar* (27).

Weibull, W. (1951), 'A statistical distribution function of wide applicability', *ASME J. Appl. Mech.* (September), 293–297.

Wereszczak, A. A., Ferber, M. K. & Musselwhite, W. (2014), 'Method for identifying and mapping flaw size distributions on glass surfaces for predicting mechanical response', *Int J Appl Glass Sci* **5**, 16–21.

Westergaard, H. M. (1939), 'Bearing pressures and cracks', *J Appl Mech* **6**, A49–53.

Wiederhorn, S. M. (1967), 'Influence of water vapor on crack propagation in soda-lime glass', *J. Am. Ceram. Soc.* **50**, 407–417.

Wiederhorn, S. M. & Tornsend, P. (1970), 'Crack healing in glass', *J. Am. Cer. Soc.* **53**, 486–489.

Yankelevsky, D., Spiller, K., Packer, J. & Seica, M. (2017), 'Fracture characteristics of laboratory-tested soda lime glass specimens', *Can J Civ Eng* **44**, 151–160.

Yankelevsky, D. Z. (2014), 'Strength prediction of annealed glass plates – A new model', *Eng Struct* **79**, 244–255.

Young, G. A. & Smith, R. L. (2005), *Essentials of Statistical Inference*, Cambridge Series in Statistical and Probabilistic Mathematics, Cambridge University Press.

Zubkov, V. A. & Kondratieva, N. V. (2014), Ultrasonic examination of sheet glass macrostructure, *in* C. Louter, F. Bos, J. Belis & J.-P. Lebet, eds, 'Challenging Glass 4 & COST Action TU0905 Final conference', pp. 755–761.

Part II

Appended publications

David Kinsella, Johan Lindström, Kent Persson

Performance of Standard Statistical Distributions for Modeling Glass Fracture

International Journal of Structural Glass and Advanced Materials Research 2 (2018) (178.190)

Paper A

International Journal of Structural Glass and Advanced Materials Research

Original Research paper

Performance of Standard Statistical Distributions for Modeling Glass Fracture

[1]David Kinsella, [2]Johan Lindström and [1]Kent Persson

[1]Construction Sciences, Lund University, Sweden
[2]Centre for Mathematical Sciences, Lund University, Sweden

Article history
Received: 07-06-2018
Revised: 13-07-2017
Accepted: 2-08-2018

Corresponding Author:
David Kinsella
Construction Sciences,
Lund University, Sweden
Email:
david.kinsella@construction.lth.se

Abstract: Experimental data on the strength of new annealed float glass tested in an ambient environment was collected. A comparison was made between four standard distributions, the normal, lognormal, Gumbel and Weibull, with respect to the performance in modelling the strength. The Weibull distribution outperformed the normal and lognormal distributions when the data contained edge only failure origins. When the data was selected to contain surface only failure origins it is indicated that the extreme value distributions performed poorly. The Weibull model is known to have a basis in a failure-mechanism concept based on the weakest-link principle. The Gumbel distribution can also be derived from failure-based mechanics and be associated with certain types of flaw size distribution. The Weibull model, however, is a better choice for a failure model of glass edge strength compared to the normal and lognormal distributions and at least as good as a Gumbel distribution. The surface strength is complicated to model and none of the standard distributions which were examined are capable of producing a proper model. The sample size also has a profound impact on the performance of the surface strength models.

Keywords: Glass, Strength, Fracture statistics, Weibull distribution

Introduction

The normal distribution was previously used by glass manufacturers to model the fracture stress. In e.g., the early Pilkington design charts, the design stress was based on the 1%-fractile of a normal distribution with a coefficient of variation of 0.20 (Calderone, 1999). Today, the Weibull distribution is commonly used to model the fracture stress data from experiments on glass. However, a number of researchers have questioned whether the Weibull distribution is in fact superior to an ordinary normal or lognormal distribution as a model of the fracture stress in glass. Based on the test results of a large set of full-size rectangular plates of both new and old annealed float glass, Calderone (1999) found that the lognormal distribution provided a better fit with the experimental data than the Weibull distribution. The lognormal distribution has support on the right half axis only and that gives it a logical advantage over the normal distribution because the strength is a positive number. Later studies by Calderone *et al*. (2001) and Calderone *et al*. (2005) recommended that the Weibull distribution should in fact not be used to predict the strength of window glass panels. However, the 32 samples of data in Calderone (1999) were of limited size ranging from 5 to 9 specimens each. Lü (1997) carried out tests on glass in three-point and four-point bending and concluded, based on the correlation coefficient of the fitted line in the probability plots, that all three standard distributions, i.e., the normal, lognormal and Weibull, were applicable as failure models. Veer *et al*. (2009) carried out tests on glass beams in four-point bending and concluded that on the one hand, the lognormal distribution provided a fit that was at least as good as the Weibull model. On the other hand, it was concluded that none of the standard distributions properly modelled the data on annealed glass.

So far and to the best of our knowledge, no one has made a comparison of the standard distributions based on a comprehensive survey of the published data results that are available in the open literature. In fact, a substantial portion of the total number of experiments that have been reported were conducted only recently within the last decade.

Moreover, it is sometimes believed that the edge strength in glass differs from the surface strength. This is reflected in the structural standards in different ways. For example, DIN 18008:2010 gives a reduction factor to be applied when calculating the edge strength, the factor of which is 0.8. Hence, the edge condition is always considered to be inferior to the surface condition. On the other hand, prEN 16612:2017 provides a different set of reduction factors for the edge strength depending on the edge treatment, i.e., cut, arrised, ground, or polished. In the case of the polished edge, the edge reduction factor is unity which amounts to no reduction at all. This implies that the polished edge condition is considered to be equal to the pristine surface. In summary it is possible then, but not self-evident perhaps, that different models should be used for the edge and surface fractures in glass.

The question of which standard distribution that provides the best fit has important implications. Currently, there is a draft for a European standard for strength of glass in building, prEN 16612:2017, that bases its estimate of the characteristic value of the strength of glass on test results that were fitted with a Weibull distribution. The characteristic value of the bending strength is defined from the 5% fractile in the distribution for monolithic panes of annealed float glass.

In this study, the performance of the following four standard statistical distributions is examined, viz. the normal, lognormal, Gumbel and Weibull distributions.

Standard Distributions

A Weibull distribution with the parameter values $m = 6$ and $k = 74$ MPa was fitted to test results on annealed float glass specimens that were performed as a basis for the DIN 1249-10:1990 (Haldimann, 2006). The tests were carried out using the R400 double ring bending device at a stress rate of approximately 2 MPa s^{-1}. The characteristic value of the bending strength was estimated at 45 MPa which was the 5% fractile in the distribution. This value was subsequently adopted in the draft standard which currently is referred to as prEN 16612:2017.

The Weibull distribution (Weibull, 1939) has the cumulative distribution function:

$$F(\sigma) = 1 - \exp\left(-\left(\frac{\sigma}{k}\right)^m\right) \tag{1}$$

where, k and $m>0$ denote the scale and shape parameters, respectively. Glass strength is governed by the existence of surface flaws which magnify the stresses locally (Griffith, 1920). The stress-raising property of a given flaw can be determined from the associated crack size and shape using fracture mechanics (Mencik, 1992). Let $f(a)$ denote the flaw size density function with a signifying the flaw size. Suppose a_c denotes the critical crack size that prompts failure of the crack. In the case of a plane crack with geometry factor Y that is subjected to a uniform uniaxial stress σ, it can be shown that:

$$a_c = \frac{K_{Ic}^2}{Y^2\sigma^2\pi} \tag{2}$$

where, K_{Ic} represents the fracture toughness (Mencik, 1992). Let $P_f(\Delta A, a_c)$ denote the failure probability in the small region ΔA at the critical crack depth a_c. It can be shown that (Lamon, 2016):

$$P_f\left(\Delta A, a_c\right) = \Delta A\int_{a_c}^{\infty} f\left(a\right)da \tag{3}$$

Suppose the total area is:

$$A = N\Delta A \tag{4}$$

for some number N. By application of the weakest link principle while assuming that the regions are non-interacting it is found that the survival probability is:

$$1 - P_f\left(A, a_c\right) = \left(1 - P_f\left(\Delta A, a_c\right)\right)^N \tag{5}$$

Substituting for Equation 3 and 4 in Equation 5 while observing the standard limit:

$$\lim_{N\to\infty}\left(1 + \frac{x}{N}\right)^N = e^x \tag{6}$$

it follows after some rearrangement that:

$$P_f\left(A, a_c\right) = 1 - \exp\left(-A\int_{a_c}^{\infty} f\left(a\right)da\right) \tag{7}$$

Suppose $f(a)$ is a Pareto density function, i.e.:

$$f\left(a\right) = ca_0^c a^{-(c+1)} \tag{8}$$

where, c and a_0 are scale and shape parameters (Forbes *et al*., 2011). Inserting Equation 8 into Equation 7 while substituting for Equation 2 yields the Weibull distribution, Equation 1, with:

$$m = 2c \tag{9}$$

and:

$$k = \frac{K_{Ic}}{Y\sqrt{\pi a_0 A^{1/c}}} \tag{10}$$

In fact, for reasons of extreme value theory (Beirlant *et al*., 2004), the Weibull distribution is the limiting distribution when the flaw size distribution decays like a power-law in the tail. This means that the Weibull distribution emerges for the strength model when the flaw size distribution is e.g., Pareto, Cauchy, *t*, or *F*. Another common extreme value distribution is the Gumbel distribution which has the density function:

$$f(\sigma) = \frac{1}{s}\exp\left(\frac{\sigma-\mu}{s}\right)\exp\left(-\exp\left(\frac{\sigma-\mu}{s}\right)\right) \quad (11)$$

where, μ and s signify the location and scale parameters, respectively. It is the limiting distribution when the flaw size distribution decays exponentially in the tail. This includes flaw size distributions such as the normal, lognormal, exponential, gamma and χ^2 (Trustrum and De Jayatilaka, 1983).

The normal distribution has the probability density function (Forbes *et al*., 2011):

$$f(\sigma) = \frac{1}{\sqrt{2\pi s^2}}\exp\left(-\frac{(\sigma-\mu)^2}{2s^2}\right) \quad (12)$$

where, μ and s^2 are the mean and variance, respectively. The use of a normal distribution as a standard model for data is due to the Central Limit Theorem (Beirlant *et al*., 2004) which states that averages of many samples will tend to follow a normal distribution.

The lognormal distribution arises from the normal distribution through a change of variables transformation. If Y is a random variable with a normal distribution, then $X = \exp(Y)$ has a lognormal distribution with the density function (Forbes *et al*., 2011):

$$f(\sigma) = \frac{1}{\sigma\sqrt{2\pi s^2}}\exp\left(-\frac{(\log\sigma-\mu)^2}{2s^2}\right) \quad (13)$$

In Equation 13, μ and s^2 denote the mean and variance of the related normal distribution. By token of the Central Limit Theorem, the lognormal distribution would be a natural model for geometric means.

Method

Data on the strength of annealed float glass was collected from a set of references, see Table 1 for the complete list including details on the experimental setups. The strength was the maximum principal tensile stress at the fracture origin location. Only those data samples were extracted from the references and included in the analysis which fulfilled the following conditions: the glass was monolithic annealed float glass in the as-received condition that was tested in an ambient environment. The experiments were conducted using either the double ring bending device, the three or four-point bending device, or the setup that allows for a uniform pressure to be applied to a laterally supported plate. In the case of four-point bending tests, the recorded strength value was discarded in case the failure origin was located outside the load span. In one case of double ring bending tests, viz. Simiu *et al*. (1984), the fracture stress values that corresponded to failure origins outside the loading ring area were adjusted using Equation 14 in order to reflect the maximum principal tensile stress at the failure origin. This was possible to do because the fracture origins were recorded by Simiu *et al*. (1984). Otherwise, all the recorded strength values were taken as-received. The radial stress outside the loading ring area in a double ring bending setup at the distance r from the centre point is:

$$\sigma_r = \frac{3F}{2\pi b^2}\left((1+\nu)\ln\frac{r_1}{r} + (1-\nu)\frac{r_0^2\left(r_1^2-r^2\right)}{2r^2r_2^2}\right),\ r > r_0 \quad (14)$$

where, r_2 is the equivalent outer radius used for a square shaped specimen with side length $2L$, viz:

$$r_2 = L\left(1+\sqrt{2}\right) \quad (15)$$

In Equation 14, F is the failure load, b is the plate thickness, ν is Poisson's ratio, r_0 is the loading ring radius and r_1 is the support ring radius.

An overview of the experiments including a more detailed presentation of each data sample can be found in Kinsella (2018). All data samples that were larger in size than 5, 15, 30 and 45, respectively, were fitted with the four standard probability distributions. The parameter estimation was performed with the maximum likelihood method. The goodness-of-fit was calculated with the Anderson-Darling statistic (D'Agostino and Stephens, 1986) and a set of four p-values were derived for each sample, the p-values being associated with the normal, lognormal, Gumbel and Weibull distributions, respectively.

The float process production method causes the diffusion of tin into the surface that was in contact with the molten tin bath and this side is termed the tin side. The other side is the air side. When the statistical models were fitted to the data samples, it was not taken into account whether the fracture origin was located on the tin side of the glass or on the air side.

The method used to measure and compare the potential of various statistical models allows for the effect of different surface area size or edge length and different stress state to be taken into account by adaptation of the

two parameter values. This is done in the maximum likelihood estimation. However, the method of analysis used in this study does not take into account that the strength in e.g., uniaxial stress states is of one type of distribution, e.g., Weibull, while in biaxial stress states is of a different type of distribution, e.g., normal.

In some experiments the fracture origin mode was not recorded while the data contained a mixture of surface and edge fractures or there was an ambiguity towards the fracture origin due to multiple potential fracture locations. Hence only a mixed failure origin mode could be determined in those cases. This pertains to a number of cases with the four-point bending device with the loading taking place out-of-plane and with laterally supported plates subjected to uniform pressure. In the examination that follows, it was assumed that when a glass beam was tested in the four-point bending device with in-plane loading, then the type of fracture produced was an edge failure origin. For an illustration of the meaning of in-plane and out-of-plane loading with the four-point bending device, see Fig. 1. The model fitting was performed in the following three cases, viz. mixed failure origins, edge only failure origins and surface only failure origins.

In a first procedure, the resulting measures of performance were visualized in the form of boxplots. Subsequently, the multiple models over multiple data sets were compared in a Friedman test (Friedman, 1937; 1940) under the null-hypothesis that all models perform equally. In case the null-hypothesis was rejected, a post-hoc test was performed to determine which of the models that were significantly different. For this, the Wilcoxon signed-rank test (Wilcoxon, 1945) was used and the family-wise error was controlled with the Bonferroni-Holm method (Holm, 1979).

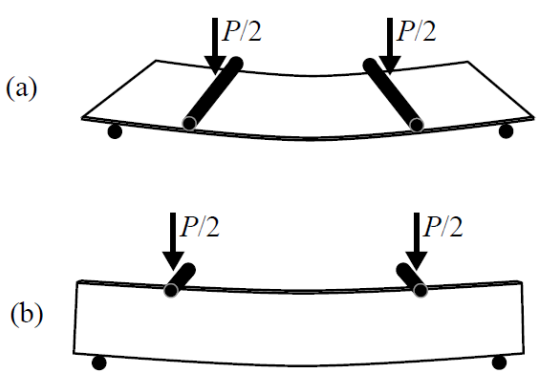

Fig. 1: Illustration of the (a) out-of-plane loading of a beam in four-point bending and the (b) in-plane loading

Friedman Test

The Friedman test is a non-parametric test for comparing models over multiple data sets. The performance of the *m* models is calculated for each of the *n* data sets and then ranked with rank 1 corresponding to the best performance. The ranks can be organized in a matrix:

$$R = \begin{bmatrix} R_{11} & R_{12} & \cdots & R_{1n} \\ R_{21} & R_{22} & \cdots & R_{2n} \\ \vdots & \vdots & \vdots & \vdots \\ R_{m1} & R_{m2} & \cdots & R_{mn} \end{bmatrix} \tag{16}$$

where, R_{ij} is the rank of model i in data set j (Benavoli *et al.*, 2016). Under the null-hypothesis, there is no difference in performance between the models, in which case the average value of each row in R is $\frac{n(m+1)}{2}$. The test statistic is:

$$T = \frac{12}{nm(m+1)} \sum_{j=1}^{n} \left(\sum_{k=1}^{n} R_{jk} - \frac{n(m+1)}{2} \right)^2 \tag{17}$$

which under the null-hypothesis is χ^2-distributed with m-1 degrees of freedom.

Wilcoxon Signed-Rank Test

The Wilcoxon signed-rank test is a non-parametric test for comparing the performance of two models over multiple data sets. Under the null-hypothesis, both models perform equally and hence the distribution of the pairwise difference is symmetrical about the value 0. Let d_i denote the difference in performance between the two models for data set number i among n sets when the first model outperforms the second. In case $d_i = 0$, i.e., a tie, one has to exclude observations. Suppose there are an odd number of ties. Then one tie is excluded and half of the remaining ties are included. Suppose there are an even number of ties. Then half of the ties are included. The rank sum R is calculated:

$$R = \sum_{d_i > 0} rank(d_i) + \frac{1}{2} \sum_{d_i = 0} rank(d_i) \tag{18}$$

The test statistic is:

$$z = \frac{R - \frac{1}{4} n(n+1)}{\sqrt{\frac{1}{24} n(n+1)(2n+1)}} \tag{19}$$

which for a large number of samples is approximately normally distributed under the null-hypothesis (Demsar, 2006).

Bonferroni-Holm Method

When making multiple comparisons between pairs of models, the Bonferroni-Holm method (Holm, 1979) can be used to adjust the significance level to control the family-wise Type 1 error, i.e. the probability of making at least one Type 1 error in any of the comparisons (Demsar 2006). Suppose the desired significance level is α. Then, with the Bonferroni method, the corrected significance level is simply $\frac{\alpha}{m}$. However, this is very conservative. Holm (1979) provided a sequentially rejective version of the Bonferroni method that has larger probability of rejecting the false hypothesis. The hypotheses are ordered by their significance levels p_1, p_2,... with $p_1 \leq p_2 \leq ... \leq p_m$. Starting with the most significant p-value, p_1 is compared with $\frac{\alpha}{m}$ and if it is greater than so, the procedure stops and no p-values are significant. If, however, $p_1 \leq \frac{\alpha}{m}$, the corresponding hypothesis is rejected and the second p-value is compared with $\frac{\alpha}{m-1}$. If the corresponding hypothesis is also rejected, the third p-value is compared with $\frac{\alpha}{m-2}$, etc. Hence, p_i is compared sequentially to $\frac{\alpha}{m-i}$ in a step-down procedure that stops when there is failure to reject the hypothesis.

Limitations

The glass included in the investigation was new and in the as-received condition when it was tested. Moreover, the glass was stressed in an ambient atmosphere, typically represented by an indoor temperature of about 20°C and a relative humidity between 40-70%. Only monolithic panes of annealed float glass was considered. Static fatigue was not taken into account in the analysis of the data.

Table 1: List of references which were the basis for an investigation. ULP = Plate bending due to Uniform Lateral Pressure, CDR = Co-axial Double Ring bending, 4PB = Four-Point Bending, 3PB = Three-Point Bending

Reference	No. samples	No. observations	Bending mode
Johar (1981)	9	78	ULP
Johar (1982)	5	106	ULP
Simiu *et al*. (1984)	2	85	CDR
Carre (1996)	5	81	4PB
Calderone (1999)	32	195	ULP
Hess (2000)	3	15	4PB
Fink (2000)	2	127	CDR
Haldimann (2006)	2	20	CDR
Veer *et al*. (2006)	3	32	4PB
Sglavo *et al*. (2007)	8	115	3PB
Veer *et al* (2009)	2	54	4PB
Postigo (2010)*	1	41	CDR
Veer and Rodichev (2011)	2	177	4PB
Veer and Rodichev (2012)	2	60	4PB
Vandebroek *et al*. (2012)	4	77	4PB
Lindqvist (2013)	32	478	4PB
Vandebroek *et al*. (2014)	8	202	4PB
Kozlowski (2014)	1	6	4PB
Kleuderlein *et al*. (2014)	33	830	4PB
Schula (2015)	1	15	CDR
Kinsella and Persson (2016)	2	58	4PB
Muniz-Calvente *et al*. (2016)	2	73	CDR 4PB
Navarrete *et al*. (2016)	8	69	CDR
Yankelevsky *et al*. (2017)	1	56	4PB
Osnes *et al*. (2018b)	3	93	4PB
Total:	173	3143	ULP CDR 3PB 4PB

*Obtained from Huerta *et al*. (2011)

Table 2: Friedman test p-values based on the samples that contained at least 15 observations of the strength

	Edge fail. origins	Surf. fail. origins
p-value	0.0000	0.0104

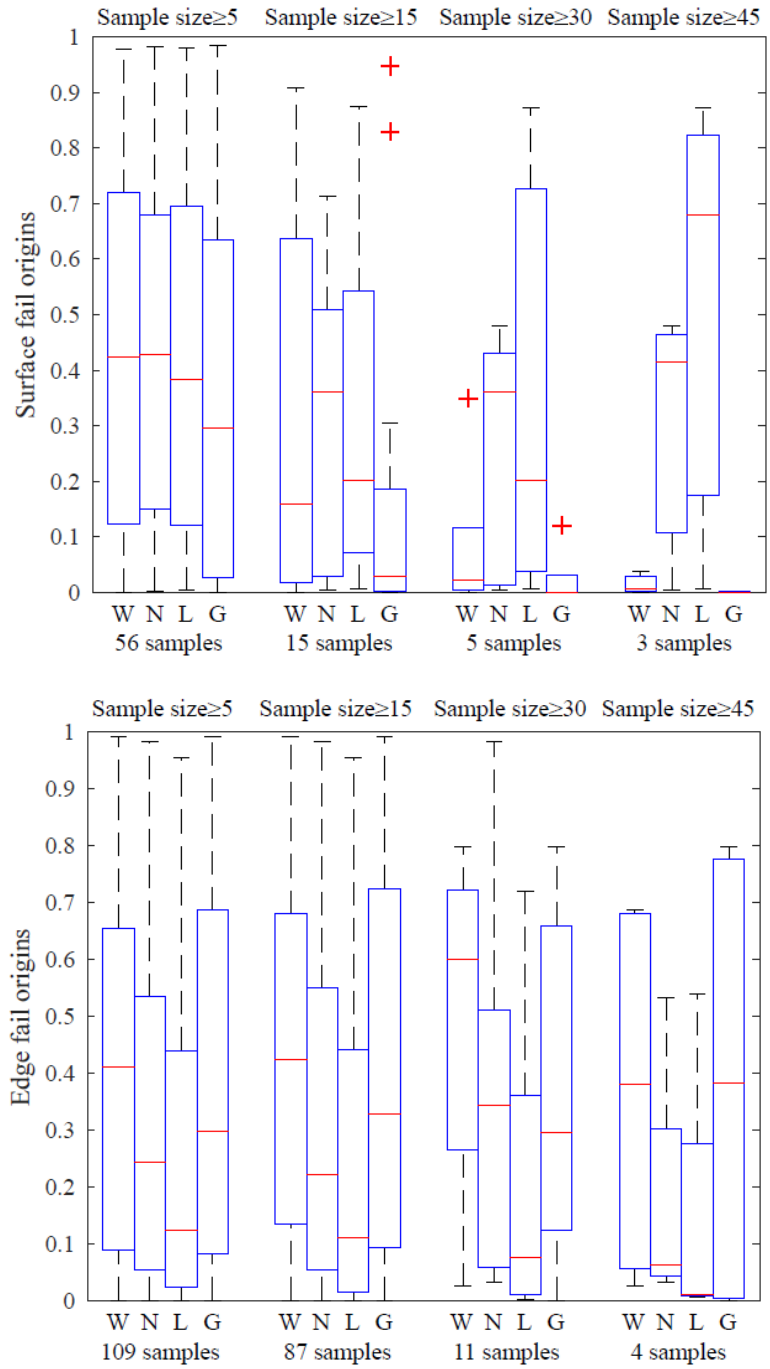

Fig. 2: Boxplots for the p-values from the Anderson-Darling tests that measured the goodness-of-fit of various standard statistical models of the fracture stress of annealed float glass. The results are separated according to the failure origin mode as well as according to the minimum number of observations per sample included in the analysis. W = Weibull, N = normal, L = lognormal and G = Gumbel distribution

Edge fails

W	N	L	G	
	+0.0017 (*)	+0.0000 (*)	+0.0722	W
		+0.0000 (*)	-0.0944	N
			-0.0011 (*)	L
				G

Surface fails

W	N	L	G	
	-0.5995	-0.8040	+0.0166	W
		-0.8904	+0.0256	N
			+0.1205	L
				G

Fig. 3: p-values for the pairwise comparison of model performance with the signed-rank test. (*) indicates that the p-value was significant while controlling for the family-wise type I error. A plus sign in front indicates that the row had a higher rank while a minus sign indicates that the column had a higher rank. Analysis comprises all samples of size 15 or greater. W = Weibull, N = Normal, L = Lognormal and G = Gumbel distribution

Results

The samples from the references in Table 1 which fulfilled the limitations, see Sec. Limitations, were modelled using the normal, lognormal, Gumbel and Weibull distributions. The goodness-of-fit was tested with the Anderson-Darling statistic. The models were fitted in the following three cases, viz. mixed failure origins, edge only failure origins and surface only failure origins. An overview of the performances is provided in Fig. 2 which contains a set of boxplots separated according to the failure origin mode as well as according to the minimum sample size in the analysis. Note that under the null-hypothesis the p-values are uniformly distributed between 0 and 1. Fig. 2 only contains the results from pure edge and surface failures, i.e., not mixed failure origins. Due to the fundamental difference that is apparent in the behaviour between edge and surface failure mode, it is not effective to combine the results in an analysis, see further the Discussion section.

A further investigation was performed based on all samples that included at least 15 observations of the strength, the results of which follow. Similar features were exhibited when the analysis was selected to comprise minimum sample sizes of 30 and 45 observations, respectively. A Friedman test was performed to make multiple comparisons over the data sets and the null-hypothesis was rejected in both cases corresponding to edge only failure origins and surface only failure origins, see further Table 2 for the p-values. Finally, pairwise comparisons were made between the models using the Wilcoxon signed-rank test and the family-wise Type I error was controlled using the Bonferroni-Holm correction method, see Fig. 3. The results show that in the case of edge failure origins, the normal and lognormal distributions did not perform as well as the Weibull distribution. In the case of surface only failure origins, however, none of the pairwise comparisons rendered a statistical significance.

Discussion

The Weibull model has been praised for its utility in a wide range of applications (Weibull, 1959). According to a recent survey (Rinne, 2009), there are a great number of papers and monographs that demonstrate the successful application of the Weibull model in some 180 distinct topics that encompass nearly all scientific disciplines. Part of the reason for the versatility may lie in the fact that the Weibull distribution is one of the three extreme value distributions. It emerges naturally as the limiting distribution of the minimum or maximum value in a sample.

The utility of the Weibull model has been called into question, however, both from within the structural glass engineering community and from outside. As was noted in the Introduction section, certain experiments on glass have indicated that the Weibull model does not perform better than a normal or lognormal distribution. These experiments have included laterally supported plates subjected to uniform loading as well as beams in three-point and four-point bending. However, the fact that the Weibull model does not appear to outperform other standard models may be due to the sample sizes being too limited. In order to illustrate this, consider Fig. 4 which illustrates the results when drawing 1000 random samples from a Weibull distribution with different sample sizes and fitting the standard distributions to the drawn samples. The Weibull parameter values were selected as m = 6 and k = 74 MPa, i.e., the same distribution as was mentioned already in Sec. Standard Distributions. The figure indicates that it may be hard or indeed impossible to distinguish properly between a Weibull model and models based on other standard distributions when the sample sizes are limited. In particular this applies to detecting a difference in performance between the Weibull model with these parameter values and the model based on a normal distribution.

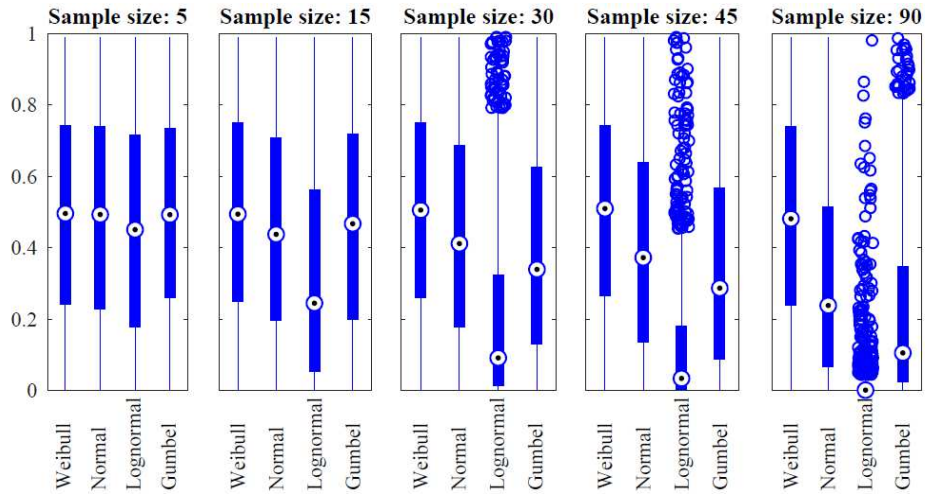

Fig. 4: Simulations of the p-values based on 1000 random samples from a Weibull distribution of varying sample size

From the point of view of structural glass engineering, however, the Weibull model has a logical basis. According to experiments with Hertzian indentation fracture (Poloniecki and Wilshaw, 1971; Poloniecki, 1974), flaw size in glass can be closely fitted by an inverse gamma distribution:

$$f(a) = \frac{r^{n-1}}{(n-2)!} a^{-n} e^{-r/a} \tag{20}$$

which is like a Pareto distribution in the tail. In Sec. Standard Distributions, it was shown that the Weibull distribution can be derived from the weakest-link principle when supposing a Pareto flaw size density function, see Equation 3 to 10. Hence, a strong case can be made for applying the Weibull distribution to model glass strength when the stress state is uniform and uniaxial over each crack (De Jayatilaka and Trustrum, 1977). Notwithstanding, a number of studies have questioned the utility of the Weibull distribution while noting that it does not perform better than a normal or lognormal distribution. In fact, some studies have recommended to abandon the Weibull model altogether and use a normal or lognormal distribution instead. However, when one is unable to distinguish between fitted distributions, preference should be given to the model that has a physical and theoretical foundation, in this case a model that is logically based on fracture mechanics.

In recent attempts to model glass surface fracture in Monte Carlo simulations with distributed Griffith flaws, it was assumed by some researchers that flaw size is governed by a density function that decays like an exponential distribution (Yankelevsky, 2014; Pathirana *et al*., 2017; Osnes *et al*., 2018a; 2018b). Assuming a single population of flaws with a size distribution that decays exponentially would naturally lead to Gumbel-like distributions for the strength in the limit, assuming a uniform and uniaxial stress normal to the crack planes. However, a Gumbel-like distribution for the strength model of the surface of glass is not supported by the empirical data.

In connection with this study, a comprehensive survey of the data on annealed glass strength was performed (Kinsella, 2018). Based on the results it was noted that when taking the whole collection of empirical data into account, the Weibull distribution turns out to be a better model for the strength than the normal and lognormal distributions in the case of edge failure origins. The performance was investigated in a statistical testing procedure and found to be significant, see Fig. 3, with the following exception: The Weibull distribution was not found to be significantly better than a Gumbel distribution. Nevertheless, it is indicated in Fig. 2 and 3 that the Weibull model is at least as good as the Gumbel distribution. The test procedure was based on the Friedman non-parametric method and a post-hoc test with the Wilcoxon signed-rank test. In the case of surface only failure origins, the multiple comparisons using the Friedman test rendered a rejection of the null-hypothesis meaning that it can be concluded that there are significant differences in performance between the four standard models in this case. In fact, the boxplots in Fig. 2 clearly suggest that the extreme value Weibull and Gumbel distributions can be dismissed as a model for the surface strength of glass. However, the number of relevant data samples is limited in the case of surface failure origin data.

The analysis depends on a choice for the minimum sample size to be included. In this study, the main analysis considered samples of size 15 or greater, cf. Fig. 3. It might be argued that even greater sample sizes are needed to distinguish properly between the different models when only a limited or moderate number of samples are available, such as is typically the case in the respective experimental campaigns considered in this study. The dependence on sample size is clearly indicated in Fig. 4 which contains simulation results of the goodness-of-fit while varying the underlying sample size. However, the empirical data only provides a limited number of samples when the sample size is 30 or greater. Nonetheless, the following conclusions can be drawn from Fig. 2 while noting the effect of the minimum sample size upon the results. When all samples are included which contain at least five observations, no particular effect can be seen between the different models for the surface strength. However, as the minimum sample size increases, the Weibull distribution performs poorly while the normal and lognormal distributions appear to perform better. In order to address this phenomenon properly, an investigation was carried out into the properties of the underlying samples. Fig. 5 illustrates the results from this investigation in the form of three diagrams. The top diagram shows the size of surface area in maximum tension as a function of the minimum sample size. The y-axis scaling is logarithmic for the sake of visual clarity. The surface areas were not included in Fig. 5 in the case of laterally supported plates subjected to uniform pressure because of the difficulty associated with assigning a value to the size of surface area in maximum tension. The diagram shows that the whole range of surface sizes are present at the first two levels, i.e., sample sizes greater than or equal to 5 and 15. However, already as the sample sizes are restricted to 15 or greater, the extreme value Gumbel distribution is clearly performing poorly as can be seen in Fig. 2. The extreme value Weibull distribution seems to be performing worse than at the first level, i.e. for sample sizes restricted to 5 or greater. Furthermore, a considerable portion of the whole range of surface sizes is still present at the third level, i.e., for sample sizes restricted to 30 or greater. However, both the extreme value distributions perform poorly as can be seen in Fig. 2. Finally, at the last level, i.e., for sample sizes restricted to 45 or greater, the surface area sizes that remain are the following, viz. approx. 2000, 2400 and 3800 mm^2. The extreme value distributions perform poorly again. The conclusion is that the poor performance of the extreme value distributions cannot simply be explained as a consequence of the surface size converging towards a small size or a large size. In other words, it is not simply the surface size that governs the features of Fig. 2. Next, consider the middle diagram in Fig. 5 which shows the bending modes of the underlying samples. Here, ULP refers to the setup that allows for a uniform lateral pressure to be applied to linearly supported plates, CDR refers to the coaxial double ring bending device, while 3PB and 4PB refer to the three and four-point bending devices, respectively. The diagram shows that both a uniaxial stress state from the four-point bending device and an equibiaxial stress state from the double ring bending device are present at all levels of samples sizes. Hence, the attributes of Fig. 2 cannot be explained as a consequence of the stress state converging towards one or the other configuration. Rather, there is a mixture of stress states present at each level. Next, the bottom diagram in Fig. 5 shows whether the fracture origin was located on the tin side, air side, or whether it was unknown because it was not recorded in the publication. With many of the samples, the publication did not record the configuration of the glass specimens in terms of the tin and air side being in the tension zone. This likely implies that there was a mixture of tin and air side failures. This would be so, because if the experimentor made the effort to identify the tin and air side of each specimen properly and configure them accordingly in the testing device, then this would probably have been recorded or at least mentioned in the ensuing publication. Hence, the conclusion can be drawn that a mixture of tin and air side failures are present at all levels of sample size. This demonstrates that the features of the surface origin failures in Fig. 2 probably cannot be explained as a consequence of the configuration of the test specimens in the testing device with respect to the air or tin side in tension. In other words, it is probably not the case that the fracture origins converge towards either pure tin side or pure air side failures as the sample sizes are restricted to at least 15, 30 and 45, respectively.

The following explanation for the features of the surface origin failures in Fig. 2 is suggested. When the surface condition in glass is considered, there is no single population of flaws that govern the failure because if so were the case, then the Weibull and Gumbel distributions would have performed much better. Hence it is indicated that multiple flaw populations are present on the surface. If the underlying flaw size distribution is governed by multiple unimodal populations which are superposed, it is natural to expect a more symmetrical and “rounded out" shape for the extreme value such as would correspond better with a normal distribution. By the same token, when the minimum sample sizes are small, then it would be logical that the Weibull and Gumbel models perform better because the probability decreases that you sample all the underlying flaw populations hence resulting in a better fit.

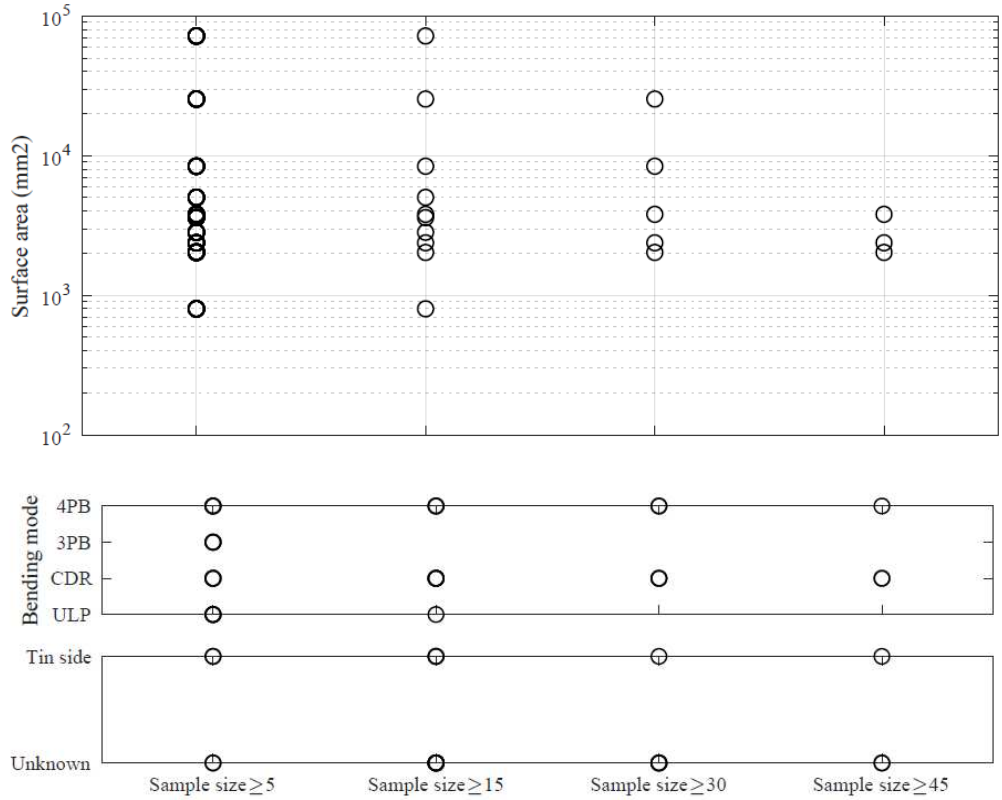

Fig. 5: Properties of the underlying samples that generated the surface origin boxplots in Fig. 2

On the other hand, the generally equal performance of the models in the case of ≤5 sample size may just as well be attributed to small-sample effects, i.e., the difficulty of detecting any effects when the sample sizes are small. Moreover, the fact that the normal distribution performs better when the sample sizes increase should not be taken as argument for adopting this distribution as a model for the surface strength. From a weakest-link perspective, the normal distribution is not suitable. As already mentioned, there may be a logical explanation for the better performance of the normal distribution compared to the extreme value distributions that has to do with the presence of multiple flaw populations.

However, attempts to address the presence of multiple flaw populations may lead to more or less exotic distributions for the flaw size. So far, attempts have been made by Pathirana *et al*. (2017), Kinsella and Persson (2018b) and Pisano and Royer-Carfagni (2017) to model surface failure in glass with a multimodal flaw size distribution approach.

With the edge strength data, the conclusions are different. Here, it is readily seen that the Weibull distribution overall performs better than the normal and lognormal distributions and at least as well as the Gumbel distribution, irrespective of the minimum sample size in the analysis. This indicates that when the edge strength is considered, there is a tendency towards a unimodal flaw size distribution that governs the failure. This may be logical when you consider the mechanical treatment of the edge which undergoes various operations such as scoring and machining. As a comparison, consider when the glass surface is artificially scratched by sandblasting (Blank, 1993; Schula, 2015). Then the result is generally to produce a better Weibull fit compared with the original pristine surface.

In summary then, it can be concluded that the edge and surface condition in glass differ fundamentally. A proper analysis of the strength has then to discriminate between these failure origins. However, it may be that certain kinds of testing device can be used as a proxy for either the edge of the surface condition. In other words, when a given test device produces failures with the majority of one kind, then it may be that this data can be combined without producing significant errors. This proxy-effect has not been quantified in the present study

but it will be considered in a future investigation. In a recent paper (Yankelevsky *et al*., 2018), it was examined whether edge failures should be excluded from the analysis of the data sample that is produced with the four-point bending device with out-of-plane loading or whether they may be included. The examination was based on a reference sample of 83 specimens that were tested in accordance with ASTM C158-02. The results from the investigation were not conclusive with regards the possible proxy-effect of the bending device, nevertheless the authors recommended to exclude edge failures.

The majority of experimental data points included in this investigation pertain to the edge strength of glass. As a matter of fact, the edge strength is of great importance for the strength design of a structural glass component. The edge is thought to contain more weaknesses than the surface, probably due to machining operations done to the edge while scoring, cutting and processing (Veer and Rodichev, 2011; Vandebroek *et al*., 2014). When a laterally supported plate is subject to uniform pressure, significant tensile stresses occur near the edges, see e.g., Kinsella and Persson (2018a) which contains an analysis of the fracture origins in laterally supported plates subject to uniform pressure. For glass beams and pillars, the edges are always subject to significant tensile stress in the design state. Hence, in practical situations the edge strength can hardly be neglected for most types of structural units, including laterally supported plates. Also during handling, transportation and maintenance, the edge is prone to damage. The fact that the Weibull distribution outperforms the normal and lognormal distributions in the case of edge only failure origins is an argument for adopting this model rather than the others.

The lognormal distribution might seem like a better candidate than the normal distribution because the strength is a positive number and the lognormal model lacks support on the left-hand side of the real axis. Nevertheless, a better fit was indicated using the normal distribution.

In summary, the Weibull distribution is recommended as a basic model for the edge strength of glass for reasons of empirical evidence and physics. The empirical evidence is that the Weibull model is generally superior to a normal and lognormal distribution and at least as good as a Gumbel distribution in the case of edge failure origins. For physics-based reasons, the extreme value Weibull and Gumbel models are preferable because they derive from the weakest-link principle and thus harmonize with an essential brittle material concept. In fact, assuming a population of material flaws with a unimodal crack size distribution that is Pareto, F, Cauchy, or t in the tail, the Weibull distribution can be deductively derived from the weakest-link principle. This supposes that the stress state is uniform and uniaxial over each crack. In the case of the normal and lognormal distributions, however, there is no such failure-mechanism basis. However, the Weibull and Gumbel models are unsuited to represent the strength of glass when the fracture originates from the surface.

Finally, there exist numerous strength prediction models for use with glass. For example, Monte Carlo simulations of glass fracture with stochastic Griffith flaws have recently been performed by Yankelevsky (2014), Pathirana *et al*. (2017), Yankelevsky *et al*. (2017), Osnes *et al*. (2018a; 2018b) and Kinsella and Persson (2018b). In such case, no closed form exists for the probability distribution. It could be an interesting future research project to compare the performance of a larger set of models over a comprehensive set of data samples.

Conclusion

Based on a large set of empirical data, the Weibull distribution outperforms the normal and lognormal distributions and is at least as good as a Gumbel distribution as a model for glass strength when the fracture data is selected to comprise edge only failure origins. In the case of surface only failure origins, it is indicated that the normal and lognormal distributions perform better than the extreme value distributions. The analysis of the surface strength is dependent on the sample size. A proper distinction between the tentative models is more straight-forward to make, the greater the sample sizes that are included in the analysis. It is suggested that when the minimum sample size is much smaller than 15 then no distinction is possible to make. The Weibull and Gumbel models have a logical basis in a failure-mechanism that applies to brittle glass behaviour assuming a weakest-link argument. The Weibull model is therefore recommended instead of a normal or lognormal distribution to model glass fracture when the edge strength is considered. The analysis of the surface strength distribution is complicated. This is probably due to the presence of multiple flaw populations. Neither extreme value Weibull or Gumbel nor normal or lognormal distributions are able to properly model the surface strength of glass.

Author's Contributions

David Kinsella: Is the main author of the article and the conceptual designer of the project, the main analysis and the interpretation of data.

Johan Lindström: Contributes to the analysis and interpretation of the data, and with suggestions to the revision of the manuscript.

Kent Persson: Contributes to the conception of the project and to reviewing, writing, and making changes to the manuscript.

Ethics

The corresponding author confirms that all of the other authors have read and approved the manuscript and there are no ethical issues involved.

References

prEN 16612, 2017. Glass in building-determination of the lateral load resistance of glass panes by calculation. CEN.

Beirlant, J., Y. Goegebeur, J. Segers and J. Teugels, 2004. Statistics of Extremes: Theory and Applications. 1st Edn., John Wiley and Sons, ISBN-10: 0471976474, pp: 522.

Benavoli, A., G. Corani and F. Mangili, 2016. Should we really use post-hoc tests based on mean-ranks? J. Mach. Learn. Res., 17: 152-161. https://dl.acm.org/citation.cfm?id=2946650

Blank, K., 1993. Dickenbemessung von Vierseitig Gelagerten Rechteckigen Glasscheiben unter Gleichförmiger Flächenlast. 2nd Edn., Institut fur Konstruktiven Glasbau, Gelsenkirchen.

Calderone, I., 1999. The equivalent wind loading for window glass design. PhD Thesis, Monash University.

Calderone, I., C. MacDonald and L. Jacob 2001. The Fallacy of the Weibull Distribution for Window Glass Design. In: Glass Performance Days, pp: 293-297.

Calderone, I., L. Jacob, J. Ltd and A. Pty, 2005. The Dangers of Using a Probabilistic Approach for Glass Design. In: Glass Performance Days, Tampere, Finland.

Carre, H., 1996. Etude du comportement à la rupture d'un matériau fragile précontraint: Le verre trempé. PhD Thesis, Ecole Nationale des Ponts et Chaussees.

D'Agostino, R.B. and M.A. Stephens, 1986. Goodness-of-Fit Techniques. 1st Edn., CRC Press, ISBN-10: 0824774876, pp: 576.

De Jayatilaka, A. and K. Trustrum, 1977. Statistical approach to brittle fracture. J. Mater. Sci., 12: 1426-1430. DOI: 10.1007/BF00540858

Demsar, J., 2006. Statistical comparisons of classifiers over multiple data sets. J. Mach. Learn. Res., 7: 1-30. https://dl.acm.org/citation.cfm?id=1248548

DIN 18008-1, 2010. Glas im Bauwesen-Bemessungs- und Konstruktionsregeln-Teil 1: Begriffe und allgemeine Grundlagen. CEN.

Fink, A., 2000. Ein Beitrag zum Einsatz von Floatglas als dauerhaft tragender Konstruktionswerkstoff im Bauwesen. PhD Thesis, TU-Darmstadt.

Forbes, C., M Evans, N. Hastings and B. Peacock, 2011. Statistical Distributions. 4th Edn., John Wiley and Sons, Hoboken, ISBN-10: 1118097823, pp: 230.

Friedman, M., 1937. The use of ranks to avoid the assumption of normality implicit in the analysis of variance. J. Am. Stat. Assoc., 32: 675-701. DOI: 10.2307/2279372

Friedman, M., 1940. A comparison of alternative tests of significance for the problem of m rankings. Ann. Math. Stat., 11: 86-92. DOI: 10.1214/aoms/1177731944

Griffith, A., 1920. The phenomena of rupture and flow in solids. Phil. Trans. R Soc. A, 221: 163-198. https://www.jstor.org/stable/91192?seq=1#page_scan_tab_contents

Haldimann, M., 2006. Fracture strength of structural glass elements: Analytical and numerical modelling, testing and design. PhD Thesis, Ecole Polytechnique Federale de Lausanne EPFL.

Hess, R., 2000. Glastrager. Forschungsbericht 20, ETH Zurich. Institut für Hochbautechnik, Zurich, Switzerland.

Holm, S., 1979. A simple sequentially rejective multiple test procedure. Scandinavian J. Stat., 6: 65-70. https://www.jstor.org/stable/4615733?seq=1#page_scan_tab_contents

Huerta, M.C., A. Pacios-Alvarez, M.J. Lamela-Rey and A. Fernandez-Canteli, 2011. Influence of experimental test type on the determination of probabilistic stress distribution. In: Glass Performance Days.

Johar, S., 1981. Dynamic fatigue of flat glass-Phase II. Technical report, Ontario Research Foundation, Department of Metals, Glass and Ceramics.

Johar, S., 1982. Dynamic fatigue of flat glass - Phase III. Technical Report, Ontario Research Foundation, Department of Metals, Glass and Ceramics.

Kinsella, D., 2018. Survey of experimental data on the strength of annealed float glass panes in the as-received condition tested in an ambient atmosphere. Tech. Rep. TVSM-7166, Division of Structural Mechanics, Lund University.

Kinsella, D. and K. Persson, 2016. On the applicability of the Weibull distribution to model annealed glass strength and future research needs. Proceedings of the Challenging Glass Conference 5, (CGC' 16), Ghent, Belgium.

Kinsella, D. and K. Persson, 2018a. An Analysis of Glass Fracture Statistics. Proceedings of the Challenging Glass Conference 6, (CGC' 18), Delft, The Netherlands.

Kinsella, D.T. and K. Persson, 2018b. A numerical method for analysis of fracture statistics of glass and simulations of a double ring bending test. Glass Struct. Eng., 3: 139-152. DOI: 10.1007/s40940-018-0063-z

Kleuderlein, J., F. Ensslen and J. Schneider, 2014. Investigation of edge strength dependent on different types of edge processing. Proceedings of the International Conference at Glasstec, (ICG' 14), Düsseldorf, Germany.

Kozlowski, M., 2014. Experimental and numerical analysis of hybrid timber-glass beams. PhD Thesis, Silesian University of Technology.

Lamon, J., 2016. Brittle Fracture and Damage of Brittle Materials and Composites: Statistical-Probabilistic Approaches. 1st Edn., ISTE Press, London, ISBN-10: 008101161X, pp: 296.

Lindqvist, M., 2013. Structural glass strength prediction based on edge flaw characterization. PhD Thesis, Ecole Polytechnique Federale de Lausanne EPFL.

Lü, B.T., 1997. Fatigue strength prediction of soda-lime glass. Theor. Applied Fract. Mech., 27: 107-114. DOI: 10.1016/S0167-8442(97)00012-8

Mencik, J., 1992. Strength and Fracture of Glass and Ceramics. 1st Edn., Elsevier, New York, ISBN-10: 0444986855, pp: 357.

Muniz-Calvente, M., A. Ramos, F. Pelayo, M.J. Lamela and A. Fernández-Canteli, 2016. Statistical joint evaluation of fracture results from distinct experimental programs: An application to annealed glass. Theor. Applied Fract. Mech., 85: 149-157. DOI: 10.1016/j.tafmec.2016.08.009

Navarrete, B., H. Juarez, L. Olmos, J. Guerrero and P. Garnica, 2016. Failure behavior of annealed glass for building windows. Eng. Struct., 141: 417-426. DOI: 10.1016/j.engstruct.2016.12.050

Osnes, K., T. Börvik and O. Hopperstad, 2018a. Shock tube testing and modelling of annealed float glass. Proceedings of the 12th International DYMAT Conference, (IDC' 18), Arcachon, France.

Osnes, K., O. Hopperstad, T. Börvik, 2018b. Quasi-static and dynamic testing of annealed float glass. Proceedings of the 18th International Conference on Experimental Mechanics, (CEM' 18), Brussels, Belgium.

Pathirana, M., N. Lam, S. Perera, L. Zhang and D. Ruan *et al*., 2017. Risks of failure of annealed glass panels subject to point contact actions. Int. J. Solids Struct., 129: 177-194. DOI: 10.1016/j.ijsolstr.2017.09.001

Pisano, G. and G. Royer-Carfagni, 2017. A micromechanical derivation of the macroscopic strength statistics for pristine or corroded/abraded float glass. J. Eur. Ceram. Soc., 37: 4197-4206.

Poloniecki, J., 1974. Statistical investigation of surface flaws. PhD Thesis, The University of Sussex.

Poloniecki, J.D. and T.R. Wilshaw, 1971. Determination of surface crack size densities in glass. Nat. Phys. Sci., 229: 226-227. DOI: 10.1038/physci229226a0

Postigo, S., 2010. Estudio teorico experimental de impactos humanos contra vidrios de acristalamientos de edificacion. PhD Thesis, Universidad de Politecnica de Madrid.

Rinne, H., 2009. The Weibull Distribution: A Handbook. 1st Edn., CRC Press, ISBN-10: 1420087444, pp: 808.

Schula, S., 2015. Charakterisierung der Kratzanfälligkeit von Gläsern im Bauwesen. 1st Edn., Springer, Berlin, ISBN-10: 3662477823, pp: 406.

Sglavo, V.M., C. Muller and F. Righetti, 2007. Influence of edge finishing on the resistance to thermal stresses of float glass. Glass Performance Days.

Simiu, E., D. Reed, C. Yancey, J. Martin and E. Hendrickson *et al*., 1984. Ring-on-ring tests and load capacity of cladding glass. Tech. Rep., NBS Building Series 162, U.S. Department of Commerce: National Bureau of Standards

Trustrum, K. and A. De Jayatilaka, 1983. Applicability of Weibull analysis for brittle materials. J. Mater. Sci., 18: 2765-2770. DOI: 10.1007/BF00547593

Vandebroek, M., J. Belis, C. Louter and G.V. Tendeloo, 2012. Experimental validation of edge strength model for glass with polished and cut edge finishing. Eng. Fract. Mech., 96: 480-489. DOI: 10.1016/j.engfracmech.2012.08.019

Vandebroek, M., C. Louter, R. Caspeele, F. Ensslen and J. Belis, 2014. Size effect model for the edge strength of glass with cut and ground edge finishing. Eng. Struct., 79: 96-105. DOI: 10.1016/j.engstruct.2014.08.004

Veer, F.A. and Y.M. Rodichev, 2011. The structural strength of glass: Hidden damage. Strength Mater+, 43: 302-315. DOI: 10.1007/s11223-011-9298-5

Veer, F.A., Y.M. Rodichev, 2012. The strength of water jet cut glass. In: Glass Performance Days, pp: 434-438.

Veer, F.A., P.C. Louter and T. Romein, 2006. Quality control and the strength of glass.

Veer, F.A., C. Louter and F.P. Bos, 2009. The strength of annealed, heat-strengthened and fully tempered float glass. Fatigue Fract. Eng. Mater., 32: 18-25. DOI: 10.1111/j.1460-2695.2008.01308.x

Weibull, W., 1939. A statistical theory of the strength of materials. Ingenjörsvetenskapsakademiens handlingar 151.

Weibull, W., 1959. A Statistical distribution function of wide applicability. ASME J. Applied Mechan., 18: 293-297.

Wilcoxon, F., 1945. Individual comparisons by ranking methods. Biometrics, 1: 80-83.

Yankelevsky, D., 2014. Strength prediction of annealed glass plates-a new model. Eng. Struct., 79: 244-255. DOI: 10.1016/j.engstruct.2014.08.017

■■

Yankelevsky, D., K. Spiller, J. Packer and M. Seica, 2017. Fracture characteristics of laboratory-tested soda lime glass specimens. Can. J. Civ. Eng., 44: 151-160. DOI: 10.1139/cjce-2016-0374

Yankelevsky, D., K. Spiller, J. Packer and M. Seica, 2018. Standard testing of glass revisited - experimental and theoretical aspects. J. Test. Eval., 46: 20170221-20170221. DOI: 10.1520/JTE20170221

David Kinsella, Kent Persson

A Numerical Method for Analysis of Fracture Statistics of Glass and Simulations of a Double Ring Bending Test

Glass Structures & Engineering 3(2) (2018) 139–152

Paper B

Glass Struct. Eng.
https://doi.org/10.1007/s40940-018-0063-z

SI: CHALLENGING GLASS PAPER

A numerical method for analysis of fracture statistics of glass and simulations of a double ring bending test

David T. Kinsella · Kent Persson

Received: 15 September 2017 / Accepted: 20 March 2018

Abstract The results from a new numerical method for simulating the strength and fracture locations of small glass specimens subjected to double ring bending are compared with experimental data. The method implements the weakest-link principle while assuming the existence of Griffith flaws. A Weibull distribution for the strength is simulated based on a single population of Pareto distributed crack sizes. The effect of using different fracture criteria is investigated. An alternative distribution is simulated based on two populations of flaws. This distribution models the apparent bimodality in the empirical data set. The numerical method is dependent on a representation of the surface flaws condition in glass. As new techniques become available for examining the surface characteristics, this numerical method is promising as a means for modelling the strength better than current methods do.

Keywords Glass · Strength · Fracture statistics · Stochastic methods

D. T. Kinsella ( ) · K. Persson
Division of Structural Mechanics, Faculty of Engineering
LTH, Lund University, P.O. Box 118, 221 00 Lund, Sweden
e-mail: david.kinsella@construction.lth.se

K. Persson
e-mail: kent.persson@construction.lth.se

1 Introduction

In order to explain and predict the strength of annealed glass a range of concepts and methods have been applied with mixed results. Typically, the strength is explained assuming the existence of Griffith flaws and supposing the weakest-link principle. Predictions are based either on some standard distribution or on tables and diagrams obtained using a modelling tool such as the Glass Failure Prediction Model (GFPM) (Beason and Morgan 1984). There is disagreement among researchers as to which prediction model is the correct one to use (Fischer-Cripps and Collins 1995). A range of experiments have shown a consistent bilinearity in the probability plots when the Weibull distribution is used for modelling the strength of annealed glass (Veer 2007; Veer et al. 2009). As regards the GFPM, it has been said that it "is best suited to representing glass strength for specific test conditions." (Reid 2007) Neither the standard distributions nor the GFPM are able to consistently provide for an acceptable goodness-of-fit while modelling data from experiments, something that is called for in a prediction model with true potential. At the same time, structural glass is gaining in popularity among designers and units are being installed in buildings and public spaces worldwide at an increasing rate. The search for a failure prediction model is therefore as topical as ever. Moreover, a study has indicated that shear stress might affect the observed strength of glass in double ring bending tests (Reid 2007). Shear stress is generally not considered in current failure models

Published online: 30 March 2018

for glass. In this article, a numerical method for predicting the failure of glass is investigated and applied to double ring bending tests. The method is general and can be applied to a range of specimen geometries, loading setups and support conditions. The results are compared with experimental data. The presented method depends on a model that is based on fracture mechanics and the weakest-link principle while assuming a preexisting population of surface cracks. Stress corrosion is not directly considered in this study. The presented method should not be taken as a complete and final strength design tool. The aim is to promote a failure model for glass that is based on a logical and tractable representation of the surface condition in glass with a suitable consideration of the fracture mechanics. With further research, this could in the end lead to an improved strength design tool for use with glass.

2 Background

Flaws in glass are capable of promoting brittle failure due to the lack in capacity for plastic flow. While assuming that the surface contains a large number of minute flaws that act like cracks, so-called Griffith flaws, it is possible to explain the scatter in fracture location observed in experiments. It also helps to explain the variation in failure stress observed and the relatively low strength attained in practice. Surface flaws arise in the production line during manufacture as well as in subsequent handling, transportation, assembly, use, and maintenance. Bulk flaws are disregarded in the following, cf. Bourhis (2008). Griffith (1920) modelled crack growth as a reversible thermodynamical process. For a crack subjected to mode I opening displacement, fracture is governed by the following criterion

$$K_{\mathrm{I}} \leq K_{\mathrm{I}c} \tag{1}$$

where K_{I} is the Stress Intensity Factor (SIF) and $K_{\mathrm{I}c}$ denotes the fracture toughness (Irwin 1957). The value of $K_{\mathrm{I}c}$ for glass has been estimated at about 0.75 MPa $\mathrm{m}^{1/2}$ (Mencik 1992). It is assumed that the individual cracks do not interact with each other. The shape of a surface crack in glass is typically conceived of as being either a long, straight-fronted plane crack or a semi-circular crack (Haldimann 2006). There exist several solutions to the calculation of the SIF for a semi-circular crack subjected to a uniform tensile stress field σ_n oriented perpendicular to the crack plane. According to one solution the SIF at the deepest point on the crack contour is (Newman and Raju 1981)

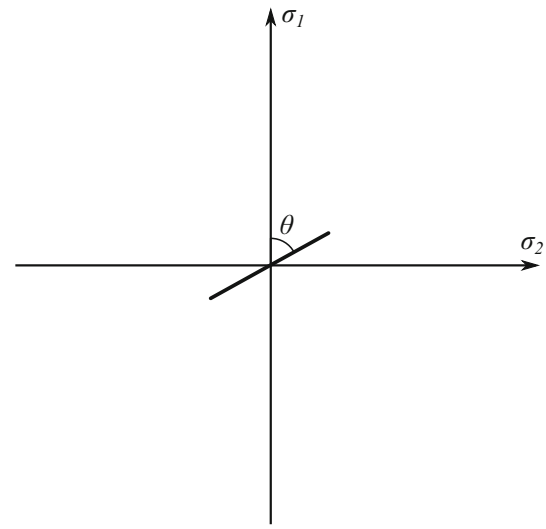

Fig. 1 A plane crack subjected to a biaxial stress field with the crack plane inclined at an angle θ in the coordinate system of the principal stresses σ_1 and σ_2

$$K_{\mathrm{I}} = 1.14 \times \frac{2}{\pi}\sqrt{\pi a} \times \sigma_n \tag{2}$$

where a denotes the crack depth, see also Thiemeier et al. (1991). Figure 1 illustrates a crack subjected to a biaxial stress field with the crack plane inclined at an angle θ in the coordinate system of the principal stresses σ_1 and σ_2. If the crack plane is oriented perpendicular to the Maximum Principal Tensile Stress (MPTS) σ_1 then

$$\sigma_n = \sigma_1 \tag{3}$$

is substituted into Eq. (2). Otherwise, the tensile stress acting normal to the crack plane can be calculated as

$$\sigma_n = \sigma_1 \cos^2\theta + \sigma_2 \sin^2\theta \tag{4}$$

The presence of shear stress does not have any effect in a pure mode I fracture criterion. There exists a range of fracture criteria for a crack subjected to both normal and shear stresses while assuming mode I crack opening and mode II in-plane shearing displacements. One such mixed mode fracture criterion which is based on the maximum non-coplanar energy release rate (Hellen and Blackburn 1975) is given by the following inequality

$$\sqrt[4]{K_{\mathrm{I}}^4 + 6K_{\mathrm{I}}^2 K_{\mathrm{II}}^2 + K_{\mathrm{II}}^4} \leq K_{\mathrm{I}c} \tag{5}$$

where the left-hand side of inequality (5) is a mode I-equivalent SIF, cf. Thiemeier et al. (1991). For a semi-circular crack K_{II} can be approximated as (Thiemeier et al. 1991)

$$K_{\mathrm{II}} = 1.14 \times \frac{4}{\pi}\frac{1}{2-\nu}\sqrt{\pi a} \times \tau \tag{6}$$

In Eq. (6) ν is Poisson's ratio. τ is the shear stress in the crack plane which can be calculated from the in-plane principal stresses as

$$\tau = \frac{1}{2}|\sigma_1 - \sigma_2| \sin 2\theta \tag{7}$$

The idea that you can calculate the distribution of macroscopic strength of a stressed solid by starting from an analysis of the microscopic defects dates back at least to Peirce (1926). Peirce (1926) formulated the Weakest-Link Principle (WLP), i.e. that the strength of a chain is governed by its weakest link, and applied it in the study of the tensile strength of cotton yarn. Also using the WLP, Weibull (1939) came up with the following distribution function for the strength of a brittle solid

$$S = 1 - e^{-B}, \quad B \geq 0 \tag{8}$$

where B, denoted "the risk of rupture", is a function of body size and tensile stress. According to Weibull (1939), a simple mathematical form that is in general accord with experimental data is

$$B = \left(\frac{\sigma}{k}\right)^m, \quad \sigma \geq 0 \tag{9}$$

where k and m denote the scale and shape parameters, respectively. Inserting Eq. (9) into Eq. (8) gives the standard two-parameter Weibull distribution function where k is also the 63rd percentile (Wachtman et al. 2009). Various derivations of the strength distribution function for a brittle solid are offered by e.g. Freudenthal (1968), Matthews et al. (1976), Batdorf and Heinisch (1978), Evans and Jones (1978) and Danzer (1992). In general, the derivation is based on a subdivision of the stressed solid into regions. It is assumed that there exists a population of non-overlapping cracks which are distributed among the regions. Each crack is associated with a critical stress. It is assumed that the stress state varies slowly so that all cracks within a subdivided region are subjected to the same nominal stress. The solution methods, which are analytical, vary. Also varying are certain assumptions, such as whether or not it is supposed that the fracture of the crack depends only on the component of stress normal to the crack plane, whether or not there exist multiple crack populations, etc. Essentially, the analytical expression for the strength distribution is obtained through a limit operation in which the region size shrinks infinitesimally while the number of subdivided regions increases indefinitely. All these solution methods are capable of producing the fundamental Eq. (8). However, the mathematics soon become intractable when all but the simplest assumptions are made for the stress state, fracture criterion, crack size distribution, flaw density, crack plane orientation, and the existence of multiple flaw populations. Yankelevsky (2014) offers a numerical solution method to the problem of determining the strength distribution of a brittle solid while building upon the same general ideas as in the aforementioned studies except that the limit operation is not carried out. In other words, it is not necessary to assume that a crack of some finite size is contained within an infinitesimally small space, cf. Afferrante et al. (2006). Yankelevsky illustrates the method in a study of a glass square plate subjected to bending. He neglects bulk flaws and considers failures starting from the surface area only. The surface area of the plate is subdivided into unit cells measuring 1 cm^2. One crack is distributed into each cell. The flaw size density function proposed by Yankelevsky (2014) and which is motivated for use with glass material can be interpreted as a truncated exponential distribution. The square plate is laterally supported along two opposite edges and subjected to a line-load at midspan producing a uniaxial state of stress in the plane of the tensioned surface. A Monte Carlo simulation is carried out for a large sample of thousands of virtual specimens. This numerical method offers a tractable way of calculating the strength distribution as well as the fracture location distribution for arbitrary stress states, fracture criteria, crack plane orientations, crack size distributions, and multiple flaw populations. However, in Yankelevsky (2014), only a uniaxial tensile stress field is considered where the cracks are stressed normal to their crack planes. Subcritical crack growth is not considered. Nor is the method applied to a double ring bending test which is quite a common and relatively inexpensive method to evaluate the strength of small glass plates (Dalgliesh and Taylor 1990).

Based on Hertzian indentation tests it has been suggested that flaw size in glass can be closely fitted by a Pareto distribution (Poloniecki and Wilshaw 1971; Poloniecki 1974; Tandon et al. 2013). The Pareto distribution has the scale and shape parameters $a_0 > 0$

and $c > 0$ and the distribution function is (Forbes et al. 2010)

$$F(x) = 1 - \left(\frac{a_0}{x}\right)^c, \quad x \geq a_0 \tag{10}$$

It has moreover been shown that the Weibull distribution function is derived from the WLP if it is assumed that the surface flaws condition is represented by a single population of cracks whose size is Pareto distributed in the tail (Jayatilaka and Trustrum 1977). In this view the Weibull shape parameter is a true material parameter. Then, the relation between the shape parameters m and c of the Weibull and Pareto distributions, respectively, is found to be

$$m = 2c \tag{11}$$

When stressed in an ambient atmosphere, glass strength is reduced over time due to a process known as static fatigue which is due to subcritical crack growth, the effects of which are only observed when the mode I SIF lies above a threshold limit value at about 0.25 MPa $\mathrm{m}^{1/2}$ (Wiederhorn and Bolz 1970). In Charles' stress corrosion rate theory (Charles 1958a, b), subcritical crack growth is explained as a thermally activated chemical process whereby water moisture interacts with tensile stress at the crack tip. Equation (12), however, often approximates observed values of subcritical crack growth (Mencik 1992)

$$v = AK_{\mathrm{I}}^n \tag{12}$$

where v is the subcritical crack growth velocity, A is a constant, and n is the stress corrosion parameter. While the value of n was repeatedly estimated at about 16 for soda-lime glass in ambient conditions, the value of A at 50% relative humidity was estimated in a range spanning more than two orders of magnitude, see Schula (2015) for an overview of those experiments. Hence, it is generally challenging to predict subcritical crack growth in ambient conditions.

3 Surface flaws concept

For the representation of the surface flaws condition, we consider two models. The first one comprises a single population of semi-circular edge cracks with a Pareto distributed crack size. The second model comprises a dual population of semi-circular edge cracks with a Pareto and Fréchet distributed crack size, respectively. In both cases, a choice of crack density at 2 cm^{-2} is made. The purpose with the dual population model presented here is to provide a logical basis for a strength distribution with a bimodality. The choice of crack density at 2 cm^{-2} is guided by the following observation. Based on optical scanning techniques applied to a pair of small soda-lime silicate glass plates in the as-received condition there were 632 flaws observed and it was noted that the flaw mean density varied between 1.2 and 2.6 cm^{-2} for flaw sizes greater than approximately 8 microns (Wereszczak et al. 2014).

3.1 Single population model

For the single population model, it is assumed that the cracks are uniformly distributed over the surface area of the original plate and that the crack planes are oriented between $[0, \pi)$ according to a uniform distribution.

The logical basis for the selected choice of single population model are the Hertzian indentation tests that have been carried out in the past (Poloniecki and Wilshaw 1971; Poloniecki 1974; Tandon et al. 2013) and which have provided data that could be closely fitted by a Pareto distribution, see Sect. 2.

3.2 Dual population model

For the dual population model it is assumed that it comprises two populations of semi-circular edge cracks with a Pareto and Fréchet distributed crack size, respectively. All cracks are uniformly distributed over the surface area of the original plate and the crack planes are oriented perpendicular to the MPTS. The Pareto population cracks represent large surface flaws. The Fréchet cracks represent small surface flaws. It is assumed that the number of Pareto cracks is a small fraction of the total number of cracks. It is assumed that the fraction is 0.002.

The logical basis for the dual population model is the following. First, glass fracture statistics tend to produce bimodalities in the probability plots according to e.g. Veer et al. (2009). In fact, the experiment considered in Sect. 5 is no exception because the histogram of the data appears to exhibit two modes, see also Fig. 3. Other researchers have suggested to represent the surface cracks using two populations. Mencik (1992) distinguishes between several populations of surface flaws

according to their origin. In doing so, Mencik (1992) distinguishes between a large flaws and a small flaws population of cracks with relevance for the practical engineering strength of glass. Mencik (1992) characterizes the large flaws population as being responsible for the tensile stress to decrease to 20–60 MPa. Substituting these values into Eq. (2) while assuming that the SIF equals to 0.75 MPa $m^{1/2}$, the corresponding crack depth is found to be 94–850 microns. Mencik (1992) characterizes the small flaws population as containing cracks smaller than a hundredth of a millimeter in depth. He associates this with a strength reduced to 60–200 MPa. Substituting these values into Eq. (2) yields a corresponding crack depth of 8–94 microns. A statistical model for characterizing glass strength when two flaw populations are superimposed due to abrasive phenomena has been proposed in Pisano and Carfagni (2017). Pathirana et al. (2017) implemented a dual population of cracks in a numerical model for the evaluation of the strength distribution in panels subjected to point contact actions. Second, the choice for the value of the fraction of large cracks, i.e. 0.002, is guided by the following observation. Out of the total number of flaws detected in the investigations by Wereszczak et al. (2014), the proportion of large flaws greater in size than or equal to about 200 microns was approximately 0.002. This corresponds with a crack depth of 100 microns assuming that the flaws are semi-circular surface cracks. Taking a crack depth of about 100 microns as a value that separates large flaws from small flaws is through adoption of the line of reasoning in Mencik (1992). Third, the logical basis for the Pareto distribution are the Hertzian indentation tests that have been carried out in the past and which have been mentioned earlier in this paper already. Fourth, the logical basis for the Fréchet distribution is motivated as follows. Assuming that small flaws are exceedingly numerous, one might select only the greatest small flaw in a given region and let this one determine the fracture mechanical behaviour of the small flaws population in that region (Freudenthal 1968). Because it is assumed that the cracks in the small population are abundant, it is supposed that the selected crack plane is oriented approximately normal to the maximum principal tensile stress. If the numerous small flaws have an independent Pareto size distribution then in the limit the largest flaw size is Fréchet distributed (Beirlant et al. 2004). For extreme-value theoretical reasons the greatest flaw size among a large set of flaws whose size is identically and independently distributed is approximately Fréchet distributed if the following holds (Horst 2009); the sampled distribution has a range which is unlimited from above and its distribution function F is such that there exist some positive numbers k, A such that

$$\lim_{x\to\infty} x^k(1 - F(x)) = A \tag{13}$$

Hence, the Pareto distribution lies in the domain of attraction of the Fréchet distribution (Beirlant et al. 2004).

4 Numerical modelling tool

Here follows a description of a numerical modelling tool for the strength of glass plates in bending based on an implementation of the weakest-link principle and some concept for the surface flaws condition. The numerical method adopted in this study is based on the Monte Carlo simulation method carried out by Yankelevsky (2014). The most important difference between the present study and Yankelevsky (2014) is that the present study considers multiple flaw populations with arbitrary crack plane orientations and a mixed mode fracture criterion.

Float glass is usually produced and shipped in a standard size so-called jumbo plate with the dimensions 3.21×6.00 m^2. Taking the standard jumbo plate as a starting point, the plate is subdivided into unit cells of 1 mm^2. This cell size provides a reasonable compromise between resolution and computational cost. A set of flaws are randomly scattered across the cells according to a uniform distribution, although in general another spatial distribution could be adopted. It is supposed that the stochastic orientation of the crack planes is uniformly distributed. This assumption might not be conservative, however, if there is a tendency for the flaws to lie in some particular direction due to e.g. machining abrasion or contact with the rollers during manufacture. The total number of flaws on the jumbo plate is fixed and depends on the flaw density. It is assumed that the flaw density is 2 cm^{-2} yielding a total of 385,200 flaws on either face of the plate. Each flaw is independently assigned a size based on some statistical distribution function which depends on the particular flaws concept that is adopted. The random flaws are resampled in each new simulation of the jumbo plate.

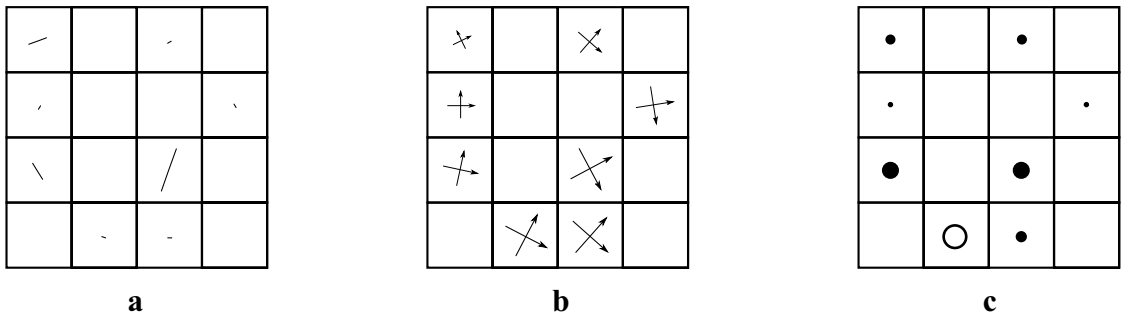

Fig. 2 Main steps leading up to the creation of the SIF envelope. **a** Random flaws are sampled and located across the unit cells. **b** The bending stresses are determined and compared with the flaws. **c** The resulting SIFs with magnitudes illustrated by discs are calculated based on one of the fracture criteria. The large white disc represents the critical event that the SIF exceeds the fracture toughness

The stochastics of the flaws are the location, the orientation in the plane, and the size. Next, a specimen of given dimensions is extracted and separated from the jumbo plate. In the following the cut out specimen is analysed.

The cut out specimen is subjected to an arbitrary loading in increments and the stress field history at the centre of each flaw-containing unit cell determined. It is supposed that the load type is such that tensile stress actually develops on the face of the cut out specimen otherwise failure will not be detected based on fracture mechanics. In general the stress response is non-linear. The loading increment is chosen so as to produce a tensile stress increase of no more than 1 MPa per increment anywhere on the specimen. However, if the response is linear then it suffices with one increment and to scale the results. The complete stress history needs only to be calculated once for a given loading type and specimen geometry because the stochastics of the cracks do not affect the distribution of nominal bending stresses. It is assumed that the sum of load increments is sufficiently large in relation to the given flaw characteristics, i.e. flaw density, flaw size distribution, etc., to prompt fracture. Otherwise, failure might not have been detected by the end of the last load increment. There exists a SIF envelope that meets with the fracture toughness at some point in time, the smallest of which is identified as the time of failure. If the crack planes are always oriented perpendicular to the MPTS then the SIF envelope is calculated using Eqs. (2) and (3). For reference, this case is denoted MPTS mode I fracture criterion. If the crack planes are inclined at an oblique angle in the coordinate system of the principal stresses while mode I opening displacement is considered then the SIF envelope is calculated using Eqs. (2) and (4). This case is denoted oblique angle mode I fracture criterion. If both mode I opening and mode II shearing displacements are accounted for then the SIF envelope is calculated using the left-hand side of inequality (5). This is the mixed mode fracture criterion. By token of the WLP, the fracture origin is determined from the first unit cell that contains a flaw with a SIF exceeding the fracture toughness. A search algorithm is used to detect this cell. By carrying out simulations on a whole series of cut out specimens it is possible to obtain a sample of the fracture stress which is defined as the MPTS at the failure origin. In this study the number of cut out specimens in a simulation series is 5,000. This sample size offers a reasonable compromise between precision and computational cost. Figure 2 illustrates the main steps leading up to the creation of the SIF envelope; (a) the flaw stochastics are sampled, (b) the in-plane principal stresses are determined at each load increment and (c) the SIF envelope is calculated per load increment based on either of the fracture criteria. Failure is prompted at the first instance of intersection between SIF envelope and fracture toughness (white disc). Likewise, the failure origin is determined by the first unit cell that contains a SIF which exceeds the fracture toughness. The so-called critical stress is the uniform tensile stress perpendicular to a given crack plane that would bring about failure with a pure mode I fracture criterion. The critical stress can be calculated with Eqs. (1) and (2).

5 Experimental data comparison

Double ring bending tests are frequently carried out to evaluate the strength of glass. In this testing device a glass plate is supported on a reaction ring and subjected to an applied loading through a smaller concentric ring on its opposite side. An equibiaxial state of stress is produced within the loading ring. Failures that start from edges are eliminated because tensile stress diminishes near the edges. Some experimenters discard any observation associated with a failure originating from outside the loading ring radius. Simiu et al. (1984) carried out experiments on 56 small square glass plates in double ring bending. The plates had the nominal dimensions $179 \times 179 \times 6$ mm^3. The mean thickness was 5.4 mm. The glass was new in the as-received condition and it had been obtained from the same manufacturer and batch. The loading ring radius was 25.4 mm and the segmented reaction ring radius 60.3 mm. All specimens were subjected to ramp loads that generated an average rate of stress of 0.8 MPa/s inside the loading ring. The load-duration until failure ranged from 48 to 117 s. It is not known whether it was the tin side or air side of the glass plates that was subjected to tensile stress. The tin side is defined as the side of the glass that was in contact with the molten tin bath in the float process production method.

This experiment is selected for a number of reasons. The data report is complete with values for the fracture stress even when the failure originated from outside the loading ring. Because Simiu et al. (1984) reported the fracture locations it is possible to make comparisons with the simulated failure origin data. The data is challenging to model. A Weibull distribution for the strength can be rejected, cf. Sect. 6.1. The modelling of the surface flaws condition is simplified when edge failures are eliminated.

Using a formula for a flat circular plate of constant thickness, Simiu et al. (1984) calculated the in-plane MPTS for each fractured specimen. The stress was calculated at the centre of the plate, even when the fracture origin was not located within the loading ring radius. Twelve of the data points, however, were associated with failures originating from outside the loading ring. Those values have been readjusted by this author in order to reflect the MPTS at the actual failure location rather than the MPTS inside the loading ring. The adjustments were made based on finite element calculations with the computer software ABAQUS/CAE (2013). The loading rings were modelled by analytic rigid surfaces. The glass part was modelled with 20-node quadratic solid elements with reduced integration, although it would also be possible to use continuum shell elements. The number of through-the-thickness elements was 5 and the number of elements in the plane was about 9500. Only a quarter of the plate was modelled for symmetry reasons. It was assumed that Young's modulus is 70 GPa and Poisson's ratio is 0.23 (Bourhis 2008). A friction coefficient of 0.1 was used in modelling the contact between loading ring and glass parts.

6 Results

Virtual glass specimens were tested until failure in double ring bending and the results were compared with data from the experiment conducted by Simiu et al. (1984). The analysis was carried out using the software ABAQUS/CAE (2013) and MATLAB (2016). The following cases were investigated, viz. a single population of Pareto distributed flaw sizes using either the MPTS mode I fracture criterion or oblique angle mode I criterion or the mixed mode criterion, and a two-population concept for the flaw sizes using only the MPTS mode I fracture criterion.

6.1 Single population of flaws

A fracture stress distribution was simulated based on the oblique angle mode I fracture criterion, cf. Eqs. (1), (2) and (4) while supposing that the surface condition is characterized by a single population of Pareto distributed flaw sizes. This is illustrated in Fig. 3a and the values shown are the MPTS at the failure origins. The histogram in Fig. 3a is normalized so as to reflect a probability density function. The area of each bar is the relative number of observations. The total sum of the bar areas is less than or equal to 1 depending on whether or not some of the data lies outside the bin limits. The sampled distribution was compared with a Weibull distribution and the goodness-of-fit was tested using the Anderson–Darling (AD) statistic (D'Agostino and Stephens 1986). No significance was obtained in a test at the 5% level. The simulated distribution appears to be indistinguishable from a Weibull distribution. An ordinary Weibull distribution was fit-

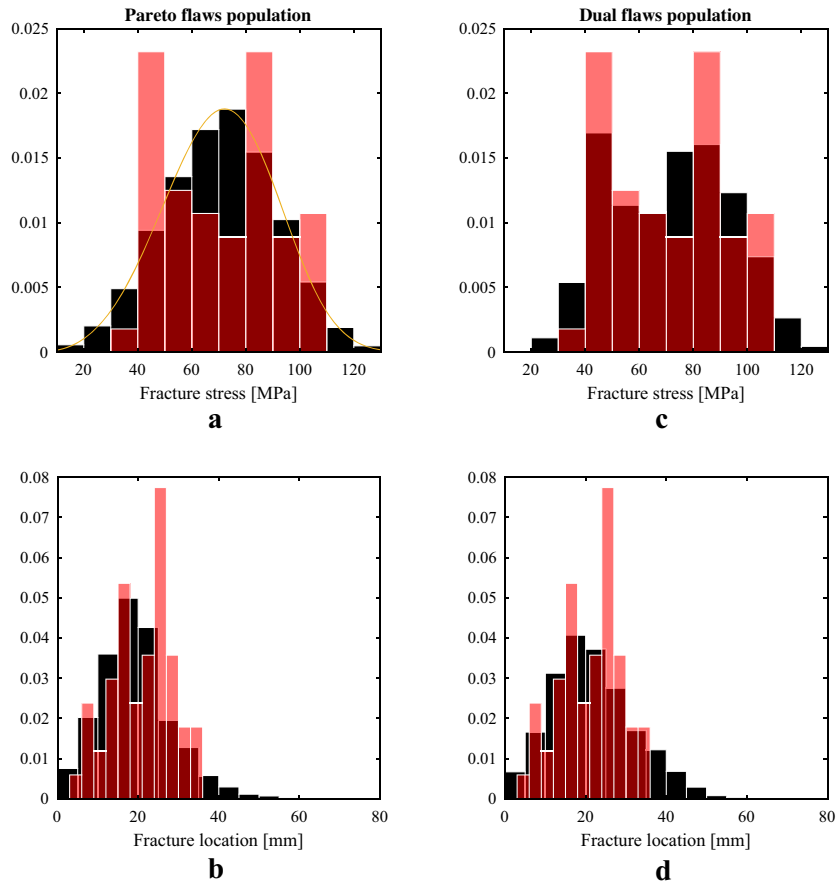

Fig. 3 Simulated and empirical fracture stress and failure location distributions. Semi-transparent (red) histograms represent the empirical data. Opaque (black) histograms represent the simulated data. Overlapping histograms are dark red. Sturges binning method was used for the simulated data sets

ted to the empirical data set using the maximum likelihood method and the estimated parameter values were $k = 78$ MPa and $m = 3.8$. Using the AD statistic it could be rejected at the 0.4% level that the empirical data set is Weibull distributed. The simulated distribution was optimized so as to match the ordinary Weibull model which was fitted to the empirical data. The optimization was carried out by varying the underlying Pareto distribution parameters until the simulated strength distribution was similar to the Weibull distribution that was fitted to the empirical data. The similarity was measured by fitting a Weibull distribution to the simulated sample and comparing the so fitted Weibull parameters with the parameter estimates of the Weibull model that was fitted to the empirical data set. See Fig. 3a where both the empirical data set (red bars), the fitted Weibull density function (solid line) and the simulated distribution (black bars) are illustrated.

Table 1 Pareto parameter values that generated an estimated Weibull distribution with the scale and shape parameters $k = 78$ MPa and $m = 3.8$ while using the numerical method

Fracture criterion	Scale param. (μm)	Shape param.
MPTS	8.4	2.34
Oblique angle	8.3	2.13
Mixed mode	8.8	2.26

The strength distribution was further simulated using the MPTS mode I criterion and the mixed mode criterion. The Pareto parameters were selected so that the strength distribution could be fitted by a Weibull distribution with scale and shape parameters $k = 78$ MPa and $m = 3.8$. Table 1 contains the Pareto parameter values so far discussed according to the three fracture criteria.

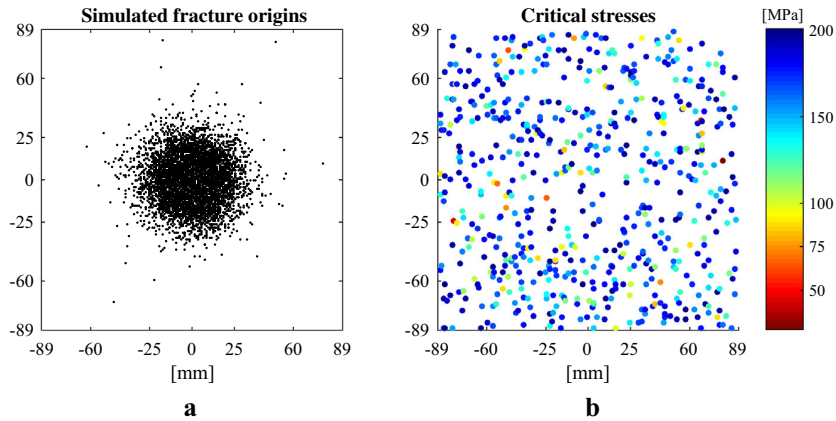

Fig. 4 Left: Simulated fracture locations. Right: Critical stresses in a single cut out specimen

In Fig. 3b the simulated fracture locations in the radial direction are shown together with the empirical for the oblique angle mode I case. Using a two-sample AD test (Scholz and Stephens 1987; Trujillo et al. 2007), a significant deviation between the pair of data sets could be detected. The spatial distribution of failures is further illustrated in Fig. 4a.

The critical stresses in a single cut out specimen are obtained by solving for σ_n in Eq. (2) after substituting for the fracture toughness value in Eq. (1) as illustrated in Fig. 4b.

Considering the various fracture criteria, the following was noted while using identical Pareto parameter values for generating the strength distribution. The mode I fracture criterion in the oblique angle case produced only a very small difference in the strength data sample compared with the mixed mode criterion, cf. Eqs. (1), (2), (4) and (5). The 63rd percentiles deviated by less than 3%. However, taking mode II shearing displacement into consideration increased the proportion of failures originating from outside the loading ring by 20%. Comparing the flaw-orientation independent MPTS mode I criterion, Eqs. (1), (2) and (3), with either of the two other criteria yielded a significant difference in the data samples; the 63rd percentile of the simulated strength was more than 10% lower while using the MPTS case. The proportion of failures originating from outside the loading ring increased by over 60%. The results are illustrated in Fig. 5.

6.2 Two populations of flaws

It is possible to obtain a simulated distribution like the one shown in Fig. 3c while assuming that the flaws originate from two different populations, see Sect. 3. The flaw model parameters are given in Table 2. The resulting distribution could not be distinguished from the empirical data set with any statistical significance at the 5% level judging from the two-sample AD test statistic ($p = 0.64$). In Fig. 3d the simulated fracture locations are shown together with the empirical. It was found using the same test statistic that a significant departure exists from the hypothesis that the experimental and simulated fracture location data sets come from equal distributions.

7 Discussion

Providing for consistency in a glass failure prediction model calls for its foundation to be laid on physically sound concepts such as the WLP. The WLP captures an essential feature of brittle material failure. The existence of Griffith flaws is another physical concept to build upon. The Weibull distribution implements the WLP which makes it an attractive choice for a glass failure prediction model, at least from a theoretical point of view. All major standards including the European draft of a Eurocode of glass acknowledge Weibull's Eq. (8) in one form or another (prEN 16612:2013). A number of studies, however, have indicated that the Weibull distribution does not provide a superior fit compared with a lognormal or normal distribution (Lü 1997; Calderone et al. 2001; Veer et al. 2009; Huerta et al. 2011; Kinsella and Persson 2016). It has been noted that the estimated value of the Weibull shape parameter varies quite significantly from one sample to another in experiments (Ritter et al. 1985; Carre 1996; Huerta et al. 2011). Some researchers have called for abandoning

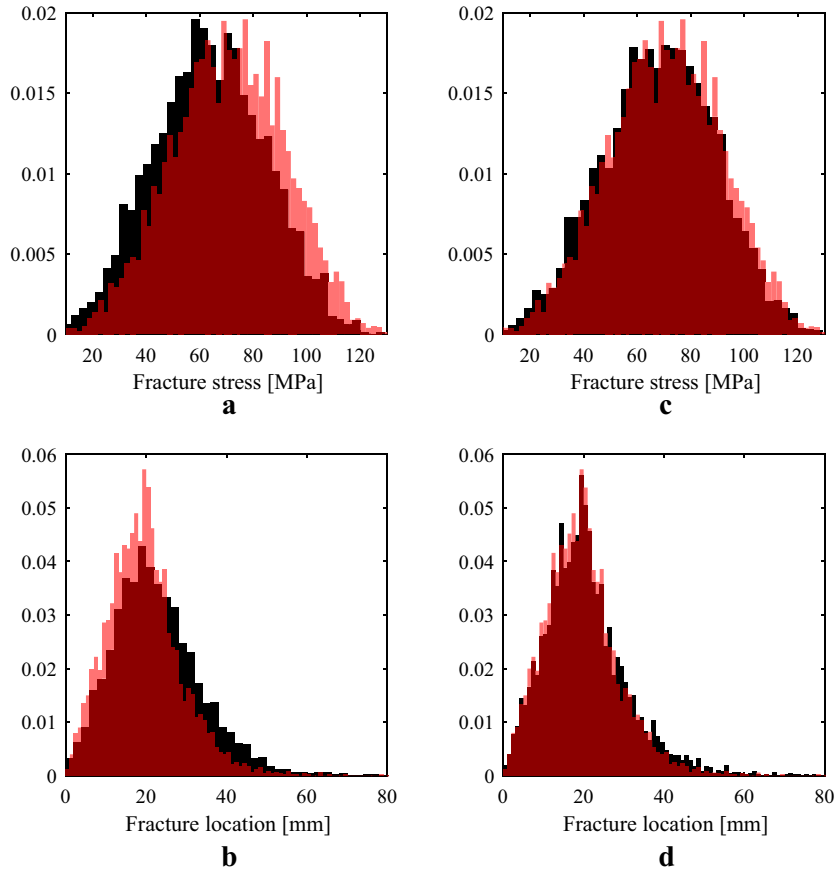

Fig. 5 Left: Oblique angle versus MPTS mode I fracture criterion. Right: Oblique angle mode I versus mixed mode fracture criterion. Semi-transparent (red) bars indicate the oblique angle mode I data. Overlapping histograms are dark red

Table 2 Pareto and Fréchet parameter values used in the dual population model that was implemented with the numerical method

Pareto		Fréchet	
Scale (μm)	Shape	Scale (μm)	Shape
130	4.0	11	3.0

the Weibull model altogether in favour of a normal or lognormal distribution (Calderone et al. 2001). But to adopt a normal distribution in this case is to favour with a model lacking in failure-based physical concept. In contrast, by using the numerical method in this paper it is possible to keep intact the WLP as well as the Griffith flaws assumption while producing data fits equal or superior to the Weibull model. Figure 3a illustrates that it is possible to simulate a Weibull distribution using this numerical tool while assuming that the surface flaws are sampled from one single population of Pareto distributed sizes. In keeping with recent experimental findings using optical scanning techniques, cf. Wereszczak et al. (2014), it was assumed that the flaw density is 2 cm^{-2}. From a theoretical point of view, the shape parameter of the simulated Weibull distribution should relate with the Pareto shape parameter according to Eq. (11) if the stress state is uniform uniaxial. At any rate, the Weibull distribution doesn't actually model the experimental data that was compared with.

While exploring the possibility of implementing two flaw populations, the idea is to distinguish between one large flaws population of flaws greater in depth than about 100 microns and one smaller flaws population. An idea along a similar line was proposed by Mencik (1992), cf. Sect. 3. The purpose is to model the bimodality that is frequently encountered in the strength distribution from practical experiments. Turning to Fig. 3c it is evident that an acceptable fit can be achieved with

Table 3 Weibull shape parameter estimates from 16 experiments on new annealed glass plates in double ring bending, tested in ambient conditions

Reference	Load. ring diam. (mm)	Approx. stress rate (MPa/s)	Sample size	Weib. shape param.
Peeken (1982)[a]	600	2	97	10.1
Peeken (1982)[a]	600	2	99	11.3
Simiu et al. (1984)	51	0.8	56	4.0
Simiu et al. (1984)	51	1.0	29	3.6
Mellmann and Maultzsch (1989)[a]	600	2	113	5.1
Mellmann and Maultzsch (1989)[a]	600	2	108	3.9
Fink (2000)	55	2	20	3.5
Fink (2000)	55	2	107	5.9
Overend (2002)	51	0.7	10	2.4
Overend (2002)	51	0.9	10	1.8
Overend (2002)	51	0.6	10	4.9
Haldimann (2006)	51	0.2	10	3.7
Haldimann (2006)	51	21	10	4.2
Postigo (2010)[b]	180	2.4	41	2.9
Schula (2015)	80	2	15	7.8
Muniz et al. (2016)	60	2	28	4.5

[a]Obtained from Sedlacek et al. (1999)
[b]Obtained from Huerta et al. (2011)

a two-population flaws concept. Moreover, this fit is at least as good as the fitted Weibull model in Fig. 3a as can be seen by comparing the p-values from the AD tests. Moreover, the tail of the distribution is important when calculating the design value. Therefore, when choosing between the simulated distributions as seen in Fig. 3a and c, as a matter of fact, the ordinary Weibull distribution appears to provide the most conservative approach.

With a two-parameter Weibull distribution, only two parameters are fitted to the data. With the numerical model presented in this paper, the Pareto and Fréchet distributions each require two parameters. As the number of parameters increase, it is only logical that a better fit might be produced. Therefore, the outcome while comparing Fig. 3a with c is rather predictable. However, if it were possible to estimate some of the surface flaw parameters a priori, the numerical modelling tool would gain in potential. Then, these parameter estimates would be based on the material physics. There is a need for more data on the surface flaws condition in glass. Up to date, the published data is scarce. As new techniques become available for examination and assessment of the surface condition in glass, more reliable input data will likely become available for use in this kind of numerical prediction tool.

Moreover, with this numerical tool it is possible to simulate the distribution of fracture locations. The simulations were not quite able to model the empirical distribution of fracture location. This is due to the lower mean value in the simulations as well as the longer tail, cf. Fig. 3b and d. However, it may also be due to the fact that a large number of fractures in the empirical data set occured at the loading ring contact circle. About one in five specimens failed under the loading ring. This could have an impact not only on the failure location statistics but also on the fracture stress statistics.

The Weibull shape parameter value that was estimated based on the double ring bending experiment carried out by Simiu et al. (1984), i.e. $m = 3.8$, might indicate a high dispersion for the experimental data because the value is quite low. The data refers to an experimental campaign carried out almost 40 years ago. In order to investigate the dispersion, a table was organized, cf. Table 3, which contains the estimated Weibull shape parameter values from a range of experiments with the double ring bending device. All listed items in Table 3 refer to experiments on new, annealed glass that was tested in ambient conditions. The experiment carried out by Simiu et al. (1984) is included in Table 3 where the estimated shape parameter value was based

on the original data, unadjusted with respect to the true stress at the fracture origin, see also Sect. 5. The results found in Table 3 show clearly that there appears to be nothing unusual about the estimated Weibull shape parameter value in the experimental data of Simiu et al. (1984). However, it is possible that the estimated shape parameter values in Table 3 were affected by the following circumstances. The table comprises both the results from glass tested with the tin side in tension and glass tested with the air side in tension. It has been noted that some experiments with the double ring bending device generate a substantial number of fractures near the loading ring contact area, see e.g. Simiu et al. (1984).

Reid (2007) studied the proportion of failures occuring inside and outside the loading ring in coaxial double ring bending tests and compared the observed results with what might be expected based on theoretical considerations using Weibull statistics. He found that a series of 59 small specimens of annealed plates 6 mm in thickness produced anomalous results. The proportion of failures occuring outside the loading ring was substantially greater than expected. Reid hypothesized that this might be related to the glass having to withstand shear stresses outside the loading ring. Due to the equibiaxial state of stress within the loading ring, shear stresses are not present there. Our results show that if a uniformly distributed flaw orientation is considered in the fracture criterion, then there is a significant effect on the observed proportion of failures originating from outside the loading ring while taking mode II shearing displacement into consideration. The proportion increases by 20% with the mixed mode failure criterion. However, disregarding flaw orientation altogether in the fracture criterion, i.e. considering only the MPTS, yields the highest proportion of failures originating from outside the loading ring. Our results are therefore not conclusive with respect to Reid's hypothesis. It depends on whether or not it is assumed that flaw orientation matters. More experiments need to be carried out in order to verify or disprove this hypothesis while taking note of the fracture statistics of failures occuring outside the loading ring.

Although the simulations are more time-consuming than fitting a standard statistical distribution, significant improvements in computational efficiency can certainly be made. There is mounting evidence in the literature, see e.g. Veer (2007), that the fitted models for glass fracture data in general are lacking in potential when using a standard distribution such as the Weibull or Normal distributions. The present study was undertaken in order to explore a novel approach towards the failure prediction of glass. In order to further validate this method, more experiments could be carried out and the surface condition of glass should be investigated further.

The effects of stress corrosion on the strength of glass were neglected in this study. In a future paper, the implementation of subcritical crack growth into the numerical method will be considered.

8 Conclusions

Using a numerical simulation tool based on the weakest-link principle and assuming the existence of Griffith flaws it is possible to simulate a Weibull distribution for the strength of glass. The incorporation of mode II shearing displacement into the fracture criterion has only a very small impact on the simulated strength distribution when the glass is subjected to double ring bending. In the case of small plates in double ring bending where edge failures can be neglected, it is feasible to model the strength based on a large-flaws and a small-flaws concept while capturing a bimodality in the data set. There is a need for more knowledge and data on the surface condition in glass.

Compliance with ethical standards

Conflict of interest On behalf of all authors, the corresponding author states that there is no conflict of interest.

References

ABAQUS/CAE Version 6.13: Dassault Systèmes (2013)

Afferrante, L., Ciavarella, M., Valenza, E.: Is Weibull's modulus really a material constant? Example case with interacting collinear cracks. Int. J. Solids Struct. **43**, 5147–5157 (2006)

Batdorf, S.B., Heinisch, H.L.: Weakest link theory reformulated for arbitrary fracture criterion. J. Am. Ceram. Soc. **61**(7–8), 355–8 (1978)

Beason, W., Morgan, J.: Glass failure prediction model. J. Struct. Eng. **110**, 197–212 (1984)
Beirlant, J., Goegebeur, Y., Teugels, J., Segers, J., De Waal, D., Ferro, C.: Statistics of Extremes: Theory and Applications. Wiley, Hoboken (2004)
Calderone, I., MacDonald, C., Jacob, L., Jacob Associates Pty Ltd: The fallacy of the Weibull distribution for window glass design. In: Glass Performance Days, vol. **2001**, pp. 293–297 (2001)
Carre, H.: Etude du comportement à la rupture d'un matériau fragile précontraint: le verre trempé. Ph.D. Thesis, Ecole Nationale des Ponts et Chaussées (1996)
Charles, R.: Static fatigue of glass. I. J. Appl. Phys. **29**, 1549–1553 (1958a)
Charles, R.: Static fatigue of glass. II. J. Appl. Phys. **29**, 1554–1560 (1958b)
D'Agostino, R.B., Stephens, M.A. (eds.): Goodness-of-fit Techniques. Marcel Dekker Inc, New York (1986)
Dalgliesh, W., Taylor, D.: The strength and testing of window glass. Can. J. Civ. Eng. **17**, 752–762 (1990)
Danzer, R.: A general strength distribution function for brittle materials. J. Eur. Ceram. Soc. **10**, 461–472 (1992)
Evans, A., Jones, R.: Evaluation of a fundamental approach for the statistical analysis of fracture. J. Am. Ceram. Soc. **61**, 156–160 (1978)
Fink, A.: Ein beitrag zum einsatz von floatglas als dauerhaft tragender konstruktionswerkstoff im bauwesen. Ph.D. Thesis Technische Universität Darmstadt (2000)
Fischer-Cripps, A., Collins, R.: Architectural glazings: design standards and failure models. Build. Environ. **30**, 29–40 (1995)
Forbes, C., Evans, M., Hastings, N., Peacock, B.: Statistical Distributions, 4th edn. Wiley, Hoboken (2010)
Freudenthal, A.: Statistical Approach to Brittle Fracture, Fracture, vol. II. Academic Press, New York (1968)
Griffith, A.: The phenomena of rupture and flow in solids. Philos. Trans. R. Soc. A **221**, 163 (1920)
Haldimann, M.: Fracture Strength of Structural Glass Elements: Analytical and Numerical Modelling, Testing and Design. Ph.D. Thesis, Ecole Polytechnique Fédérale de Lausanne EPFL (2006)
Hellen, T., Blackburn, W.: The calculation of stress intensity factors for combined tensile and shear loading. Int. J. Fract. **11**, 605 (1975)
Horst, R.: The Weibull Distribution: A Handbook. Taylor & Francis Group, London (2009)
Huerta, M.C., Pacios-Alvarez, A., Lamela-Rey, M.J., Fernandez-Canteli, A.: Influence of experimental test type on the determination of probabilistic stress distribution. In: Glass Performance Days 2011 (2011)
Irwin, G.: Analysis of stresses and strains near the end of a crack traversing a plate. J. Appl. Mech. **24**, 361 (1957)
Jayatilaka, A., Trustrum, K.: Statistical approach to brittle fracture. J. Mater. Sci. **12**, 1426–1430 (1977)
Kinsella, D., Persson, K.: On the applicability of the Weibull distribution to model annealed glass strength and future research needs. In: Challenging Glass Conference, vol. 5 (2016)
Le Bourhis, E.: Glass. Wiley-VCH Verlag GmbH & Co KGaA, Weinheim (2008)
Lü, B.T.: Fatigue strength prediction of soda-lime glass. Theor. Appl. Fract. Mech. **27**, 107–114 (1997)
MATLAB Version 9.1 (R2016b). The MathWorks Inc (2016)
Matthews, J., McClintock, F., Shack, W.: Statistical determination of surface flaw density in brittle materials. J. Am. Ceram. Soc. **59**, 304–8 (1976)
Mellmann, G., Maultzsch, M.: Untersuchung zur ermittlung der biegefestigkeit von flachglas für bauliche anlagen. BAM-Forschungsbericht 161, Bundesanstalt für Materialforschung und -prüfung, Berlin (1989)
Mencik, J.: Strength and Fracture of Glass and Ceramics, Glass Science and Technology, vol. 12. Elsevier, Amsterdam (1992)
Muniz-Calvente, M., Ramos, A., Pelayo, F., Lamela, M., Fernández-Canteli, A.: Statistical joint evaluation of fracture results from distinct experimental programs: an application to annealed glass. Theor. Appl. Fract. Mech. **85**(Part A), 149–157 (2016)
Newman, J., Raju, I.: An empirical stress intensity factor equation for the surface crack. Eng. Fract. Mech. **15**, 185–92 (1981)
Overend, M.: The Appraisal of Structural Glass Assemblies. Ph.D. Thesis, University of Surrey (2002)
Pathirana, M., Lam, N., Perera, S., Zhang, L., Ruan, D., Gad, E.: Risks of failure of annealed glass panels subject to point contact actions. Int. J. Solids Struct. **129**, 177–194 (2017)
Peeken, H.: Bruchfestigkeitsuntersuchungen an quadratischen floatgläsern der kantenlänge 1000 mm nach der doppelringmethode mit überlagertem gasdruck. Bericht Nr. 10-82, Institut für Maschinelemente und Maschinengestaltung der RWTH Aachen, Aachen (1982)
Peirce, F.: Tensile tests for cotton yarns. J. Text. Inst. Trans. **17**, 355 (1926)
Pisano, G., Carfagni, G.R.: A micromechanical derivation of the macroscopic strength statistics for pristine or corroded/abraded float glass. J. Eur. Ceram. Soc. **37**, 4197–4206 (2017)
Poloniecki, J.: Statistical Investigation of Surface Flaws. Ph.D. Thesis, The University of Sussex (1974)
Poloniecki, J., Wilshaw, T.: Determination of surface crack size densities in glass. Nat. Phys. Sci. **229**, 226–227 (1971)
Postigo, S.: Estudio teorico experimental de impactos humanos contra vidrios de acristalamientos de edificacion. Ph.D. Thesis, Universidad de Politecnica de Madrid (2010)
prEN 16612: Glass in building-determination of the load resistance of glass panes by calculation and testing. CEN (2013)
Reid, S.: Effects of spatial variability of glass strength in ring-on-ring tests. Civ. Eng. Environ. Syst. **24**, 139–148 (2007)
Ritter, J., Service, T., Guillemet, C.: Strength and fatigue parameters for soda-lime glass. Glass Technol. **26**, 273–278 (1985)
Scholz, F.W., Stephens, M.A.: K-sample Anderson–Darling tests. J. Am. Stat. Assoc. **82**(399), 918–924 (1987). https://doi.org/10.1080/01621459.1987.10478517
Schula, S.: Charakterisierung der Kratzanfälligkeit von Gläsern im Bauwesen. Springer, Berlin (2015)
Sedlacek, G., Blank, K., Laufs, W., Güsgen, J.: Glas im Konstruktiven Ingenieurbau. Ernst & Sohn, Berlin (1999)
Simiu, E., Reed, D., Yancey, C., Martin, J., Hendrickson, E., Gonzalez, A., Koike, M., Lechner, J., Batts, M.: Ring-on-ring Tests and Load Capacity of Cladding Glass. Technical Report, NBS Building Series 162, U.S. Department of Commerce–National Bureau of Standards (1984)

Tandon, R., Paliwal, B., Gibson, C.: Practical aspects of using Hertzian ring crack initiation to measure surface flaw densities in glasses: influence of humidity, friction and searched areas. Philos. Mag. **93**, 2847–2863 (2013)

Thiemeier, T., Brückner-Foit, A., Kölker, H.: Influence of the fracture criterion on the failure prediction of ceramics loaded in biaxial flexure. J. Am. Ceram. Soc. **74**(1), 48–52 (1991)

Trujillo-Ortiz, A., Hernandez-Walls, R., Barba-Rojo, K., Cupul-Magana, L., Zavala-Garcia, R.: Andarksamtest: Anderson–Darling k-sample procedure to test the hypothesis that the populations of the drawned groups are identical. A MATLAB file. http://www.mathworks.com/matlabcentral/fileexchange/loadFile.do?objectId=17451 (2007)

Veer, F.: The strength of glass, a nontransparent value. HERON **52**, 87–104 (2007)

Veer, F., Louter, C., Bos, F.: The strength of annealed, heat-strengthened and fully tempered float glass. Fatigue Fract. Eng. Mater. Struct. **32**, 18–25 (2009)

Wachtman, J., Cannon, W., Matthewson, M.: Mechanical Properties of Ceramics. Wiley, Hoboken (2009)

Weibull, W.: A statistical theory of the strength of materials. Ingenjörsvetenskapsakademiens handlingar 151 (1939)

Wereszczak, A., Ferber, M., Musselwhite, W.: Method for identifying and mapping flaw size distributions on glass surfaces for predicting mechanical response. Int. J. Appl. Glass Sci. **5**, 16–21 (2014)

Wiederhorn, S., Bolz, L.: Stress corrosion and static fatigue of glass. J. Am. Ceram. Soc. **53**, 543–548 (1970)

Yankelevsky, D.: Strength prediction of annealed glass plates: a new model. Eng. Struct. **79**, 244–255 (2014)

David Kinsella, Kent Persson

An Analysis of Glass Fracture Statistics

In: Challenging Glass Conference 6: Conference on Architectural and Structural Applications of Glass (2018), Delft, The Netherlands

Paper C

Challenging Glass 6
Conference on Architectural and Structural Applications of Glass
Delft University of Technology, May 2018.

An Analysis of Glass Fracture Statistics

David T. Kinsella [a], Kent Persson
[a] *Lund University, Sweden, david.kinsella@construction.lth.se*

A numerical method is applied to model the fracture stress and failure location in glass panes subjected to various bending arrangements. The method assumes the weakest-link principle and the existence of surface microcracks. The fracture stress and failure origin are revealed through a search algorithm. The magnitude of strength and the location of fracture are stochastic in nature and can be predicted based on a suitable representation of the surface flaws condition. When the crack size distribution is assumed to be Pareto, the strength distribution is found to be very similar to a Weibull distribution. The stresses in large laterally supported plates which are subjected to uniform pressure are modelled and the distribution of fracture location is determined based on a single population of cracks with a Pareto distributed crack size. Two types of gasket support materials are considered, neoprene and nylon. The softer gasket material produces a greater number of fractures nearer the corners of the plate. A comparison is made with the recorded fracture locations according to various experiments. In addition, a tall vertical panel of laminated glass with a complex geometry and which is subjected to dynamic impact loading is modelled and the distribution of fracture location is determined based on a single population of cracks with a Pareto distributed crack size.

Keywords: Glass, fracture statistics, fracture mechanics, Monte Carlo

1. Introduction

Various models for predicting the fracture stress have been proposed for use on glass (Beason and Morgan 1984, Sedlacek et al. 1999). Some of the models have been implemented in national building codes (DIN 18008-1, ASTM E 1300-04). The failure models proved to have potential for prediction-making within limited domains. However, making accurate predictions of the strength remains a challenge to the general design case of a glass structure with varying boundary conditions and loading types. In fact, large safety factors are implemented in the building codes. Until recently, little attention was paid to the prediction of fracture location. In the following, a method for predicting the failure stress as well as the failure origin of a glass plate subjected to both static and dynamic loading is investigated. The method which assumes the existence of surface microcracks and the governing principle of the weakest-link is applied to different specimen geometries and loading setups. The results are compared with experimental data.

2. Background

The strength of a glass pane can be revealed by subjecting it to bending until it breaks while noting the fracture load (or pressure). The fracture stress at the origin of failure can be calculated assuming that the fracture location is known. The observed fracture stress varies generally within a large range of about 20-200 MPa and is further dependent on a number of factors including the load history, the surface condition (new or weathered or artificially scratched), the size of surface area in tension, the environmental conditions in particular the relative humidity, and the origin of failure, i.e. edge or surface (Mencik 1992).

It has been suggested to use a Weibull distribution for predicting the strength of a structural unit made from annealed float glass (Weibull 1939; prEN 16612:2017). In Eq. (1), the Weibull distribution function for the strength σ is given where k and m denote the scale and shape parameters, respectively.

$$F(\sigma) = 1 - e^{-\left(\frac{\sigma}{k}\right)^m} \tag{1}$$

It has also been suggested to make predictions of the strength based on the Glass Failure Prediction Model (GFPM) (Beason and Morgan 1984). The GFPM was calibrated with experiments in which uniform lateral pressure was applied to full-scale plates with continuous lateral support along all four edges. The American building code ASTM E 1300 implements the GFPM.

The scatter in failure stress magnitude can be explained by assuming that fracture is governed by microscopic surface flaws. Tensile stress is magnified in a localized region near the flaw tip (Griffith 1920). Flaws in glass can cause brittle failure because of the lack in capacity for plastic flow. Surface flaws arise in the production line during manufacture as well as in subsequent handling, transportation, assembly, use, and maintenance. Bulk flaws are disregarded as potential fracture sites in the following.

Variations in the surface condition of glass causes the observed strength to scatter, in general, for some given set of glass specimens, even when identical testing arrangements and specimen geometries are maintained. In fact, experiments have shown that even when the specimens are extracted from the same original standard size plate, the so-called jumbo plate, significant variations in the observed strength remain (Veer et al. 2009; Veer and Rodichev 2011; Vandebroek et al. 2014). Hence, surface flaw characteristics vary significantly not just between plates from different manufacturing batches but also between plates in the same batch.

In this paper, we consider semi-circular cracks that are uniformly distributed over the surface of some glass specimen. The corresponding mode I stress intensity factor (SIF) is determined using the following equation with a referring to the crack depth (Irwin 1957; Newman and Raju 1981)

$$K_I = 1.14\frac{2}{\pi}\sqrt{\pi a}\sigma_n \tag{2}$$

In Eq. (2), σ_n is the tensile stress normal to the crack plane. The mode I fracture criterion is

$$K_I \le K_{Ic} \tag{3}$$

and it is assumed that the fracture toughness K_{Ic} equals to 0.75 MPa $m^{½}$ (Mencik 1992). It is assumed that the individual cracks do not interact with each other. As a mixed mode criterion we take

$$\sqrt[4]{K_I^{\,4} + 6(K_I^{\,2} + K_{II}^{\,2}) + K_{II}^{\,4}} \le K_{Ic} \tag{4}$$

which is based on the maximum non-coplanar energy release rate (Hellen and Blackburn 1975), see also Thiemeier et al. (1991). In Eq. (4), K_{II} can be approximated as (Thiemeier et al. 1991)

$$K_{II} = 1.14\frac{4}{\pi}\frac{1}{2-\nu}\sqrt{\pi a}\tau \tag{5}$$

with ν referring to Poisson's ratio and τ the shear stress in the crack plane.

According to experimens with Hertzian indentation fracture in glass, flaw size can be closely fitted by a Pareto distribution (Poloniecki and Wilshaw 1971; Tandon et al. 2013). The Pareto distribution is (Forbes et al. 2010)

$$F(a) = 1 - \left(\frac{a_0}{a}\right)^c \tag{6}$$

where the scale and shape parameters are a_0 and c, respectively. It has been demonstrated that the Weibull distribution function can be derived from the WLP while assuming that the surface flaws condition is represented by a single population of cracks with a crack depth that is Pareto distributed (Jayatilaka and Trustrum 1977). It is then supposed that the stress state is uniform tensile and that the crack planes are oriented normal to the uniaxial stress. Let $f(a)$ denote the probability density function of the crack depth. Then the probability of failure at stress σ for a single crack is

$$F(\sigma) = \int_{a_c}^{\infty} f(a)da \tag{7}$$

where a_c is the critical crack depth that prompts failure for a crack subjected to tensile stress perpendicular to the crack plane. The critical crack depth is obtained through combination of Eqs. (2) and (3)

$$a_c = \frac{K_{Ic}^{\,2}}{Y^2\pi\sigma^2} \tag{8}$$

where for the sake of convenience, the geometry factor Y has been substituted for. The geometry factor is in this case given by

$$Y = 1.14\frac{2}{\pi} \tag{9}$$

Supposing that crack depth is Pareto distributed, we derive from Eqs. (6) and (7) while substituting for Eq. (8) that

$$F(\sigma) = \left(\frac{Y\sqrt{\pi a_0}\sigma}{K_{Ic}} \right)^{2c} \tag{10}$$

For N cracks, the probability of failure, P_f, is given by the following equation, supposing the WLP

$$P_f = 1 - \left(1 - F(\sigma)\right)^N \tag{11}$$

When N is large, Eq. (11) can be approximated by the following equation which can be shown by performing a Taylor series expansion

$$P_f = 1 - \exp\left(-NF(\sigma)\right) \tag{12}$$

so that for large N, we have approximately

$$P_f = 1 - \exp\left(-\left(\frac{Y\sqrt{\pi a_0}N^{\frac{1}{2c}}}{K_{Ic}}\sigma \right)^{2c} \right) \tag{13}$$

Eq. (13) can be simplified to Eq. (1), i.e. the Weibull distribution function, with the scale parameter

$$k = \frac{K_{Ic}}{Y\sqrt{\pi a_0}N^{\frac{1}{2c}}} \tag{14}$$

and the shape parameter

$$m = 2c \tag{15}$$

Hence, it is possible to calculate the distribution of macroscopic strength of a stressed solid by starting from an analysis of the microscopic defects and applying the WLP. Others who have considered this include e.g. Matthews et al. (1976) and Batdorf and Heinisch (1978). However, the mathematics soon become intractable as various assumptions are made for the stress state, fracture criterion, crack size distribution, flaw density, crack plane orientation, and the existence of multiple flaw populations.

Stress corrosion causes subcritical crack growth when the glass is stressed in tension in an ambient atmosphere which relates, in particular, to the relative humidity being greater than zero (Charles 1958a, 1958b). However, subcritical crack growth is only observed when the mode I SIF exceeds a threshold limit value estimated at about 0.25 MPa $m^{1/2}$ (Wiederhorn and Bolz 1970). In this paper the effect of stress corrosion is neglected.

3. Numerical method

Yankelevsky (2014) proposed a numerical solution method for calculating the strength distribution of a brittle solid that starts from an analysis of the microscopic defects. The weakest-link principle was applied in Monte Carlo simulations with Griffith flaws to model the fracture stress and fracture location of square glass plates subjected to bending. In Yankelevsky (2014), the plates were laterally supported along two opposite edges and subjected to a line-load at midspan. A Monte Carlo simulation was carried out for a large sample of 5000 virtual specimens. The method offers a tractable way to calculate the distribution of strength and fracture location for arbitrary stress states, fracture criteria, crack plane orientations, and crack size distributions, while allowing for the implementation of multiple flaw populations. The standard size so-called jumbo plate which measures 3.21x6.00 m^2 is taken as a starting point. The surface area is divided into unit cells and cracks are distributed over the cells according to a uniform distribution. It is supposed that the orientation of the crack plane is uniformly distributed. In this study, the

total number of cracks on the jumbo plate is fixed and depends on the flaw density. It is assumed for the model that the flaw density is 2 cm^{-2} (Wereszczak et al. 2014). The sampled crack size is based on some statistical distribution, e.g. the Pareto distribution. The random flaws are resampled each time a new jumbo plate is modelled. In summary, the stochastics of the flaws comprise the location, the crack plane orientation, and the size. A specimen is extracted from the jumbo plate and analyzed. The analysis depends on a comparison of the cracks with the time-dependent stress field using fracture mechanics. However, the stress distribution over time only needs to be calculated once for any given specimen type and bending arrangement. It is the distributed set of cracks that is resampled in each new simulation of the glass fracture. Fracture is prompted when the SIF envelope for the first time intersects with the fracture toughness. When this happens, the fracture stress and location can be determined based on the first unit cell that contains a failing crack.

In a recent paper (Kinsella and Persson 2018), this type of numerical method was applied to model the fracture stress and failure location of small glass plates subjected to double ring bending. The results allowed for making comparisons between different fracture criteria. Furthermore, a dual population concept of flaws was fitted to model the fracture stress in an empirical data set, the purpose of which was to model the apparent bimodality in the fracture stress distribution (Simiu et al. 1984). Glass fracture data tends to exhibit bimodalities (Veer et al. 2009).

This kind of numerical method was also used by Pathirana et al. (2017) who implemented a dual population concept in Monte Carlo simulations of Griffith flaws for the determination of the strength distribution in panels subjected to point contact actions.

4. Application to laterally supported plates subjected to uniform pressure

In this paper, the results from new simulations are presented that were carried out using the numerical method described in Sec. 3. The results pertain to laterally supported plates subjected to uniform pressure. As a background, the following is noted. Bending tests that record the fracture location in new full-scale plates which are laterally supported along all four edges and subjected to uniform pressure have previously been carried out by Johar (1981, 1982), Kanabolo and Norville (1985), and Calderone (1999). In Johar's and Kanabolo and Norville's experiments, the glass plates were supported between (approximately) 6 mm wide neoprene gaskets. In Calderone's experiment, 20 mm thick nylon gaskets were used. The plate nominal thickness was 6 mm in all experiments whereas the average thickness was 5.8 mm. Tab. 1 lists the sample sizes as well as the relative frequency of surface failures to edge failures. In Tab. 1, only those failures which were unambiguously identified as originating from either the surface or the edge were included in the statistics. In other words, when there was recorded multiple potential fracture origins which included a mixture of surface and edge sites, these were not counted and included in the Tab. 1 statistics. This was done for the sake of consistency because it is generally believed that the edge condition and hence the edge strength differs from the surface condition. Fig. 1 shows the recorded fracture locations and depicts the various plate dimensions that were used in the experiments.

Two square plates measuring 1200x1200 mm^2 and with a thickness of 5.8 mm were modelled using the FEM with ABAQUS/CAE (2013). The plates were laterally supported along all four edges between continuous 6 mm wide gaskets which were 6 mm in thickness. In one case the gasket material was neoprene (Shore A55) and in the other case it was nylon. The neoprene was modelled as an incompressible Neo-Hookean hyperelastic material with shear modulus G=1 MPa (Gent 2012). The nylon was modelled as an isotropic linear elastic material with Young's modulus E=3 GPa and Poisson's ratio ν=0.34. The gaskets were rigidly supported on the side opposite to the contact surface with the glass. A friction coefficient of 0.19 was adopted for the contact between gasket and glass. The glass material was assumed to have a Young's modulus E=72 GPa and a Poisson's ratio ν=0.23. Solid-shell elements were used for the glass part while employing a quadrilateral mesh generator. Hybrid elements were used for the hyperelastic material parts. In the case of the neoprene material, an adaptive meshing technique was employed for the gasket parts to improve the convergence. For symmetry reasons only one quarter of the plate was modelled. The plate was subjected to uniform lateral pressure. Fig. 2 shows the deformed state of the plate as seen from one corner when the gasket material was neoprene. Figs. 3 and 4 show the maximum in-plane principal stresses on the "tension" and "compression" sides of the plate, respectively, for both plates at a pressure magnitude of 40 kPa. The maximum tensile stress at this pressure was 97 MPa (nylon) and 164 MPa (neoprene), respectively, on the "tension" side, and 165 MPa (nylon) and 48 MPa (neoprene), respectively, on the "compression" side. The "tension" side refers to the side of the plate that is in tension at the centre point. The results show that with the softer gasket material, the tensile stresses concentrated nearer towards the edges of the plate. In fact, on the "tension" side, the maximum tensile stress was also significantly greater in this case. However, with the harder gasket material, it was observed that on the "compression" side, there is a very high build-up of tensile stress near the edges.

Table 1: Sample size and relative frequency of surface to edge failure in experiments with laterally supported plates subjected to uniform pressure. Some data points were excluded in the case of multiple potential fracture locations which contained a mixture of surface and edge failure sites.

Reference	Total no. of failures	No. of surface fail's	Rel. freq. of surf. fail's
Johar (1981)	78	54	0.69
Johar (1982)	106	71	0.67
Kanabolo and Norville (1985)	206	152	0.74
Calderone (1999)	195	152	0.78

The strength and fracture locations were simulated using the numerical method that was described in Sec. 3. It was assumed that the surface condition is characterized by a single population of semi-circular cracks with a Pareto distributed crack depth. The Pareto scale and shape parameter values were chosen as a_0=4 µm and c=3.0, respectively, cf. Eq. (6). The cracks were uniformly distributed over the surface area and the unit cell size was 5x5 mm^2. The crack density was 2 cm^{-2}. The motivation behind the choice of Pareto distribution parameter values comes from assuming a Weibull distribution for the strength with the parameter values k=74 MPa and m=6. Eq. (14) and (15) then give (approximately) the said Pareto parameter values with N=5655. In fact, this Weibull distribution gives a characteristic value of the bending strength $\sigma_{b,ch}$=45 MPa defined as the 5% fractile, cf. Sedlacek et al. (1999). According to Haldimann (2006), this Weibull distribution represents the breakage stress of new glass plates in R400 double ring bending tests at a stress rate of 2 MPa s^{-1} the tests of which were conducted as a basis for the DIN 1249-10:1990. With an assumed flaw density of 2 cm^{-2} the number N=5655 is obtained because the stressed area within the loading ring is 0.2827 m^2.

Figs. 5 and 6 show the simulated fracture locations based on a series of 5000 simulations each for the two types of gaskets, i.e. neoprene and nylon. In Fig. 5, the fracture criterion that was used assumes that the crack planes are oriented normal to the maximum principal stress, whereas in Fig. 6, the mixed mode fracture criterion, Eq. (4), was used. In this case, it was assumed that the crack plane angles were uniformly distributed in $[0,\pi)$.

Fig. 7 depicts the distribution in fracture stress for both types of gasket materials while assuming a mode I criterion with the crack planes oriented perpendicular to the maximum principal tensile stress. A two-parameter Weibull distribution was fitted to the data samples and is also shown in the diagrams. It can be noted that the mean fracture stress is slightly lower with the mixed mode fracture criterion.

5. Application to tall panels subjected to impact load

The dynamic impact load case is often relevant when performing a strength design of a glass structure. With an accurate description of the stress distribution in the impacted pane, it is possible to predict the likely fracture location. However, it is not necessarily the case that the failure location coincides with the maximum principal tensile stress (Natividad et al. 2016). By implementing the numerical method described in Sec. 3 it is possible to model the distribution of fracture location. The European standard EN-12600 details a method for testing glass to classify it in terms of impact strength.

The distribution in fracture location was studied for a tall vertical panel subjected to an impact load. The panel consists of a laminated unit with two glass plies. The panel measures approximately 1x4 m^2 in surface area and each ply has a thickness of 10 mm. The full transient FE simulation of the panel and impactor were based on a previous model which is described in Fröling et al. (2014). The panel was supported on two sides (top and bottom edges) and it had a 6x6 array of ventilation holes near the bottom edge, cf. Fig. 8a for an illustration. The impactor consists of a weight encased in two tyres, the weight of the impactor being 50 kg according to standard (EN-12600). The tyre was swung into the panel in a pendulum motion thus generating a soft impact with a long pulse time. The glass and PVB interlayer parts were modelled by means of a hexahedral solid-shell element. The rubber supports were modelled using a solid element. The glass, interlayer and supports were modelled as linear elastic materials and the material parameters which were adopted from Persson and Doepker (2009) and prEN 16612:2017 are shown in Tab. 2. The initial velocity of the impactor was 2.97 m s^{-1} which corresponds to a fall height of 0.450 m. The centrical impact occurred at a height of 1.2 m.

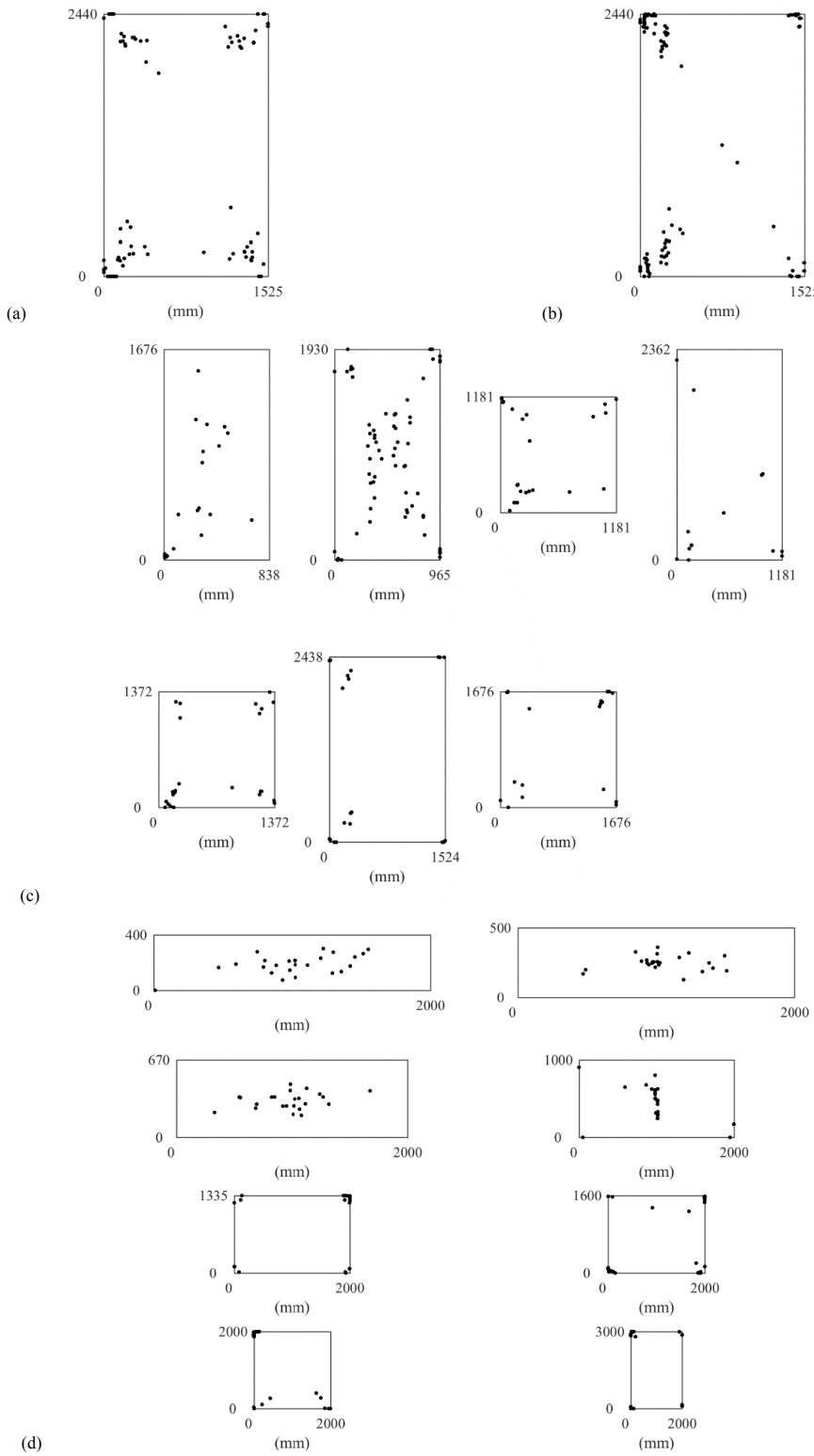

Fig. 1 Fracture origins according to four experiments (a) Johar (1981), (b) Johar (1982), (c) Kanabolo and Norville (1985), and (d) Calderone (1999).

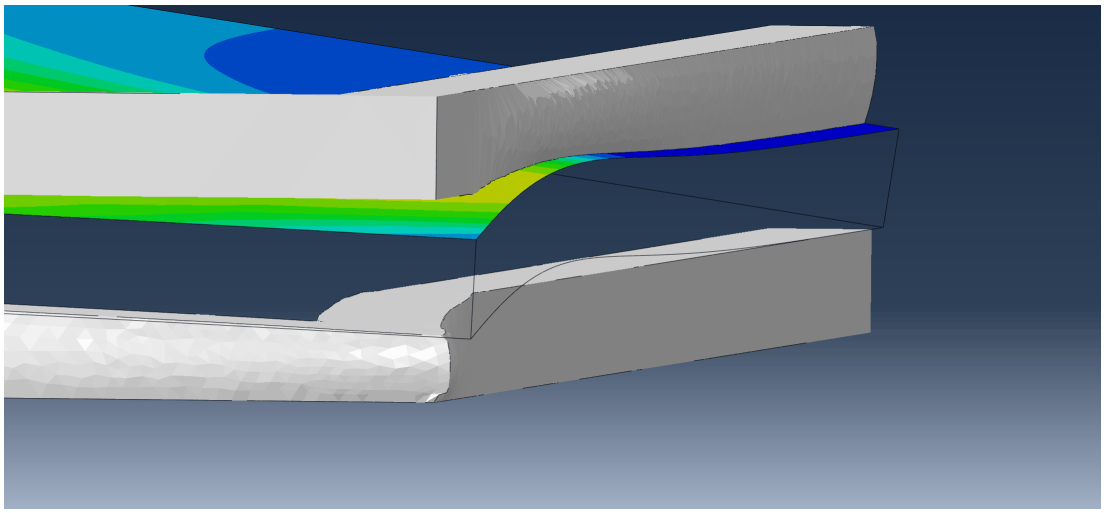

Fig. 2 Deformed state of a plate which is supported laterally between neoprene gaskets and subjected to uniform pressure. As seen from one corner. For symmetry reasons only one quarter of the plate is visible.

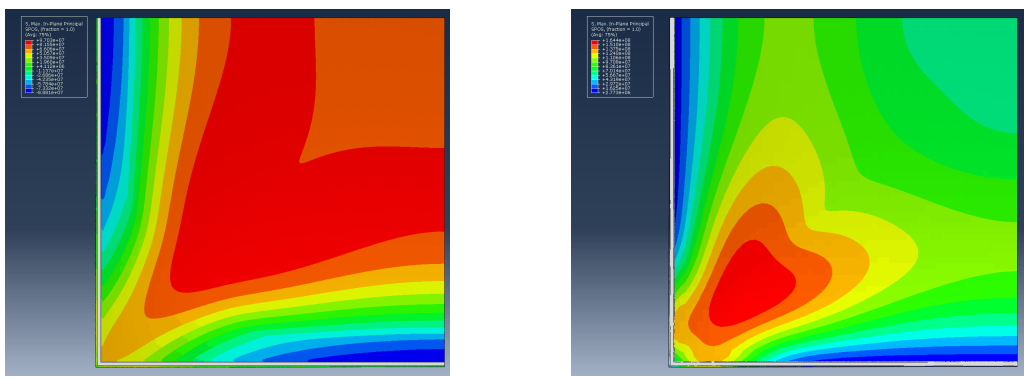

Fig. 3 Stress contours (maximum in-plane principal) on the "tension" side of the plate with (left) nylon gaskets and with (right) neoprene gaskets at the lateral pressure magnitude 40 kPa.

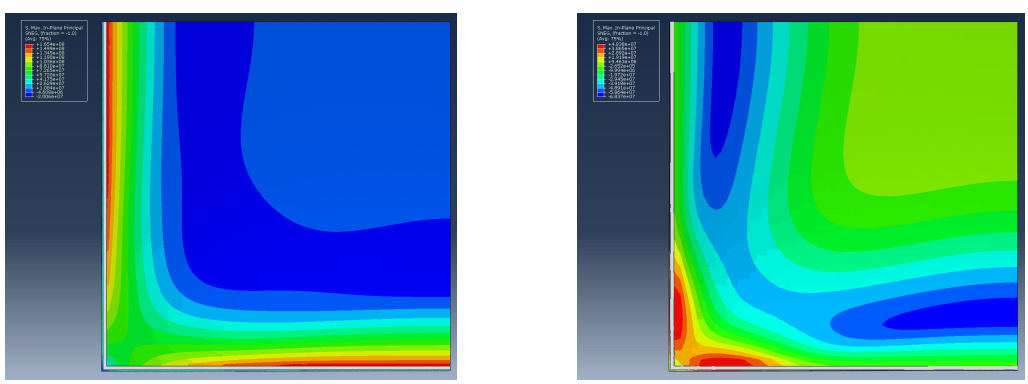

Fig. 4 Stress contours (maximum in-plane principal) on the "compression" side of the plate with (left) nylon gaskets and with (right) neoprene gaskets at the lateral pressure magnitude 40 kPa.

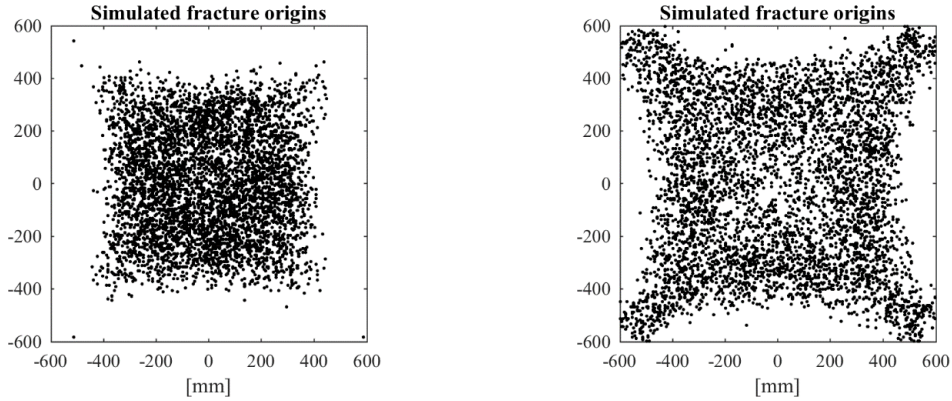

Fig. 5 Simulated fracture locations in the case of (left) nylon gaskets and (right) neoprene gaskets with a pure mode I fracture criterion assuming all crack planes to be oriented perpendicular to the max. princ. stress.

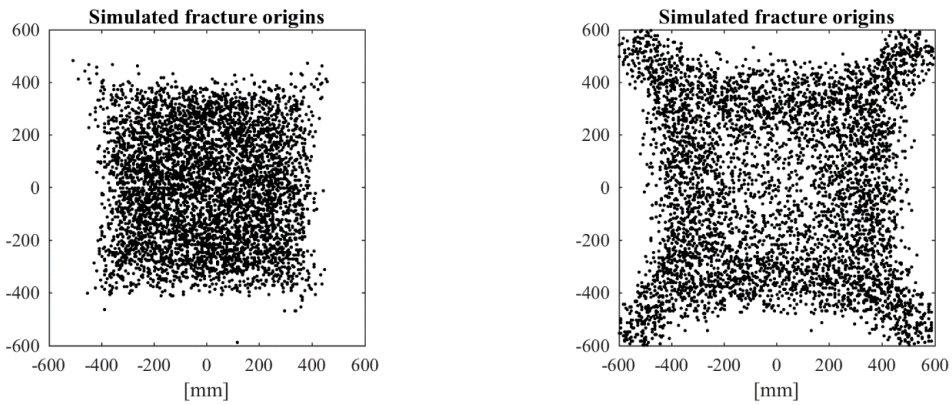

Fig. 6 Simulated fracture locations in the case of (left) nylon gaskets and (right) neoprene gaskets with a mixed mode fracture criterion.

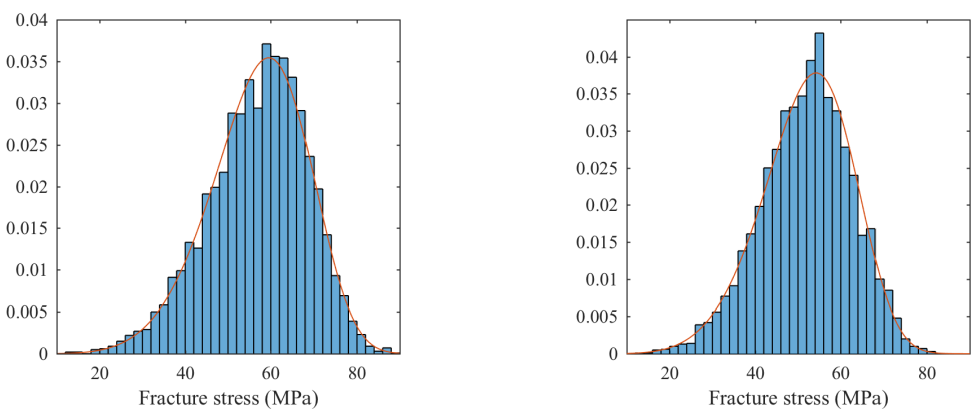

Fig. 7 Simulated fracture stress in the case of (left) nylon gaskets and (right) neoprene gaskets with the MPTS fracture criterion, i.e. assuming all crack planes to be oriented perpendicular to the max. princ. stress. Solid line corresponds to a fitted Weibull distribution. The histograms are normalized to reflect a probability density.

Fig. 8b shows the maximum in-plane principal stress contours at time equal to 15 ms when the maximum stress was about 45 MPa. Fig. 8c shows the stress contours at time equal to 30 ms when the maximum stress had reached about 82 MPa. The greatest stress (82 MPa) was located near the top row of ventilation holes. Fig. 9a shows the distribution of fracture location using a mode I fracture criterion without consideration of crack plane orientation, i.e. assuming that all crack planes are oriented normal to the maximum principal tensile stress. It was assumed that the surface condition is represented by a single population of cracks with a Pareto distributed depth with parameter values a_0=4 μm and c=3.0, and that the crack density is 2 cm^{-2}. Fig. 9a depicts in total 989 fractures which occurred during the simulation of 5000 virtual panel impacts. About 40% of the failures in total occurred near one of the ventilation holes. The area near a ventilation hole was in this case defined by a bounding box around the whole 6x6 array. Fig. 9b shows the resulting strength distribution which is not necessarily in agreement with a Weibull distribution.

Table 2: Material parameters

Material	E (MPa)	ν	ρ (kg m^{-3})
Glass	70000	0.2	2500
PVB interlayer	180	0.49	1250
Rubber support	15	0.44	1250
Impactor	2	0.3	900

Discussion

In theory, brittle fracture in glass is promoted by the existence of a large set of surface microcracks with a location and size distribution that can be described using some random variable. Because of the limited capacity for plasticity in glass, the failure mode is governed by the WLP, i.e. the first fracturing flaw prompts global breakage. A failure prediction model that is consistent with theory must therefore take into account the existence of surface microcracks including the stochastics of these, and the WLP. The Weibull model adopts the WLP and can, in theory, be associated with a single population of surface cracks having a Pareto distributed crack size. The Weibull model is preferred in major standards including the European draft prEN 16612:2017. However, the Weibull models that are fitted to empirical data are so different in scale and shape that is hard to predict the strength in general while adopting this type of distribution. A similar limitation appears to apply to the GFPM of which it has been said that it "is best suited to representing glass strength for specific test conditions." (Reid 2007) As a matter of fact, it is not just the fracture stress magnitude that scatters, the failure location is also variable. It has been shown that the fracture origin rarely occurs at the point of MPTS in laterally supported plates subjected to uniform out-of-plane loading (Natividad et al. 2016).

The method which was investigated in this paper offers a promising alternative to the ordinary Weibull model for use in failure prediction of structural glass units. Firstly, the method is based on the physics of brittle fracture. A representation of the surface condition is implemented and fracture mechanics are combined with the WLP to reveal the breakage stress and location. By assuming that the surface condition is represented by a single population of cracks with a Pareto size distribution, it is possible to obtain a Weibull distribution for the strength. The new model differs from the Weibull model in that a greater freedom is afforded towards the representation of the surface condition in glass. Now, the available data on the surface condition is scarce. As current techniques are improved, and new methods are developed to probe the surface condition, more reliable data can be supplied as input to this kind of failure model. It is moreover possible to evaluate failure based on different fracture criteria including mixed mode criteria in a way that would be more tractable than while using the ordinary Weibull distribution. The mathematics soon become intractable when evaluating the analytical expressions necessary to implement different fracture criteria, cf. e.g. Batdorf and Heinisch (1978). With the new method, it is possible to control the crack plane orientations in a way that would not be feasible using the ordinary Weibull distribution. If one for instance assumes that the crack planes lie in some particular direction on certain parts of the surface due to, for example, mechanical abrasion, then it would be quite possible to implement this in the new model through a suitable setup of the surface condition. It is also possible to implement multiple flaw populations. The new method offers the possibility to predict the fracture location which can be useful in certain situations. For example, glass structures with more complicated geometry containing corners and holes, and glass structures subjected to more advanced loading situations such as uneven static loading and dynamic loading.

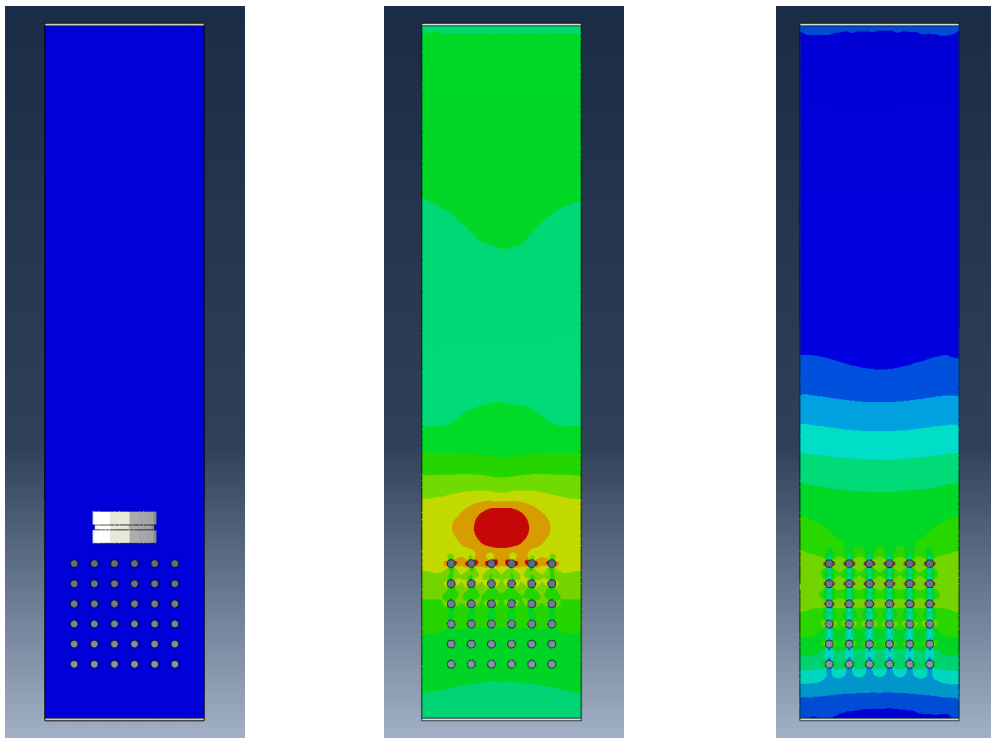

(a) (b) (c)

Fig. 8 (a) Tall panel and soft impactor. (b) Stress contours (max. in-plane princ.) when the max stress had reached 45 MPa at time 15 ms. (c) Stress contours when the max stress had reached 82 MPa at time 30 ms. NB, maximum stress in (c) is near the edges of the top row of ventilation holes. Red colour corresponds to tensile stress.

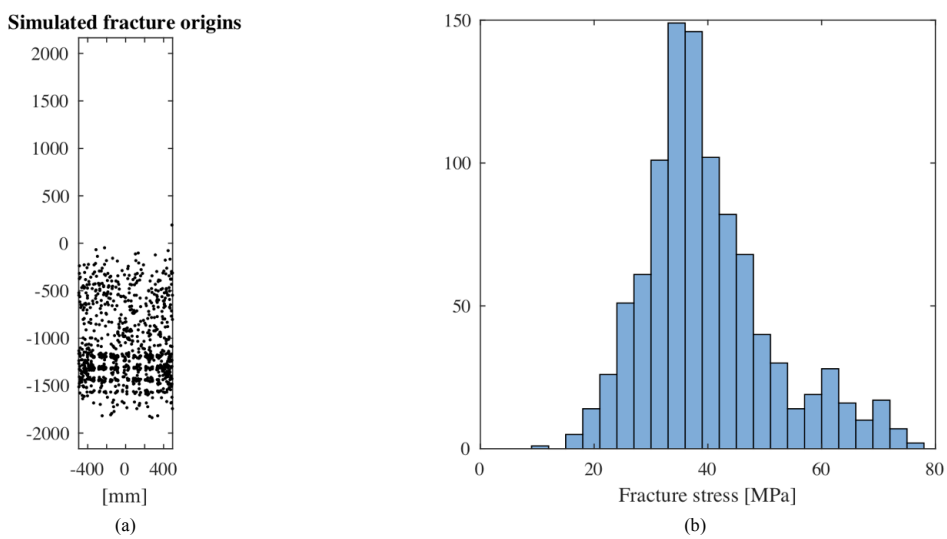

(a) (b)

Fig. 9 (a) Simulated fracture origins. (b) Strength distribution.

In the present study, a method was applied to model the strength and fracture location of laterally supported plates subjected to uniform pressure. The comparison of the empirical data appears to indicate that a significant portion of failures in tests of large plates occur near or on the edges. This might indicate that failure is sensitive to shear stress. According to one study (Reid 2007), a series of 59 small specimens of annealed glass plates generated unexpected results when tested in a double ring bending device. The proportion of failures outside the loading ring was much

greater than expected based on Weibull statistics which do not factor shear stress into the failure criterion. There is no shear stress in the loading ring area because the stress state is equibiaxial. In the case of a large laterally supported plate subjected to uniform pressure, there emerges shear stress near the corners of the plate. In this paper, such large plates were investigated while using both a mode I fracture criterion and a shear sensitive mixed mode criterion. However, from the simulation results, it is hard to see a significant impact on the fracture location due to the presence of shear stress near the corners of the plate. Nevertheless, the fracture origin was increasingly located nearer the corners when the support gaskets were made from a softer material, i.e. neoprene. As the Figs. 3 and 4 show, the tensile stress on the "compression" side of the plates are significant, especially in the case with the nylon gaskets. At the applied pressure 40 kPa, the maximum tensile stress on the "compression" side of the nylon supported plate was in fact on par with the maximum tensile stress on the "tension" side of the neoprene supported plate. This implies that a thorough analysis of the failure of laterally supported plates subjected to uniform pressure should consider both faces of the plate. This was not done in the present study but could be conducted in a future investigation. However, according to one study on large plates subjected to uniform loading (Calderone 1999), there were only two fractures occurring from the "compression" side of 195 specimens tested in total corresponding to a relative frequency of about 1%. In that study, nylon gaskets were used and the glass was fixed firmly between the nylon supports. This indicates that failures from the "compression" side are unlikely in practical situations. However, further investigation is required in order to verify this. More important perhaps, is the fact that a significant proportion of failures occur from the edges according to experimental data, cf. Tab. 1. In the modelling that was done in connection with this paper, only the surface condition in glass was considered. The edge condition was not represented separately. This is an important issue, however, that might be considered in future research work.

The case with the vertical panel impacted by a soft body illustrates how the new method can be applied to model specimens with a more complex geometry subjected to dynamic loading. This loading leads to a time-dependent stress distribution that initially affects a relatively large portion of the glass surface to moderate tensile stress and subsequently a much smaller portion is affected, in particular at the ventilation holes, to higher tensile stress. Even if the strength distribution is known a priori, i.e. a Weibull distribution, the question remains as to how the fracture location is distributed. The simulations which were carried out show that ultimately about 40% of the failures occurred near the holes. However, the edge condition in glass is very relevant in this case and should perhaps be represented differently than the surface condition. Further research needs to be conducted in order to properly model this load case while taking the edge condition into consideration. In the simulation of the panel, stress corrosion was not considered. However, in this particular case, the dynamic impact load produces a very high stress rate. In fact, the overall maximum tensile stress was reached within about 30 ms which corresponds to an average stress rate of approximately 2700 MPa s^{-1}. Presumably, any effects of static fatigue would be limited because there would be very little time for stress corrosion to take place. It is therefore believed that stress corrosion in this case would have only a negligible effect on the results. Interestingly, Haldimann (2006) carried out experiments on glass plates which were loaded at both low and very high stress rates (0.2 MPa s^{-1} and 21 MPa s^{-1}, respectively) and compared the results. His findings seemed to indicate that the behaviour of a specimen subjected to a stress rate of as much as 21 MPa s^{-1} in ambient conditions nearly approaches that of a specimen in inert conditions.

6. Conclusions

The distribution of fracture stress and failure location in glass can be modelled using a numerical method that is based on well-established concepts including the WLP and the existence of surface microcracks. The method is applied to model the strength and fracture origin in large laterally supported plates subjected to uniform pressure and in a tall panel with a complex geometry that is subjected to impact loading. By assuming that the surface condition is represented by a single population of cracks with a Pareto distributed crack size it is possible to obtain a strength distribution that is similar to a Weibull distribution. As current methods are refined and new techniques are developed to probe the surface condition of glass, this new numerical tool has potential for greater versatility in modelling glass fracture statistics since it allows for various surface flaws conditions and fracture criterions to be used.

7. References

ABAQUS/CAE: Version 6.13. Dassault Systèmes, (2013)
ASTM E 1300-04: Standard Practice for Determining Load Resistance of Glass in Buildings. (2004)
Batdorf, S.B., Heinisch, H.L.: Weakest Link Theory Reformulated for Arbitrary Fracture Criterion. J Am Ceram Soc **61**(7-8), 355-358 (1978)
Beason, W.L., Morgan, J.R.: Glass Failure Prediction Model. J Struct Eng **110**, 197-212 (1984)
Calderone, I.J.: The equivalent wind loading for window glass design. Monash University (1999)
Charles, R.J.: Static Fatigue of Glass I. J Appl Phys **29**, 1549-1553 (1958a)
Charles, R.J.: Static Fatigue of Glass II. J Appl Phys **29**, 1554-1560 (1958b)
DIN 18008-1:2010: Glas im Bauwesen - Bemessungs- und Konstruktionsregeln - Teil 1: Begriffe und allgemeine Grundlagen. (2010)
DIN 1249-10:1990: Flachglas im Bauwesen - Teil 10: Chemische und physikalische Eigenschaften. (1990)
EN 12600: Glass in building - Pendulum test - Impact test method and classification for flat glass. CEN (2003)
Forbes, C., Evans, M., Hastings, N., Peacock, B.: Statistical distributions. John Wiley and sons, Inc., (2010)
Fröling, M., Persson, K., Austrell, P.E.: A reduced model for the design of glass structures subjected to impact loads. Engineering Structures **80**, 53-60 (2014)
Gent, A.: Engineering with Rubber. Hanser, (2012)

Griffith, A.A.: The Phenomena of Rupture and Flow in Solids. Phil. Trans. R. Soc. **A221**, 163-163 (1920)
Haldimann, M.: Fracture strength of structural glass elements -- analytical and numerical modelling, testing and design. Ecole Polytechnique Fédérale de Lausanne EPFL (2006)
Hellen, T.K., Blackburn, W.S.: The Calculation of Stress Intensity Factors for Combined Tensile and Shear Loading. Int J Fract **11**, 605-605 (1975)
Irwin, G.R.: Analysis of Stresses and Strains Near the End of a Crack Traversing a Plate. J. Appl. Mech. **24**, 361-361 (1957)
Jayatilaka, A.D., Trustrum, K.: Statistical approach to brittle fracture. J Mater Sci **12**, 1426-1430 (1977)
Johar, S.: Dynamic fatigue of flat glass - Phase II. In. ORF, (1981)
Johar, S.: Dynamic fatigue of flat glass - Phase III. In. ORF, (1982)
Kanabolo, D.C., Norville, H.S.: The strength of new window glass using surface characteristics. Texas Tech University (1985)
Kinsella, D.T., Persson, K.: A Numerical Method for Analysis of Fracture Statistics of Glass and Simulations of a Double Ring Bending Test. Glass Struct & Eng (2018). doi:10.1007/s40940-018-0063-z
Matthews, J.R., McClintock, F.A., Shack, W.J.: Statistical determination of surface flaw density in brittle materials. J. Am. Ceram. Soc. **59**, 304-308 (1976)
Mencik, J.: Strength and Fracture of Glass and Ceramics, vol. 12. Elsevier, (1992)
Natividad, K., Morse, S.M., Norville, H.S.: Fracture Origins and Maximum Principal Stresses in Rectangular Glass Lites. Journal of Architectural Engineering **22**(2), 04015014 (2016). doi:10.1061/(ASCE)AE.1943-5568.0000197
Newman, J.C., Raju, I.S.: An empirical stress intensity factor equation for the surface crack. Eng. Fract. Mech. **15**, 185-192 (1981)
Pathirana M., Lam N., Perera S., Zhang L., Ruan D., Gad E.: Risks of failure of annealed glass panels subject to point contact actions. Int J Solids Struct **129**, 177–194 (2017)
Persson, K., Doepker, B.: Glass panes subjected to dynamic impact loads. Proc. of the XXIV A.T.I.V. Conference, Parma, 9-10 July (2009)
Poloniecki, J.D., Wilshaw, T.R.: Determination of Surface Crack Size Densities in Glass. Nature Physical Science **229**, 226-227 (1971)
prEN 16612:2017: Glass in building - Determination of the lateral load resistance of glass panes by calculation. CEN, (2017)
Reid, S.G.: Effects of spatial variability of glass strength in ring-on-ring tests. Civ Eng Environ Syst **24**, 139-148 (2007)
Sedlacek, G., Blank, K., Laufs, W., Güsgen, J.: Glas im Konstruktiven Ingenieurbau. Ernst & Sohn, (1999)
Simiu, E., Reed, D.A., Yancey, C.W.C., Martin, J.W., Hendrickson, E.M., Gonzalez, A.C., Koike, M., Lechner, J.A., Batts, M.E.: Ring-on-ring tests and load capacity of cladding glass. In. (1984)
Tandon, R., Paliwal, B., Gibson, C.: Practical aspects of using Hertzian ring crack initiation to measure surface flaw densities in glasses: influence of humidity, friction and searched areas. Philos Mag **93**, 2847-2863 (2013)
Thiemeier, T., Brückner-Foit, A., Kölker, H.: Influence of the fracture criterion on the failure prediction of ceramics loaded in biaxial flexure. J. Am. Ceram. Soc. **74**(1), 48-52 (1991)
Vandebroek, M., Louter, C., Caspeele, R., Ensslen, F., Belis, J.: Size effect model for the edge strength of glass with cut and ground edge finishing. Engineering Structures **79**, 96 -105 (2014)
Veer, F.A., Louter, C., Bos, F.P.: The strength of annealed, heat-strengthened and fully tempered float glass. Fatigue Fract Eng M **32**, 18-25 (2009)
Veer, F.A., Rodichev, Y.M.: The structural strength of glass: Hidden damage. Strength Mater+ **43**, 302-315 (2011)
Weibull, W.: A Statistical Theory of the Strength of Materials. Ingenjörsvetenskapsakademiens handlingar **151** (1939)
Wereszczak, A.A., Ferber, M.K., Musselwhite, W.: Method for Identifying and Mapping Flaw Size Distributions on Glass Surfaces for Predicting Mechanical Response. Int J Appl Glass Sci **5**, 16-21 (2014)
Wiederhorn, S.M., Bolz, L.H.: Stress corrosion and static fatigue of glass. J. Am. Ceram. Soc. **53**, 543-548 (1970)
Yankelevsky, D.Z.: Strength prediction of annealed glass plates -- A new model. Eng Struct **79**, 244-255 (2014)

David Kinsella, Johan Lindström

Using a Hierarchical Weibull Model to Predict Failure Strength of Different Glass Edge Profiles

International Journal of Structural Glass and Advanced Materials Research 4 (2020) (130.148)

Paper D

International Journal of Structural Glass and Advanced Materials Research

Original Research Paper

Using a Hierarchical Weibull model to Predict Failure Strength of Different Glass Edge Profiles

[1]David Thomas Kinsella and [2]Johan Lindström

[1]*Construction Sciences, Lund University, Sweden*
[2]*Centre for Mathematical Sciences, Lund University, Sweden*

Article history
Received: 27-02-2020
Revised: 01-04-2020
Accepted: 30-04-2020

Corresponding Author
David Thomas Kinsella
Construction Sciences, Lund University, Sweden
Email: david.kinsella@construction.lth.se

Abstract: The edge strength of glass is analyzed using a Weibull statistical framework based on 78 data samples from a range of experiments recorded in literature. Based on the analysis, a 45 MPa strength value (computed as the lower bound in a one-sided confidence interval at the 75% level for the 5-percentile in the distribution) could be conservatively used with arrised, ground and polished edges when related to a reference length of 100 mm at an applied stress rate of 2 MPa/s. The size effect can be represented by the usual weakest-link scaling formula with the Weibull modulus taken to be 8.0, 12.0, 8.0 and 6.5, respectively, for as-cut, arrised, ground and polished edges. It is estimated that static fatigue is best accounted for with a value of stress corrosion parameter about n = 16. The results are obtained with random sampling MC in a hierarchical modelling approach with the Weibull parameters treated as nested random variables. By accounting for the influence of glass supplier as a mixed-effect in a linear statistical model, it is found that supplier effects are significant and important to consider along with others due to, e.g., stress rate and edge length exposed to maximum stress. The data samples which are limited to glass tested in an ambient environment using four-point bending fixture, show that Weibull statistics generally scatter considerably. Numerical investigations with random sampling show that shape parameter estimates scatter substantially when sample size is limited, which can explain some of the observed variability in shape more so for ground and polished edges than for as-cut and arrised. For the as-cut edge, it is suggested that the shape parameter is scale-dependent. The Weibull parameters are also estimated using a clustered likelihood estimator under the condition that the shape factor has constant value for each edge type.

Keywords: Glass, Edge, Strength, Statistics, Weibull, Hierarchical Modelling

Introduction

According to the latest European standard for glass in building, EN 16612:2019, there has not been a large-scale assessment of edge strength of the type undertaken for surface strength. From a practical perspective, it is conservative to assume that the edge is exposed to significant stress when a structure is subjected to the design load. For instance, even though maximum tensile stress occurs at the surface center point in a laterally supported plate subjected to uniform pressure, nevertheless, the corner edges are subject to considerable tension. Regarding other kinds of structural elements, such as beams and columns, it is evident that edge resistance cannot be neglected in the design process, in particular if edge resistance is deemed to be inferior to surface strength as standards would have it (EN 16612:2019, compare also DIN 18008-1:2010).

Experimental measurements of edge strength can be found in a wide range of journal articles, conference proceedings and academic dissertations which are available in the open literature (Table 1 gives a summary of the data used here). A comprehensive investigation into these results allow for an unprecedented analysis of glass edge strength within a Weibull statistical framework.

Background

Manufacture

The manufacture of float glass involves a long process line with production operations comprising a range of parameters of importance for the mechanical properties of the glass end-product, e.g., the thermal history which is carefully controlled to design the

DOI: 10.3844/sgamrsp.2020.130.148

residual stresses (Le Bourhis, 2008; McLellan and Shand, 1984). The float process causes diffusion of tin into the surface that was in contact with the molten tin bath. This side is denoted the tin side whereas the opposite side is termed the air side (Krohn *et al*., 2002). The annealed glass is transferred to automatic cutting machines that produce standard size sheets with dimensions 6×3.21 m^2 (EN 572-1, 2012). When glass is cut it is first scribed under a sharp roller with oil applied in front of the cutting head to generate cracks which are subsequently driven through the thickness of the pane by flexuring the glass and breaking it in two. The result of the cut depends on the type of roller and the force, angle and velocity applied to it, in addition to the composition of cutting oil, all of which are controlled to generate median cracks and limit the introduction of lateral cracks, which degrade the edge quality, see also Müller-Braun *et al*. (2020) (Lawn, 1993; Le Bourhis, 2008). Moreover, the quality depends on the flexure stress and magnitude of surface residual stresses that may be present. In addition, the environment plays a role in the result (Le Bourhis, 2008).

By subjecting the as-cut edge to grinding operations, a range of edge profiles are produced. Here we consider the arrised, ground and polished types as illustrated schematically in Fig. 1. The arrising is performed with a cross-belt or cup wheel edging machine which introduce bevels at an angle of about 45° to the surface. The result of arrising depends on the belt speed and direction for crossbelt machines and on the rotation speed for machines with cup wheels, as well as on the grinding pressure, the selected grain size and the order of application of grit sizes, in addition to the total age and usage of the machines (Kleuderlein *et al*., 2014; Veer, 2007). The optical quality of the ground edge is characterised by its roughness and smooth spots of as-cut glass may be present on the surface edge (site S23 in Fig. 1) depending on the amount of grinding performed (Vandebroek *et al*., 2014). The action of polishing is carried out in a similar manner to grinding, however, very little material is removed in the process (McLellan and Shand, 1984).

Weibull Distribution

The Weibull distribution (Weibull *et al*., 1952) for the strength σ is:

$$F(\sigma) = 1 - \exp\left(-\left(\frac{\sigma}{k}\right)^m\right), k > 0, m > 0, \sigma \geq 0 \tag{1}$$

where, k and m are scale and shape parameters. The corresponding density function is:

$$f(k,m;\sigma) = \frac{m}{k}\left(\frac{\sigma}{k}\right)^{m-1} \exp\left(-\left(\frac{\sigma}{k}\right)^m\right), \tag{2}$$

and the coefficient of variation is:

$$COV = \sqrt{\frac{\Gamma\left(\frac{m+2}{m}\right)}{\Gamma\left(\frac{m+1}{m}\right)} - 1}, \tag{3}$$

where, $\Gamma(\cdot)$ is the Gamma function, i.e., $\Gamma(m) = (m-1)!$ and generalized for non-integer m (Rinne, 2009). For glass the Weibull distribution has been derived from assumptions regarding crack occurrences and sizes (see overview in Sec. Mathematical development of the Weibull model), providing links between the parameters in Equation (1) and the physical parameters of the glass; these links can be used when modelling glass strength.

Parameters of the Weibull distribution can be estimated using standard statistical theory, see Appendix A. To illustrate how the uncertainty in parameter estimates depends on the sample size, 50 point estimates of Weibull scale and shape parameters together with confidence bounds obtained from numerical simulations with random Weibull samples are shown in Fig. 2. The underlying scale and shape parameter values are $k = 75$ and $m = 10$.

Mathematical Development of the Weibull Model

The strength of glass is governed by the presence of flaws which turn into fracture sites when tensile stress reaches a critical level. The flaws are represented by cracks and the extension of a crack is modelled by an energy balance. Crack growth is prompted by either of three modes of deformation, viz. mode I, mode II and mode III (Irwin, 1958). Mode I refers to crack opening due to displacements normal to the crack plane surface. Mode II and III describe in-plane and out-of-plane shearing displacement cracking (Broek, 1983). As a simplification we consider only the impact of Mode I displacements. Failure is governed by the critical release rate of elastic strain energy. The mode I Stress Intensity Factor (SIF) for a sharp crack subjected to far-field tensile stress σ acting perpendicular to the crack plane is:

$$K_I = \sigma Y \sqrt{a\pi}, \tag{4}$$

where, a is the crack size and Y is a geometrical configuration factor whose value in many cases is roughly equal to unity (Irwin, 1957; Hellan, 1984); e.g., for a straight-fronted planar edge crack $Y = 1.12$ (Irwin, 1958). The fracture criterion is:

$$K_I \geq K_{Ic}, \tag{5}$$

where, K_{Ic} is the fracture toughness which for sodalime glass equals to about 0.75 MPa m$^{1/2}$ (Mencik, 1992).

DOI: 10.3844/sgamrsp.2020.130.148

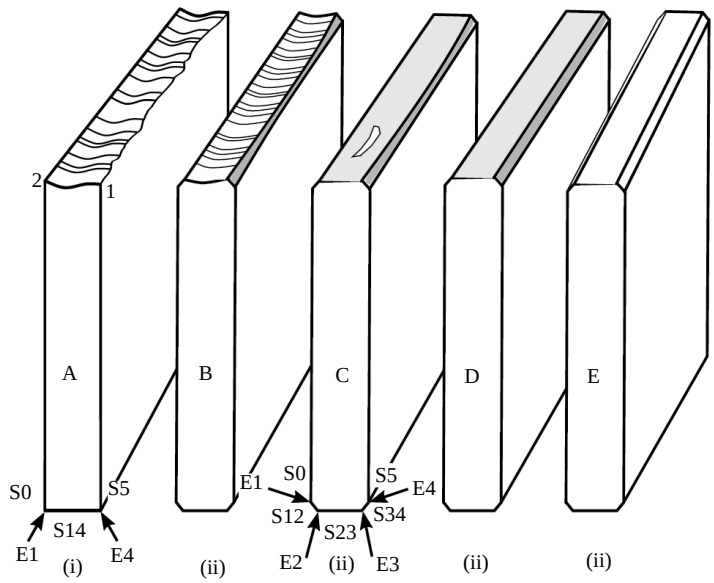

Fig. 1: Edge types. (A) As-cut with scored, 1 and non-scored, 2, edge. (B) Arrised. (C) Ground with smooth spots of as-cut glass remaining visible. (D) Ground. (E) Polished. Cross-sectional edge perimeter for (i) as-cut and (ii) arrised, ground and polished, respectively, is divided into zones where S = surface, E = edge

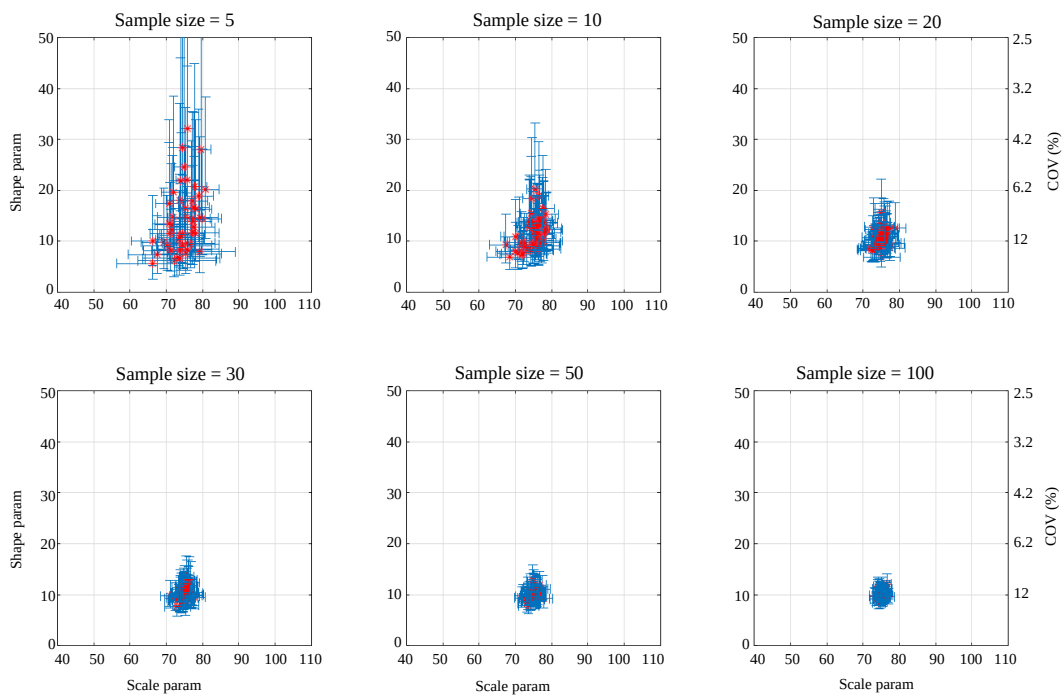

Fig. 2: Estimated confidence bounds for Weibull scale and shape parameters in numerical simulations of samples with varying size. True values: k = 75 and m = 10

Combining Equation (4) with (5) and assuming a homogeneous Poisson process for crack occurrence with Pareto distributed crack sizes, it can be shown (Mesarovic *et al*., 1992; Haldimann, 2006) that the total failure probability for an edge of length L subjected to uniform stress is:

$$P_f\left(L;\sigma_f\right)=1-\exp\left[-\lambda_0\frac{L}{L_0}a_0^r\left(\frac{\sigma_f Y\sqrt{\pi}}{K_{Ic}}\right)^{2r}\right], \tag{6}$$

where, λ_0/L_0 is the crack density, a_0 and r are Pareto scale and shape parameters and the Pareto distribution is:

$$F_A\left(a_i\right)=1-\left(\frac{a_0}{a_i}\right)^r, a_0>0, r>0. \tag{7}$$

While subjected to tensile stress in an atmosphere that contains water moisture, cracks in glass propagate subcritically due to stress corrosion (Charles, 1958a,b). For structural glass design considerations, subcritical crack growth is modelled using Equation (8) in which v_0 and n are stress corrosion parameters and K_{th} is a threshold value of SIF below which crack growth arrest occurs, at approximately 0.20-0.27 MPa $m^{1/2}$ (Evans, 1974; Haldimann, 2006):

$$da=\begin{cases}v_0\left(\frac{K_I}{K_{Ic}}\right)^n dt, K_{th}<K_I<K_{Ic},\\ 0, \qquad\qquad 0\le K_I\le K_{th}.\end{cases} \tag{8}$$

Combining Equation (4) to (8), neglecting the crack growth arrest limit and assuming in addition a constant applied stress rate until failure, subcritical crack growth is accounted for in an approximation of the total failure probability as expressed in Equation (9) (Haldimann, 2006):

$$P_f\left(L;\sigma_f\right)=1-\exp\left[\begin{array}{l}-\lambda_0\frac{L}{L_0}a_0^r\cdot\ldots\\ \ldots\cdot\left(\frac{1}{2}\cdot\frac{n-2}{n+1}\cdot\frac{v_0}{\dot\sigma}\right)^{\frac{2r}{n-2}}\left(\frac{Y\sqrt{\pi}}{K_{Ic}}\right)^{\frac{2rn}{n-2}}\sigma_f^{\frac{2r(n+1)}{n-2}}\end{array}\right] \tag{9}$$

Equation (9) is a good approximation in the case of low to moderate loading rates when v_0 is large enough (Haldimann, 2006).

Both Equation (6) and (9) can be written in the form of the Weibull distribution (1). For Equation (9), the corresponding scale and shape parameters are identified as:

$$k=\left(\frac{1}{\lambda_0}\cdot\frac{L_0}{L}\right)^{\frac{1}{m}}\left(\frac{1}{a_0}\right)^{\frac{n-2}{2(n+1)}}\cdot\ldots \\ \ldots\cdot\left(2\cdot\frac{n+1}{n-2}\cdot\frac{\dot\sigma}{v_0}\right)^{\frac{1}{n+1}}\left(\frac{K_{Ic}}{Y\sqrt{\pi}}\right)^{\frac{n}{n+1}} \tag{10a}$$

$$m=2r\cdot\frac{n+1}{n-2} \tag{10b}$$

Four-Point Bending Test Results Reviewed

A schematic of the four-point bending arrangement is shown in Fig. 3. The bending strength is calculated as:

$$\sigma=3\frac{Fl_0}{wd^2} \tag{11}$$

where, l_0 is the distance between force and support and d and w refer to the cross-sectional width and height, respectively. Here, the beam is standing up on its edge and subjected to an in-plane configuration of bending. The maximum stress rate as function of deformation rate, $\dot u$, is given by:

$$\dot\sigma=\dot u\frac{3Ed}{3L-4l_0} \tag{12}$$

where, E is Young's modulus equal to about 72 GPa and L is the distance between the supports (Mencik, 1992).

A total of 78 samples from four-point bending tests comprising some 1800 observations of edge strength were collected from literature and reviewed, see Table 1 for an overview. The data samples were obtained from experiments conducted on new annealed glass specimens broken in a four-point bending fixture in an ambient environment. No special coating was applied to the tension side of glass. The configuration of bending fixture was such that it took place in the plane of the specimen, i.e., with the glass beam standing up on its edge. The edge type was either as-cut, arrised, ground, or polished. The experiments were by all accounts consistently performed according to best practices and in many cases the procedure was guided by some standard document, e.g., EN 1288-3:2000. About 85% of recorded data was observed using a stress rate lower than 3 MPa/s. The maximum stress rate used in any of the experiments was below approx. 55 MPa/s. In total 19 suppliers of glass were identified, however, where it was not verified in a few cases that those are not confounded with each other, as indicated in the table; the reason being that it was not verified that the glass tested in Veer *et al*. (2006; 2009) and Veer and Rodichev (2011) and Vandebroek *et al*. (2012; 2014), respectively, were obtained from separate original batches even though it is likely so because experiment designs including specimen dimensions were different.

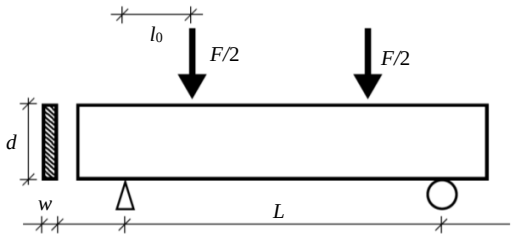

Fig. 3: Four-point bending test setup

According to one study on beams tested with an in-plane configuration of bending, on average 20% and 13% of failures in as-cut and ground specimens, respectively, occurred from either site S0 or S5 in Fig. 1, i.e., from the main surfaces (Vandebroek *et al*., 2014). For the distribution of failure origins between sites E1, S14 and E4, for the as-cut edge, Kleuderlein *et al*. (2014) found that some 92% occurred at the scored part of edge while in Vandebroek *et al*. (2014) it was 75%. The statistics in Kleuderlein *et al*. (2014) and Vandebroek *et al*. (2014) show that failure origins in beams subjected to in-plane bending are distributed over the entire cross-sectional edge perimeter and extend even beyond into the main surface. In this context, we consider the surface to be defined by the pristine surfaces of glass that were in contact with the molten tin or air in the float process, whereas the edge is those parts of material subjected to various mechanical actions of scoring, cutting, arrising and grinding operations, etc. As a simplification, in this paper it is assumed that the in-plane bending configuration is a proxy for edge failures.

Ritter *et al*. (1984) reports the results from a wide-ranging testing programme on small annealed glass plates with ground edges subjected to four-point bending. A significant strength variability from laboratory to laboratory was noted and the estimated Weibull shape parameter for the edge population ranged from about 4.6 to 12.5.

Hierarchical Modelling of a Weibull Random Variable

To model the 1782 observations we use a hierarchical approach with Weibull distributed errors:

$$\sigma_{ij} \sim Weibull\left(k_i, m_i\right) \tag{13}$$

where, σ_{ij} is the j^{th} observation from the i^{th} sample. Models for the resulting 78 shape and scale parameters, k_i and m_i, are obtained by taking logarithms of Equation (10) and rewriting as:

$$\begin{aligned}\log k = {} & \frac{1}{m}\log\frac{L_0}{L} + \frac{1}{n+1}\log\frac{\dot{\sigma}}{\dot{\sigma}_{eq}} + \ldots \\ & \ldots + \frac{n-2}{2(n+1)}\left(\log\frac{1}{a_0} - \frac{\log\lambda_0}{r}\right) + \ldots \\ & \ldots + \frac{n}{n+1}\log\frac{K_{Ic}}{Y\sqrt{\pi}} + \ldots \\ & \ldots + \frac{1}{n+1}\log\left(2\cdot\frac{n+1}{n-2}\frac{\dot{\sigma}_{eq}}{v_0}\right),\end{aligned} \tag{14a}$$

$$\log m = \log\frac{n+1}{n-2} + \log(2r). \tag{14b}$$

Equation (14) is then used as a basis to formulate a statistical linear mixed effects model (McCulloch *et al*., 2008, Ch. 6) as follows:

$$\begin{aligned}\log k_i - \frac{1}{m_i}\log\frac{L_0}{L_i} = {} & \sum_{l=1}^{4}\beta_l \mathbb{I}_{edgetype=l,i} + \ldots \\ & \ldots + \beta_5 \log\frac{\dot{\sigma}_i}{\dot{\sigma}_{eq}} + \sum_{l=1}^{17} b_l \mathbb{I}_{\text{supplier}=l,i} + \varepsilon_i,\end{aligned} \tag{15a}$$

$$\begin{aligned}\log m_i = {} & \sum_{l=1}^{4}\gamma_l \mathbb{I}_{edgetype=l,i} + \ldots \\ & \ldots + \sum_{l=1}^{17} c_l \mathbb{I}_{\text{supplier}=l,i} + \varepsilon_i\end{aligned} \tag{15b}$$

Here $\mathbb{I}$ are indicator functions for the categorical regressors; L_i and $\dot{\sigma}_i$ are the recorded load span and stress rate in the i^{th} sample; and we have chosen the reference load span and reference (or "equivalent") stress rate as L_0 = 100 mm and $\dot{\sigma}_{eq}$ = 2 MPa s^{-1} respectively.

The model in Equation (15) is obtained from Equation (14) by the following steps and assumptions:

1. The first term on the Right-Hand Side (RHS) of Equation (14a), representing edge length (size) effect, has been included in the response variable on the LHS of Equation (15a)
2. The second term on the RHS of Equation (14a) represents the effect of the constant stress rate and depends on the stress corrosion parameter n. The reciprocal of $n + 1$ is identified with the fixed-effect β_5 in Equation (15a)
3. Term number three on the RHS of Equation (14a) and the second term on the RHS of Equation (14b) correspond to the edge condition of glass. This depends on manufacturing processes (as outlined in Sec. *Manufacture*) and edge type, which governs the characteristics of flaw population, as modelled by a_0, r and λ_0 in the Poisson process and Pareto distribution. The different edge types are considered as fixed-effects, given by β_l and γ_l for l = 1 through 4, while the supplier is a random effect captured in b_l and c_l

4. Term number four on the RHS in Equation (14a) contains both a material parameter K_{Ic} and the fracture mechanics geometrical configuration factor Y the latter of which is assumed to be approximately equal to unity. The effect of these are incorporated in the intercept value of the linear model
5. The last term on the RHS of Equation (14a) contains both stress corrosion parameters n and v_0 of which the latter is assumed to be, on average, constant as long as the environmental conditions (temperature and RH) are similar between experiments. Any random variability in v_0 will be captured in the error term ϵ_i and the dependence on n is neglected as a simplification in the linear model
6. Finally, since $n \gg 1$, it is assumed that the ratios $n/(n + 1)$ and $(n - 2)/(n + 1)$ are approximately constant

The motivation for using a mixed effects model is that the effect of edge types and stress rate have physical interpretation, but differences between suppliers (and batches) are due to variability in the manufacturing process. Thus we are interested in the actual effect of edges and stress rate, while for the manufacturers we are more interested in categorizing the amount of variability among different manufacturers (see also Appendix B for a longer discussion).

Ideally the hierarchical model defined by Equation (13) and (15) should be estimated jointly, while accounting for the coupling in Equation (15). This could potentially be done using more advanced statistical algorithms such as Markov chain Monte Carlo and expectation maximization (Givens and Hoeting, 2013). However, to obtain a practically useful model we use a pragmatic two step approach where shape and scale for each sample are first estimated from Equation (13) and then used as response variables in two separate regressions in Equation (15) (Sampson *et al*., 2011, for a similar pragmatic approach to air pollution data.). In addition, a more involved model with mixed-effects for laboratory or with interactions between edge type and supplier would be desirable, but such a model is infeasible due to data sparsity; e.g., there are no cases in the published data where two (or more) laboratories uses the same batch of glass.

Given values of edge-type, stress rate and load span the model in Equation (15) can be used to predict shape and scale parameters; these parameters can then be used in Equation (13) to compute 5-percentile values. However, this would ignore the uncertainty due to different suppliers, a more correct model is obtained by integrating out (e.g., averaging over) the effect of different suppliers:

$$f(\sigma) = \int f(\sigma \mid \text{supp}) \cdot p(\text{supp}) d\text{supp} \approx \frac{1}{N} \sum_{i=1}^{N} f(\sigma \mid k_i, m_i). \quad (16)$$

Here, $f(\sigma|\text{supp})$ is the Weibull distribution with parameters from Equation (15) given a known supplier and $p(\text{supp})$ characterises the uncertainty in supplier effect, e.g., the variance of b_l and c_l. The integral in Equation (16) is intractable and we use Monte Carlo integration to compute the distribution $f(\sigma)$ using the following steps:

1. Sample pairs of scale and shape parameters from Equation (15) while assuming that the glass could have been obtained from any supplier
2. Given scale and shape parameters the corresponding Weibull density, Equation (13), is computed
3. Steps 1 and 2 are repeated 10 000 times and the results are averaged, providing a numerical approximation of the integral in Equation (16)

Results

The ordinary ML-estimates of the Weibull parameters, cf. Equation (19), for the data sets included in Table 1 are computed and illustrated in Fig. 4 where also the confidence bounds are shown. The results are grouped according to edge-type and load span dimension, additionally differences in supplier/batch (cf. Table 1) and edge thickness are indicated. For the as-cut and polished edge types additional samples with edge failures recorded in out-of-plane configuration of four-point bending are included. These additional samples were obtained from Veer and Rodichev (2011), Muniz-Calvente *et al*. (2016) and Osnes *et al*. (2018) and were given supplier/batch indices 4, 22 and 23, respectively, cf. Table 1 and see also Table. 4.

Using Equation (15b), a LME model is applied and a constant shape factor per edge type is computed as fixed-effect, the value of which is provided in Table 2. The LME model of the shape factor is further illustrated in Fig. 5 which shows the computed fixed and random effects with approximate and simultaneous 95% confidence bounds.

Figure 6 illustrates the results for the scale factor when the LME model, Equation (15a), is fitted. In the middle is a subplot of the fixed-effects with approximate and simultaneous 95% confidence bounds included. In the bottom is a subplot of the fixed+random effects. The fixed-effect in Equation (15a) that corresponds to the reciprocal of $n + 1$ is estimated at 0.0612 which produces a value of stress corrosion parameter at $n = 15.3$ with approximate 95% confidence bounds [14.0, 16.9].

DOI: 10.3844/sgamrsp.2020.130.148

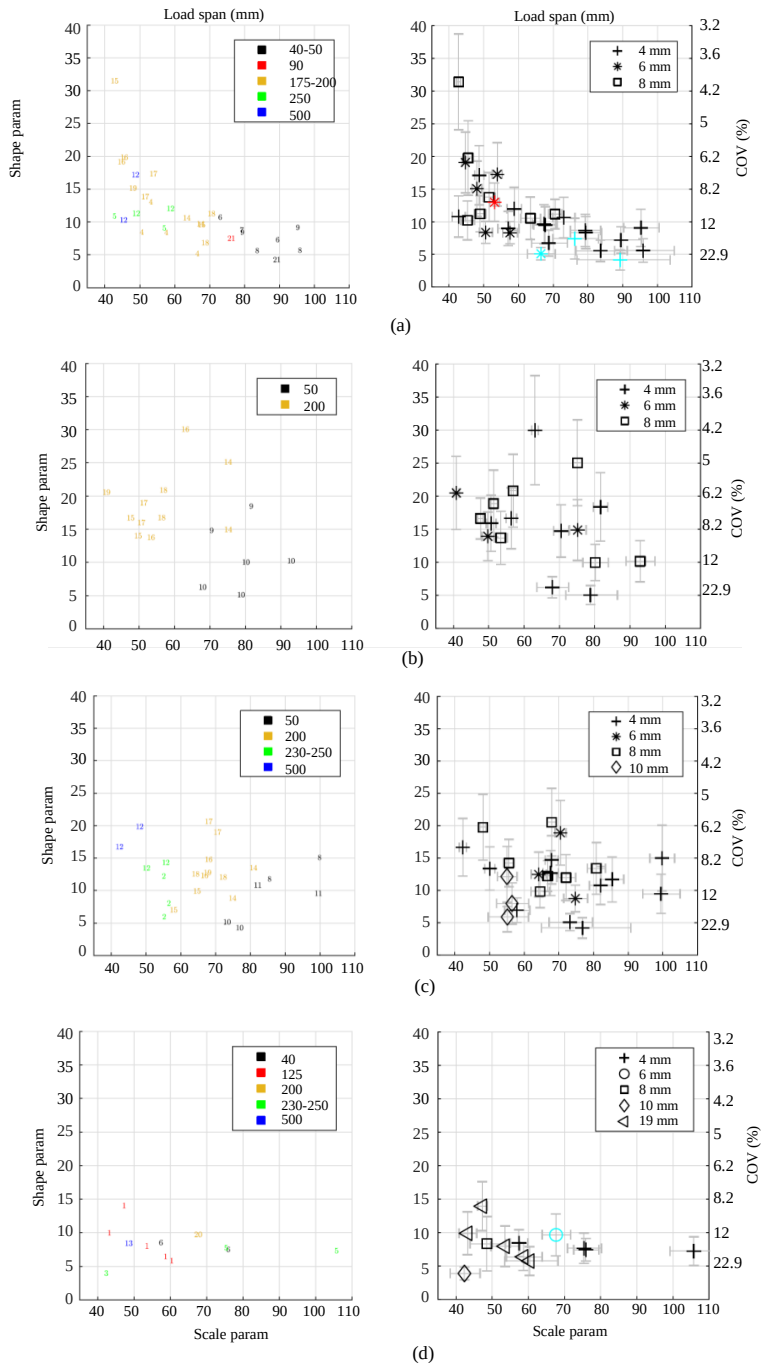

Fig. 4: Weibull statistics and sample data for the as-cut, arrised, ground and polished edge type in tests with in-plane bending configuration. Supplier/batch numbers are indicated on left-hand side and nominal edge thickness is indicated in symbolic marker +, o, *, etc., on right-hand side. For comparison additional points are added corresponding to fracture statistics with out-of-plane bending where the originally scored edge was in the tension (green marker) and compression (red marker) zone, respectively, as indicated in the right-hand subplots

DOI: 10.3844/sgamrsp.2020.130.148

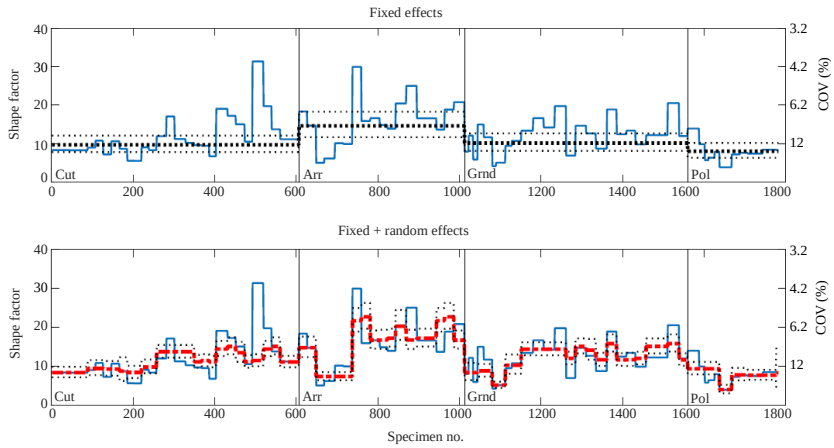

Fig. 5: Shape factor fixed and random effects according to LME model Equation (15b)

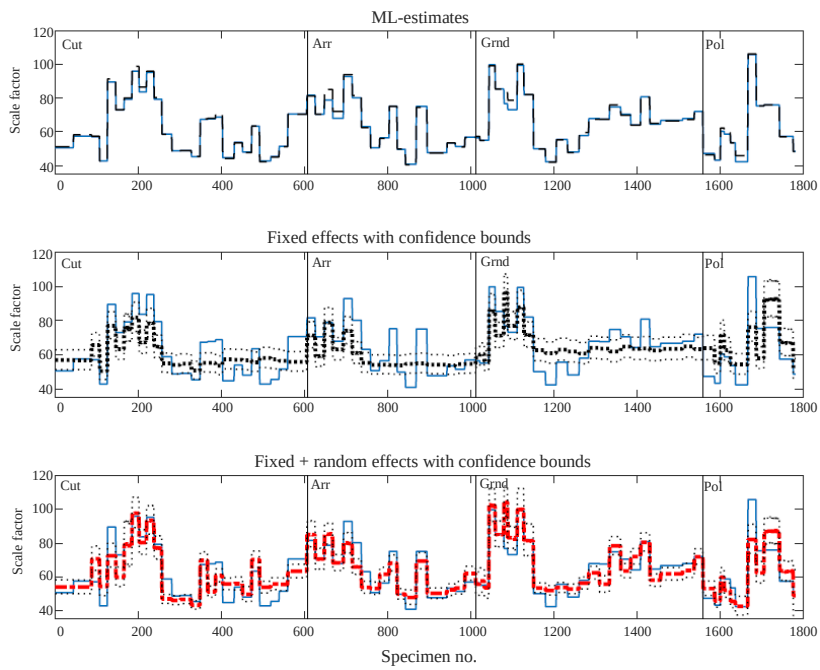

Fig. 6: Scale factor fixed and random effects according to LME model Equation (15a)

10,000 pairs of values of scale and shape parameter are drawn in random samples using the LME models, Equation (15b) and (15a), while assuming that the glass could have been obtained from either supplier (but with the same supplier, edge type, load span, etc., per each pair of parameters sampled). The stress rate is assumed to be 2 MPa s^{-1}. Since Equation (15a) contains the value of shape parameter, the shape factor is first simulated and then inserted into the model for scale parameter which is subsequently sampled. Then, median, 5% fractile and 1 in 10,000 probability values of strength are computed in MC-simulations of Weibull distributions using the sampled pairs of random scale and shape parameters and the results are illustrated in Fig. 7 for each edge type and separated according to assumed load span dimension. The whiskers in the

DOI: 10.3844/sgamrsp.2020.130.148

boxplots are extended beyond the quartile by one and a half times the interquartile range which implies about 99% coverage if the data are normally distributed. Also in these figures is indicated the lower bound of a one-sided confidence interval for the 5-percentile value at the approximate 75% confidence level. In addition, a mixture distribution function is computed, assuming that the glass could have been obtained from either supplier, in a MC-simulation based on the approximation formula in (16). Figure 8 shows the resulting mixture distributions per edge type and load span.

The proportion of variability in the response explained by the fitted models is given in Table 3 in addition to the fraction of the total unexplained variance that is explained by differences in supplier, $\sigma_c^2/\left(\sigma_c^2+\sigma_\epsilon^2\right)$. σ_c^2 is the supplier variance, σ_ϵ^2 the residual variance (see also App. B) and $\sigma_c^2+\sigma_\epsilon^2$ is the total variance not explained by fixed effects.

The LME model described so far results in the same shape factor for all data corresponding to the same edge-type. In the following, this is compared with the results from a clustered likelihood estimator, the clusters corresponding to each edge type, see also App. A. Given in Table 2 are the estimated shape factors calculated using Equation (20) and (15b). With Equation (20), the same edge-type has the same shape factor. The computation is based on the derivatives (21a) and (21b) and on the second derivatives (22a), (22b) and (22c) and is performed using a nonlinear minimization algorithm in MATLAB (MathWorks Inc., 2018). When the ML-estimates are computed using either of Equation (19) and (20), i.e. with ordinary ML-estimation or alternatively with an estimation procedure that conditions the same edge-type to have the same shape factor, there is hardly any difference in resulting scale factor, as can be seen in the top subplot in Fig. 6 which compares these values.

Table 1: Batch/supplier index numbers corresponding to cited publication with samples of strength in in-plane conguration of four-point bending tests. Items marked with a star or dagger, respectively, refer to batches for which it was not verified that they are not confounded with each other. Edge finishing: c = as-cut, *a* = arrised, *g* = ground, *p* = polished

Publication	No. of samples	Total no. edge fail's	Batch index no.	Edge finishing
Carre (1996)	6	81	1	p
Veer *et al*. (2006)	3	32	2*	g
Veer *et al*. (2009)	1	30	3*	p
Veer and Rodichev (2011)	2	83	4*	c
Vandebroek *et al*. (2012)	4	77	5†	cp
Lindqvist (2013)	4	110	6	cp
"	1	19	7	c
"	4	73	8	cg
"	4	84	9	ca
"	6	101	10	ag
"	2	39	11	g
Vandebroek *et al*. (2014)	8	202	12†	cg
Kozlowski (2014)	1	6	13	p
Kleuderlein *et al*. (2014)	6	131	14	cag
"	6	163	15	cag
"	6	169	16	cag
"	6	138	17	cag
"	6	157	18	cag
"	3	74	19	cag

Table 2: Estimated shape factor per edge type using Equation (20) or (15b) with approximate 95% confidence bounds within parentheses

	As-cut	Arrised	Ground	Polished
ML-estimation procedure	10.3	13.6	11.0	7.2
LME modelxed-effect	9.7 (8.4, 11.2)	14.6 (12.2, 17.5)	10.2 (8.5, 12.2)	8.0 (6.4, 10.0)

Table 3: The proportion of variability in the response explained by the fitted model and the fraction of the total unexplained variance that is explained by differences in supplier

LME model	R^2	$\sigma_c^2/\left(\sigma_c^2+\sigma_\epsilon^2\right)$
Scale factor	0.66	0.55
Shape factor	0.66	0.59

DOI: 10.3844/sgamrsp.2020.130.148

Table 4: Data on the relative frequency of edge failures in laterally supported plates subjected to Uniform Pressure (ULP) and in Four-Point Bending (4PB) tests. For the ULP tests, only those edge failures are included that were unambiguosly identified as such. In some cases the experimenter recorded multiple potential fracture origins for a single specimen. In case of a mixture of potential surface and edge fracture sites for the same specimen, the associated observation was not included in the edge failure statistic. Hence, the statistic represents a lower bound on the relative frequency. OP = out-of-plane bending configuration

Reference	Bend. type	Total no. fail's	No. edge fail's	Rel. freq. edge fail.
Johar (1981)	ULP	78	17	0.22
Johar (1982)	ULP	106	23	0.22
Kanabolo and Norville (1985)	ULP	206	54	0.26
Calderone (1999)	ULP	195	41	0.21
Veer and Rodichev (2011)	4PB OP	89	84	0.94
Muniz-Calvente *et al*. (2016)	4PB OP	30	14*	0.47
Osnes *et al*. (2018)	4PB OP	93	21*	0.23
Ritter *et al*. (1984)	4PB OP	1263†	1015†	0.80†

*According to private correspondence
†Test conducted either in distilled water or in dry nitrogen gas

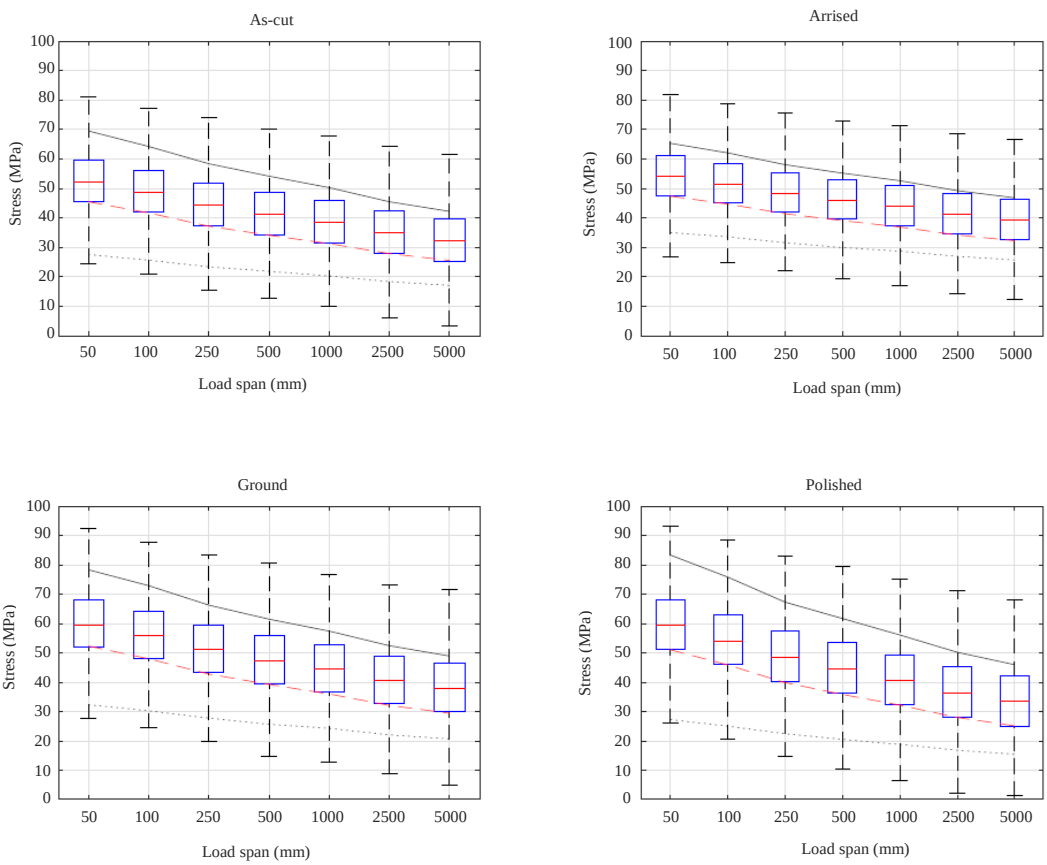

Fig. 7: Simulation of various strength percentiles per edge type at 2 MPa/s stress rate as function of load span dimension. The boxplots correspond with 5-percentile values. Dashed line is a curve fitted to the lower bound in a 75% one-sided confidence interval for the 5-percentile. Solid line traces the estimated median strength (computed as median value of 10,000 point estimates per load span). Dotted line is the 1 in 10,000 probability failure stress (median value of point estimates)

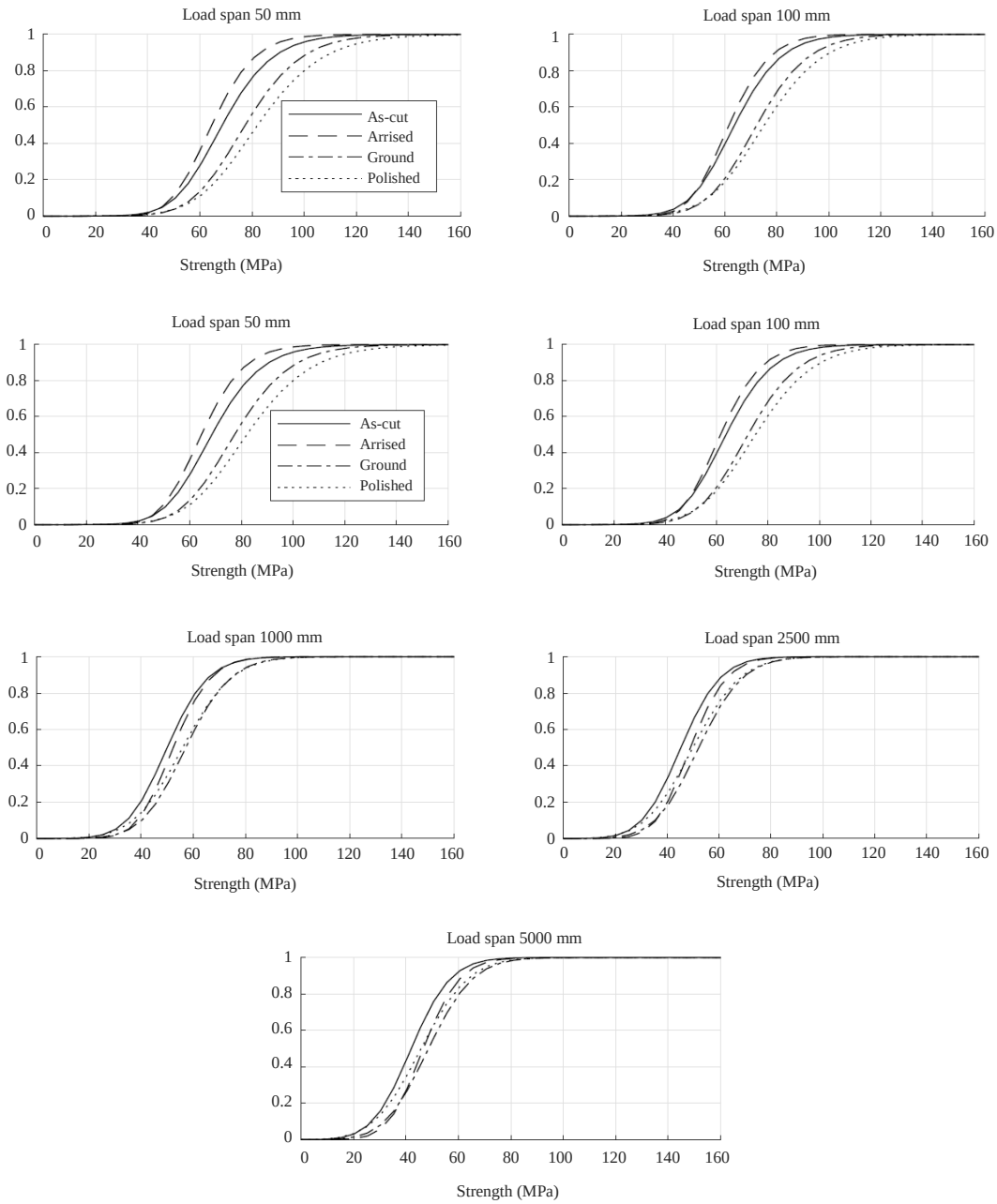

Fig. 8: Simulated mixture distributions for the strength at 2 MPa/s stress rate per edge type as function of load span

Discussion

The edge strength is important to consider in design of glass structures because in practice, the edge is prone to significant tensile stress even when maximum stress occurs away from the edge elsewhere on the surface. This is demonstrated in various experiments with four-sided laterally supported plates subjected to uniform pressure for which the maximum tensile stress occurs at the centre point of the surface. According to a recent re-

view of test results from hundreds of large laterally supported panes subjected to uniform pressure, it was found that none failed at the location of maximum principal tensile stress (Natividad *et al*., 2016). Moreover, according to a survey of almost 600 specimens tested with uniform lateral pressure, more than one in five failed at the edge, see Table 4. In addition, Table 4 shows that in four-point bending tests, on average more than half of failures originated from the edge when the configuration of bending was out-of-plane.

The additional mechanical action to the edge that occurs during production processes suggests that strength properties of the edge may not be equal to those of the pristine surface. According to EN 16612:2019, edge strength is generally considered to be inferior to surface strength and this is reflected in the prescription of an edge strength factor; the largest reduction is applied to the raw-cut edge and none at all to the polished edge. In a study involving eight participating laboratories (Ritter *et al*., 1984), it was found that for the results from seven out of eight laboratories the surface and edge failures were evenly mixed throughout the distribution so that a unimodal strength distribution often fitted the data well. However, it was also reported that with the results from one of eight laboratories, there was no intermixing of strength values from the edge and surface flaw populations and moreover, all of the surface failures were in the low strength portion of the distribution while edge failures were in the high strength portion. This clearly indicates that in some cases there can be significant differences in surface and edge strength distribution even as the specimens in this case (Ritter *et al*., 1984) were obtained from the same supplier and were randomized prior to being delivered to each of the participating laboratories. Moreover, these results apparently contradict the concept in EN 16612:2019 where the edge strength is deemed to be inferior to surface strength. Evidently, more research is needed to verify if the edge reduction factors adopted in the standards are correct. Figure 8 indicates that polished edges are generally the strongest.

Comparing different edge types with each other, see also Fig. 4, the polished edge corresponds with samples of either a similar or a larger coefficient of variation, on average, than other edge types. The optical appearance of the polished edge is superior, however, prediction-making of its strength value is potentially associated with greater uncertainty than for other finishings. The selected values for edge strength factor in EN 16612: 2019 could be non-conservative.

The edge strength is complex to model due to the range of factors that can have a confounding effect. Even when the number of factors are limited by restricting the analysis to e.g., a fixed load span for a specific edge type at a specified rate of applied stress in a controlled environment, it is seen that strength values scatter substantially and it is concluded that the variation cannot be accounted for by a single standard statistical distribution, compare also Veer (2007). Rather, samples are fitted by Weibull distributions with scale and shape parameters that exhibit random variability in addition to systematic effects according to e.g., weakest-link scaling.

Considering the recorded data results in a Weibull statistical framework, it appears that a major confounding factor is related to manufacturing and production line processes which can be assumed to vary with location and over time due to e.g., variability in grinding wheel settings and machine properties, presence of residual compressive stresses and variations in environmental conditions during manufacture to the extent that it may affect the end-product (Veer, 2007; Kleuderlein *et al*., 2014; Le Bourhis, 2008). Table 3 shows that about two thirds of the variability in the LME models fitted to the Weibull scale and shape factors is explained by physical interpretation (edge-type, stress rate, weakest-link scaling). Of the remaining variability, between 55%-60% is related to supplier or batch effects. Approx. 14% of total variability is not explained by the model and can be attributed to, e.g., local effects during testing of each individual specimen and sample-to-sample effects including inter-laboratory differences, presence of residual compressive stresses and of course errors in the treatment of stress corrosion with the approximate theory applied.

The numerical investigation into sample size effect on computed Weibull parameter estimates, see Fig. 2, shows clearly that when sample size is limited, the shape parameter estimate scatters substantially to produce what might appear like a statistical artefact. This might explain most of the variability in observed shape parameter estimates from recorded test results for ground and polished edges (cf. Fig. 4c and 4d). It corresponds to the conclusion drawn in a previous large scale investigation of the strength of small glass plates with ground edges according to Ritter *et al*. (1984), where it was noted that whereas "the variability observed in the Weibull slope parameter, *m*, was close to that expected from the statistical reproducibility of the strength test [...] the variability in the median strength from laboratory to laboratory was much greater than that due only to statistical considerations." For the arrised and in particular as-cut edge (Fig. 4a and 4b), however, variability in shape parameter is hardly within statistical reproducibility.

The environmental conditions are known to significantly affect the observed strength due to stress corrosion (Charles, 1958b; Brown, 1974); at higher rates of applied loading, the strength is increased. In the present analysis, it was assumed that the environmental conditions during testing were approximately identical. This is a simplifying assumption however, as the recorded values of temperature and relative humidity in the experiments ranged from 15°C to 25°C and from

about 23% to 70%, respectively. According to a survey of measurements of stress corrosion parameter v_0 in Haldimann (2006) and Schula (2015), its value was found to vary substantially even under seemingly identical environmental conditions. This points to a potentially confounding effect on the estimation of scale factor in the present study and it is expected to contribute to the error terms in the LME model (15a). In addition, while applying Equation (9), the existence of the threshold limit value K_{Ith} is ignored, however, this is assumed to have a limited effect on the results.

Although a general size effect is evident when considering Fig. 4, due to the scatter of individual statistics it is hard to verify that a proper assessment of it was made when based on a few sample statistics alone. The variation in estimated scale parameter for an identical load span at the same loading rate can be considerably large as the results for the as-cut and arrised edge type demonstrate. In conclusion it is recommended that size effect for glass edge be addressed in wide-ranging studies with a diversity in glass supplier, thickness, etc., perhaps also including diversity in participating laboratories. According to results from MC-simulations, see Fig. 7, the size effect can be expressed in terms of the value of 5-percentile strength with the ordinary weakest-link scaling formula, Equation (17), i.e., the decrease in strength from σ_1 to σ_2 as the load span increases from L_1 to L_2 is approximated well by the usual formula:

$$\sigma_2 = \sigma_1 \left(\frac{L_1}{L_2} \right)^{\frac{1}{m}} \tag{17}$$

if m is taken as 8.0, 12.0, 8.0 and 6.5, respectively, for the as-cut, arrised, ground and polished edge types. These values are close to those given in Table. 2. The corresponding fit is illustrated in Fig. 7 with a dashed red line where scaling is performed from a baseline strength value at load span 100 mm. The load spans represented in the experiment data range from about 50 mm to 500 mm. In practical circumstances when glass is used in structures, the effective load span can be larger than so and more research is needed to verify how the size effect is manifest and properly extrapolated. Figure 4 also shows the 1 in 10,000 probability failure stress with a dotted line which lies above 20 MPa for all load spans that are represented in the data that was used to fit the model.

The characteristic 5-percentile strength values that were estimated in the present study, see Fig. 7, suggest that the 45 MPa value for glass strength that is mentioned in EN 572-1:2012 (and which is further discussed in an annex to EN 16612:2019) could be used for the edge if it is computed as the lower bound in a one-sided confidence interval at the 75% level and, if it is related to a reference length of 100 mm at an applied stress rate of 2 MPa s^{-1} except for the as-cut edge which warrants a reduction of about 5% and the ground edge which allows for a increase of 5%. The size scaling would then follow from Equation (17). However, the difference in estimated strength between edge types is not large and a simplification could be made. So long as the as-cut edge is not considered, the characteristic values for the polished edge in Fig. 7 could be adopted conservatively for either of the arrised, ground and polished edge types.

In the present study, the edge size was measured by its length, however, weakest-link scaling could be considered in terms of edge area rather than edge length so that if w_0 denotes a reference thickness then:

$$\log k \propto \frac{1}{m} \log \frac{L_0 \cdot w_0}{L \cdot w} \tag{18}$$

where, $L_0 w_0$ is the reference area and Lw is the given edge area. With increasing thickness, edge size is greater and in consequence, the probability for the edge to contain a severe flaw increases according to classical weakest-link scaling argument. Or, another measure might be used, such as a representative volume that extends into part of the main surfaces (zone S0 and S5 in Fig. 1) in which case edge size would no longer be a simple product of thickness times length. However, increasing thickness is associated with differently chosen cutting angles in the production method. Therefore, it can be assumed that flaw population characteristics vary with thickness (Lindqvist, 2013; Veer, 2007). For such reason, glass thickness may interact with edge length and edge type to produce an effect on strength in ways that may not be self-evident. Consequently, Equation (18), although logical from the point of view of classical weakest link scaling principles, does not sufficiently express the effect on strength due to edge thickness variations. This was noted in the present study when various adaptations of the LME in (15a) and (15b) were investigated and compared using the AIC information, see App. A. For the shape parameter, it was seen that supplier/batch, edge type and thickness where the most important factors (in the given order) to consider in search of better performing models. For the scale parameter, slightly better performing models where produced when edge thickness was included as a fixed-effect rather than accounted for by using Equation (18) and, in fact, the same was seen for load span length, too. This indicates that weakest-link scaling of strength due to edge size is not entirely a simple matter of scaling according to the formula in Equation (18). Instead, it is suggested that edge characteristics in terms of flaw population vary with thickness and even with length. More research is needed to verify the effect on strength due to edge thickness and to better understand the proper way to measure edge size for weakest-link scaling purposes.

According to Veer and Rodichev (2011), lateral cracks generated by scribing are located at a greater depth than the initial surface microcracks. The length of lateral cracks is also greater than the width of the score itself. The hypothesis laid forward in Veer and Rodichev (2011) is that some of the lateral cracks are so large and are located at such depth that they remain partially or in full even after grinding and polishing operations. Others, however, appear to disagree. In Vandebroek *et al*. (2014) it is said that "[a]fter grinding, one can assume that the damage caused by cutting has vanished." And in Kleuderlein *et al*. (2014) it is suggested that "damages in the form of microcracks caused by the cutting process are eliminated or at least significantly reduced by arrising or grinding." On a similar note, Sglavo *et al*. (2007) who performed three-point bending tests on monolithic glass beams with an out-of-plane configuration of the bending, reported that the position of the originally scored edge, i.e., in the tension zone or in the compression zone, had an insignificant effect on the strength when the glass was processed, i.e., arrised, ground or polished. At the same time, Sglavo *et al*. (2007) write that the various edge processing methods are responsible for creating new flaw populations. This is in agreement with Veer (2007), who claims that grinding operations might increase the damage because the experimental data results he obtained indicated that some as-cut specimens were stronger on average. This has been noted by others too (Lindqvist, 2013; Vandebroek *et al*., 2014). In summary, there is an on-going debate in the literature over the significance of grinding and polishing operations on edge flaw population characteristics. The data in the present study suggests that grinding and polishing operations could be responsible for increasing the average value of COV for strength.

Figure 4a representing the as-cut edge statistics indicates a possible scale-dependency of the shape parameter. Although such scale-dependency has not been addressed previously in the context of structural glass engineering so far as the authors are aware, it has been noted elsewhere for metal fatigue in components such as gears, shafts and turbine blades, the strength of gear pairs made from plastic and roller bearings (Juskowiak and Bertsche, 2014, see also Seo *et al*., 2009). The salient feature is that the shape parameter decreases with increasing scale within a Weibull analysis framework. Considering the statistics in Fig. 4, it appears that one effect of grinding and polishing could be to remove a scale-dependency on the shape of the Weibull distribution, although more research is needed to verify this.

Considering the as-cut edge type, for which one side has been scribed and thus subjected to mechanical action (compare Fig. 1A), it is logical to expect the mean strength to increase when the non-scored edge (part 1 in Fig. 1A) is positioned in the tension zone compared to the scored edge (part 2 Fig. 1A) when applying four-point bending with an out-of-plane configuration. This is also reflected in Fig. 4a for the four data samples that represent this type of bending configuration (green marker colour in the figure corresponds to out-of-plane bending configuration with the scored edge positioned in tension zone while red marker corresponds to the non-scored edge subjected to tension). However, what about potential differences in edge strength with an in-plane bending configuration compared to an out-of-plane configuration? Most of the data on the edge strength comes from specimens loaded with an in-plane configuration of bending. There are significant ad- vantages with the in-plane compared to the out-of-plane configuration when measurements of edge strength are sought if it is assumed that results from in-plane bending tests can be used as a proxy for edge strength. In contrast, with an out-of-plane configuration, a substantial portion of failures may not occur from the edge, but on the centre part of the surface. Table 4 provides an indication of the ratio of edge to surface failures that may occur in practical circumstances. If the purpose is to obtain a sample of, e.g., 30 observations of edge strength using an out-of-plane bending configuration then according to Table 4 one may in the worst case have to be prepared to put some 150 specimens to the test, although on average about 60 will suffice. There is the additional time and effort involved in identifying each fractured specimen according to whether it failed at the surface or from the edge. More research is needed however, to verify whether the recorded edge strength distribution is the same for in-plane loading as for out-of-plane.

In this study, the influence of the cross-sectional and longitudinal fracture location was generally not considered except in the analysis of the as-cut edge, cf. Fig. 1. The influence of these location descriptors was studied by Vandebroek *et al*. (2014) who found that in the case of raw-cut edges, a considerably larger number of failures originated from the mechanically scribed edge. The same was found by Kleuderlein *et al*. (2014). However, according to Vandebroek *et al*. (2014), the observed strength was "almost not depending" on cross-sectional location. Moreover, the edge strength value was "hardly dependent" on longitudinal failure location, although the frequency of failures varied in the longitudinal direction (Vandebroek *et al*. 2014). This is in general accord with the results reported in Sglavo *et al*. (2007).

Kleuderlein *et al*. (2014) obtained their glass specimens from six different suppliers. The process parameters were documented by each manufacturer and the protocols were compared. The results showed that the suppliers used cutting machines from different companies and moreover, used different cutting pressure, cutting speed, cutting wheel angle and cutting fluid, even for the same glass thickness. Kleuderlein *et al*. (2014) also noted significant differences in how the arrised edge type in particular was produced, e.g. in terms of the

optical quality. Their results are not entirely conclusive as to the effect on strength due to edge processing type, i.e. cut, arrised, or ground. However, they conclude that different production parameters lead to different strength levels. This is in general agreement with other studies, see e.g. Veer *et al*. (2006); Le Bourhis (2008); Lindqvist (2013); Vandebroek *et al*. (2014). According to Veer (2007), the degree of maintenance is more important for the strength than the other settings of the grinding machine. According to EN 16612:2019, the edge strength reduction factor is defined so that when the abrasive action is across the edge, the strength is 11% lower than when the abrasive action is along the length of edge for arrised and ground processing types. Vandebroek *et al*. (2014) note that glass which originates from different manufacturers and which is processed at different points in time or in different factories might exhibit varying strength levels due to the presence of residual compressive stresses. Residual stresses develop as a consequence of the annealing process. The pre-stress levels are not very consistent according to Veer *et al.* (2009) who measured the residual stresses in specimens prior to testing them until failure and they conclude that the production process is less controlled than commonly assumed. All of this suggests that it is relevant to quantify and include in a model the potentially confounding effect due to glass supplier/batch. This was also considered in the present analysis where the supplier was included as a mixed-effect in a linear statistical model. The results show that the incorporation of supplier effects can help to explain a significant part of the total variability in observed Weibull parameter estimates.

Conclusion

A comprehensive analysis of glass edge strength is performed based on a survey of experimental measurements which can be found in a range of journal articles, conference proceedings and academic dissertations available in the open literature. Tests with four types of glass edge in a four-point bending fixture show that there is substantial variability in Weibull distribution parameter estimates, even when specimens with the same dimensions from the same supplier are subjected to the same loading rate in an in-door climate. Numerical investigations show that when sample size is limited, Weibull shape parameter estimates scatter substantially and this can provide an explanation for some of the observed variability (in shape). Data from some 1800 measurements comprising up to 19 suppliers of glass strongly suggest that there are differences in Weibull shape factor between edge types. The polished edge is associated with the lowest Weibull shape factor on average and the arrised with the highest whereas as-cut and ground edges lie in-between. Additionally, the data indicates that for the as-cut edge, the shape parameter is scale-dependent with an inverse proportionality, i.e., the lower the scale the higher is the shape value. This scale-dependency of shape appears to vanish with ground and polished edge types thus indicating a possible effect of grinding operations on the strength distribution.

The variability in parameter estimates can be further explained by considering the parameters as random variables nested within a Weibull random variable. The linear mixed-effects statistical model is used with the supplier as mixed-effect. Predictions made while assuming that glass is obtained from an unknown batch or supplier (i.e., from any of the suppliers in the study) show that the characteristic, 5-percentile strength (considering its lower bound in a one-sided confidence interval at the 75% level) is 42 MPa, 45 MPa, 48 MPa and 46 MPa for the as-cut, arrised, ground and polished edge type, respectively, on a reference 100 mm load span at 2 MPa s^{-1} stress rate. The size effect can be represented by the usual weakest-link scaling formula if the Weibull modulus is taken to be 8.0, 12.0, 8.0, 6.5, for the respective edge-types. The estimated stress corrosion parameter is close to $n = 16$ with an approximate 95% confidence interval (14.0, 16.9). The size effect in this study is based on a simplified representation of the edge as a line and thickness is neglected. In reality, glass thickness may interact with edge length and edge type to produce an effect on strength in ways that may not be self-evident, e.g. due to modified machine settings that apply when cutting glass of different thickness. More research is needed to assess the effect on strength due to thickness and how this may interact with edge length and edge profile. The equations used in this study to motivate the chosen linear mixed-effects statistical models are in reality coupled and this was neglected in a simplified approach. In future work this may be addressed and resolved more fully.

The hierarchical modelling approach results in the same distribution shape parameter for all data corresponding to the same edge-type. By considering the data sets in groups according to edge type, it is possible to estimate the Weibull parameters using a clustered likelihood estimator under the condition that the shape value is the same for the same edge type. It is found that the as-cut, arrised, ground and polished edge has a shape value quite close to those estimated with the hierarchical model and a very similar scale value.

Author Contributions

David Kinsella: Is the main author of the article and the conceptual designer of the project, the main analysis and the interpretation of data.

Johan Lindström: Contributes to the statistical analysis and interpretation of data and to the revision of the manuscript.

Conflict of Interest

On behalf of all authors, the corresponding author states that there is no conflict of interest.

References

Akaike, H., 1969. Fitting autoregressive models for prediction. Annals Institute Stat. Math., 21: 243-247.

Broek, D., 1983. Elementary Engineering Fracture Mechanics. 3rd Edn., Springer Netherlands, ISBN-10: 9401183708, pp: 469.

Brown, W.G., 1974. A Practicable Formulation for the Strength of Glass and its Special Application to Large Plates. 2nd Edn., National Research Council Canada, pp: 62.

Burnham, K.P. and D.R. Anderson, 1998. Model selection and inference.

Calderone, I., 1999. The equivalent wind loading for window glass design. PhD Thesis, Monash University.

Carre, H., 1996. Etude du comportementa la rupture d'un materiau fragile precontraint: Le verre trempe. PhD Thesis, Ecole Nationale des Pontset Chauss´ees.

Charles, R.J., 1958a. Static fatigue of glass I. J. Applied Phys., 29: 1549-1553.

Charles, R.J., 1958b. Static fatigue of glass II. J. Applied. Phys., 29: 1554-1560.

DIN 18008-1, 2010. Glas im Bauwesen- Bemessungsund Konstruktionsregeln - Teil 1: Begriffe und allgemeine Grundlagen. CEN

EN 1288-3, 2000. Glass in building - Determination of the bending strength of glass - Part 3: Test with specimen supported at two points (four point bending). CEN

EN 16612, 2019. Glass in building - Determination of the lateral load resistance of glass panes by calculation. CEN

EN 572-1, 2012. Glass in building - Basic soda lime silicate glass products - Part 1: Definitions and general physical and mechanical properties. CEN

Evans, A.G., 1974. Slow crack growth in brittle materials under dynamic loading conditions. Int. J. Fracture, 10: 251-259.

Givens, G.H. and J.A. Hoeting, 2013. Computational Statistics. 2nd Edn., John Wiley and Sons, ISBN-10: 0387981454, pp: 728.

Haldimann, M., 2006. Fracture strength of structural glass elements-analytical and numerical model- ling, testing and design. PhD Thesis, Ecole Poly-technique Federale de Lausanne EPFL.

Hellan, K., 1984. Introduction to Fracture Mechanics. 1st Edn., McGraw-Hill, ISBN-10: 0070663505, pp: 302.

Irwin, G., 1958. Fracture. In: Handbuch der Physik, Irwin, G. (Ed), Springer, p: 551.

Irwin, G.R., 1957. Analysis of stresses and strains near the end of a crack traversing a plate. J. Applied Mech., 24: 361-361.

Johar, S., 1981. Dynamic fatigue of flat glass-phase technical report, Ontario research foundation, Department of Metals, Glass and Ceramics.

Johar, S., 1982. Dynamic fatigue of flat glass - Phase. Technical report, Ontario Research Foundation, Department of Metals, Glass and Ceramics

Juskowiak, J. and B. Bertsche, 2014. Stress-dependent Weibull shape parameter based on field data. In: Probabilistic Safety Assessment and Management PSAM 12, Juskowiak, J. and B. Bertsche, Honolulu, Hawaii

Kanabolo, D.C. and H.S. Norville, 1985. The strength of new window glass using surface characteristics. MSc Thesis, Texas Tech University.

Kleuderlein, J., F. Ensslen and J. Schneider, 2014. Investigation of edge strength dependent on different types of edge processing. Proceedings of the International Conference at Glasstec Du¨sseldorf Engineered Transparency, (DET' 14). Germany.

Kozlowski, M., 2014. Experimental and numerical analysis of hybrid timber-glass beams. PhD Thesis, Silesian University of Technology.

Krohn, M.H., J.R. Hellmann, D.L. Shelleman and C.D. Pantano, 2002. Biaxial flexure strength and dynamic fatigue of soda-lime-silica float glass. J. Am. Ceram Soc., 85: 1777-1782.

Lawn, B., 1993. Fracture of Brittle Solids. 2nd Edn., Cambridge University Press, ISBN-10: 0521409721, pp: 378.

Le Bourhis, E., 2008. Glass. Wiley-VCH Verlag GmbH and Co KGaA, Weinheim

Lehmann, E.L. and G. Casella, 1998. Theory of Point Estimation. 1st Edn., Springer Texts in Statistics, ISBN-13: 978-0-387-22728-3.

Lindqvist, M., 2013. Structural glass strength prediction based on edge flaw characterization. PhD Thesis, Ecole Polytechnique F´ed´erale de Lausanne EPFL.

MathWorks, Inc., 2018. www.mathworks.com

McCulloch, C.E., S.R. Searle and J.M. Neuhaus, 2008. Generalized, Linear and Mixed Models. 2nd Edn., Wiley, ISBN-10: 0470073713, pp: 424.

McLellan, G.W. and E.B. Shand, 1984. Glass Engineering Handbook. 3rd Edn., McGraw-Hill, ISBN-10: 007044823X, pp: 471.

Mencik, J., 1992. Strength and fracture of glass and ceramics, glass science and technology.

Mesarovic, S., D. Gasparini, S. Muju and M. McNelis, 1992. Probability of crack growth in Poisson field of penny cracks. J. Eng. Mech., 118: 961-978.

Müller-Braun, S., M. Seel, M. König, P. Hof and J. Schneider *et al*., 2020. Cut edge of annealed float glass: crack system and possibilities to in- crease the edge strength by adjusting the cutting process. Glass Struct. Eng., 5: 3-25. DOI: 10.1007/s40940-019-00108-3

Muniz-Calvente, M., A. Ramos, F. Pelayo, M.J. Lamela and A. Fernandez-Canteli, 2016. Statistical joint evaluation of fracture results from distinct experimental programs: An application to annealed glass. Theor. Applied Fract. Mec., 85: 149-157.

Natividad, K., S.M. Morse, H.S. Norville, 2016. Fracture origins and maximum principal stresses in rectangular glass lites. J. Archit. Eng., 22:1-1. DOI: 10.1061/(ASCE)AE.1943-5568.0000197

Osnes, K., O. Hopperstad and T. Børvik, 2018. Quasi-static and Dynamic testing of annealed float glass. Proceedings of the 18th International Conference on Experimental Mechanics (CEM' 18), Brussels, Belgium.

Rinne, H., 2009. The Weibull Distribution - a Hand-book. 1st Edn., Taylor and Francis Group CRC Press, ISBN-10: 1420087444, pp: 808.

Ritter, J.E., P. Strzepa, K. Jakus, L. Rosenfeld and K.J. Buckman, 1984. Erosion damage in glass and alumina. J. Am. Ceram Soc., 67: 769-774.

Sampson, P.D., A.A. Szpiro, L. Sheppard, J. Lindstr¨om and J.D. Kaufman, 2011. Pragmatic Estimation of a Spatiotemporal air quality model with irregular monitoring data. Atmospheric Environ., 45: 6593-6606.

Schula, S., 2015. Charakterisierung der Kratzanf¨alligkeit von Glasernim Bauwesen. 1st Edn., Springer-Verlag, ISBN-10: 3662477823, pp: 406.

Seo, J., M. Jung and C. Kim, 2009. Design of accelerated life test sampling plans with a nonconstant shape parameter. Eur. J. Oper., 197: 659-666.

Sglavo, V.M., C. Muller and F. Righetti, 2007. Influence of edge finishing on the resistance to thermal stresses of float glass. Glass Performance.

Vandebroek, M., C. Louter, R. Caspeele, F. Ensslen and J. Belis, 2014. Size effect model for the edge strength of glass with cut and ground edge finishing. Eng. Struct., 79: 96-105.

Vandebroek, M., J. Belis, C. Louter, G.V. Tendeloo, 2012. Experimental validation of edge strength model for glass with polished and cut edge finishing. Eng. Fract. Mech., 96: 480-489.

Veer, F.A. and Y.M. Rodichev, 2011. The structural strength of glass: Hidden damage. Strength Mater, 43: 302-315.

Veer, F.A., 2007. The strength of glass, a nontransparent value. HERON, 52: 87-104.

Veer, F.A., C. Louter and F.P. Bos, 2009. The strength of annealed, heat-strengthened and fully tempered float glass. Fatigue Fract. Eng., 32: 18-25.

Veer, F.A., P.C. Louter and T. Romein, 2006. Quality Control and the Strength of Glass. In: Fracture of Nano and Engineering Materials and Structures, Gdoutos, E.E. (Ed), Springer, ISBN-13: 978-1-4020-4972-9.

Weibull, W., T.C. Tsu, R.A. Mugele and F.A. McClintock, 1952. Discussion of A statistical distribution function of wide applicability. ASME J. Applied Mech.

A) Maximum Likelihood Estimation

The Weibull parameters can be estimated with the maximum likelihood (ML) method (Lehmann and Casella, 1998, Ch. 6.3), as the (numerical) maximum of the log-likelihood function for the two-parameter distribution in Equation (1):

$$\begin{aligned}&\log L(k,m;\sigma) = n_0 \log m - n_0 m \log k + \dots \\ &\dots + (m-1)\sum_{i=1}^{n_0} \log \sigma_i - k^{-m} \sum_{i=1}^{n_0} \sigma_i^m,\end{aligned} \tag{19}$$

where, n_0 is the sample size. Approximate confidence intervals for the parameters can be computed using asymptotic theory for ML-estimators (Lehmann and Casella, 1998, Ch. 6.3, for details.). In practice the computations are performed by the wblfit-function in MATLAB (Math Works Inc., 2018).

Likelihood Function for Grouped Data

An alternative to the model in Equation (19) is to assume that the shape parameter is constant for all samples with the same edge type, while still allowing for different scale parameters. Figure 9 for an illustration of this model. The resulting log-likelihood for all samples from the q^{th} edge-type becomes:

$$\begin{aligned}&\log L\left(k_q 1,...,k_q N_q, m_q; \sigma\right) = n_q \log m_q - \dots \\ &-\dots m_q \sum_{j=1}^{N_q} n_{qj} \log k_{qj} + \dots \\ &\dots + \left(m_q - 1\right) \sum_{j=1}^{N_q} \sum_{i=1}^{n_{qj}} \log \sigma_{qji} - \dots \\ &-\dots \sum_{j=1}^{N_q} k_{qj}^{-m_q} \sum_{i=1}^{n_{qj}} \sigma_{qji}^{mq}.\end{aligned} \tag{20}$$

Here mq is the shape parameter of the q^{th} edge-type, k_{qj} is the j^{th} sample for that edge-type, n_{qj} are the number of observation in the j^{th} sample, $n_q = j\ n_{qj}$ is the total number of observations for the q^{th} edge-type and σ_{qji} are the observations (indexed by edge-type, sample and observation number).

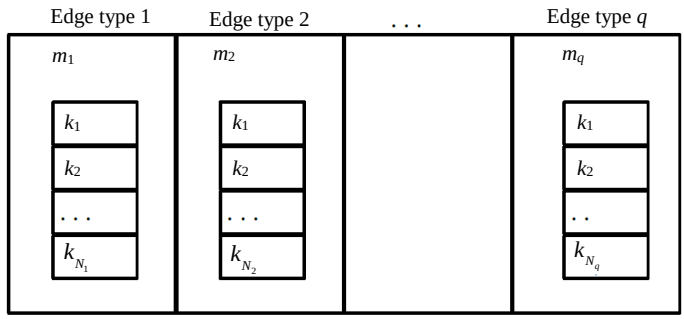

Fig. 9: Model assuming different scale parameters for each sample but a fixed shape parameter for each edge type

To obtain ML-estimates of the parameters in Equation (20) we use the fminunc nonlinear minimization algorithm in MATLAB. The numerical optimization is aided by the computation of first and second derivatives of Equation (20). For a given q and ignoring the q subscripts to simplify notation, we have first:

$$\frac{\partial \log L}{\partial k_j} = \frac{m}{k_j^{m+1}} \sum_{i=1}^{n_j} \sigma_{ji}^m - \frac{m n_j}{k_j}, \tag{21a}$$

$$\frac{\partial \log L}{\partial m} = \frac{n}{m} \sum_{j=1}^{N} n_j \log k_j + \sum_{j=1}^{N} \sum_{i=1}^{n_j} \log \sigma_{ji} + \ldots \\ \ldots + \sum_{j=1}^{N} \frac{1}{k_j^m} \sum_{i=1}^{n_j} \sigma_{ji}^m \log \frac{k_j}{\sigma_{ji}}, \tag{21b}$$

and second derivatives:

$$\frac{\partial^2 \log L}{\partial k_j \partial k l} = \begin{cases} -\frac{m(m+1)}{k_j^{m+2}} \sum_{i=1}^{n_j} \sigma_{ji}^m + \frac{m n_j}{k_j^2}, & \text{if } l = j, \\ 0, & \text{if } l \neq j, \end{cases} \tag{22a}$$

$$\frac{\partial^2 \log L}{\partial m \partial k_j} = \frac{1}{k_j^{m+1}} \left(\left(1 - m \log k_j\right) \sum_{i=1}^{n_j} \sigma_{ji}^m + \ldots \right. \\ \left. \ldots + m \sum_{i=1}^{n_j} \sigma_{ji}^m \log \sigma_{ji} \right) - \frac{n_j}{k_j}, \tag{22b}$$

$$\frac{\partial^2 \log L}{\partial m^2} = -\frac{n}{m^2} + \sum_{j=1}^{N} \frac{1}{k_j^m} \sum_{i=1}^{n_j} \sigma_{ji}^m \left(\log \frac{k_j}{\sigma_{ji}} \right)^2. \tag{22b}$$

Model Comparison

For likelihood based parameter estimation different models can be compared using information criteria, such as the Akaike information criterion (Akaike, 1969), with smaller values indicating better models. The AIC for a model is given by:

$$AIC = 2k - 2\log\left(L\right), \tag{23}$$

where, k is the number of unknown (or estimated) parameters and $\log(\hat{L})$ is the maximum-value of the log-likelihood. The AIC provides a trade-off between better models (higher value of $\hat{L}$) and increasing model complexity (more parameters, k). When comparing models those within 2 units are considered equivalent, 3-7 units indicates some differences and more than 10 units of difference is seen as strong evidence against the model with larger AIC (Burnham and Anderson 1998, pp. 75- 117).

B) Linear Mixed Effects Statistical Model

Linear Mixed Effects (LME) models are used to identify the source of variation and correlation that arise from clustered data, e.g., when data-collection is undertaken in a hierarchical manner where observational units are related, violating assumptions of independence (McCulloch et al., 2008, Ch. 6). Considering Equation (15b):

$$\log m_i = \sum_{l=1}^{4} \lambda_l \mathbb{I}_{edgetype=l,i} + \sum_{l=1}^{17} c_l \mathbb{I}_{\text{supplier}=l,i} + \varepsilon_i,$$

this constitutes a LME model where we see the effect of edge-type, γ_l, as fixed regression coefficients but assume that both the supplier (or batch) effect, c_l and the residuals, ε_i, are samples from normal distributions:

$$c_l \sim N\left(0, \sigma_c^2\right), \text{ and } \varepsilon_i \sim N\left(0, \sigma_\varepsilon^2\right). \tag{24}$$

The suppliers/batch are seen as random effects since: (1) we could expect substantially similar behaviour for glass from the same batch, violating the independence

DOI: 10.3844/sgamrsp.2020.130.148

assumptions regarding residuals in a standard regression. (2) It is unlikely that the list of suppliers considered here is exhaustive, i.e., that we include all suppliers on the market. (3) Due to the large number of supplier and batches it is more realistic (and useful) to characterise the variability between suppliers/batches than to try to form a complete list of supplier effects. The relative values of the estimated variances in Equation (24) will indicate how much of the variability in shape and scale parameters is due to supplier and how much has to be considered random errors not captured by the regression models in Equation (15).

When predicting from the LME the division in fixed and random effects allows us to consider both the case of a known edge-type and supplier, or the case of a known edge-type but unknown supplier. In both cases standard predictions for the LME will produce expected values for shape and scale parameters, as well as associated uncertainties in these predictions. The uncertainties will be based on the Normal models in Equation (24), with variances estimated from the data.

David Kinsella, Erik Serrano

Failure Modelling of Glass Plates in Biaxial Loading: Using Flaw-Size Based Weakest-Link Systems

Paper E

Submitted for possible journal publication